STUDIES OF INDIUM-DOPED SILICON

By

C.E. Jones, Project Investigator (612) 887-4415
D.E. Schafer, Project Scientist (612) 887-4419
M.W. Scott, Project Scientist (612) 887-4445
R.J. Hager, Research Assistant (612) 887-4505

HONEYWELL INC.
CORPORATE MATERIAL SCIENCES CENTER
10701 Lyndale Avenue South
Bloomington, Minnesota 55420

Final Report - June 1980

Effective Date: 1 August 1977
Expiration Date: 31 October 1979

Sponsored by

Defense Advanced Research Projects Agency (DoD)
ARPA Order No. 3211

Monitored by NVL Contract No. DAAK70-77-C-0194

UNCLASSIFIED

SECURITY CLASSIFICATION OF THIS PAGE (WHEN OATA ENTEREO)

REPORT DOCUMENTATION PAGE		READ INSTRUCTIONS BEFORE COMPLETING FORM
1. REPORT NUMBER	2. GOV'T ACCESSION NUMBER	3. RECIPIENT'S CATALOG NUMBER
4. TITLE (ANO SUBTITLE) STUDIES OF INDIUM-DOPED SILICON		5. TYPE OF REPORT/PERIOO COVERED FINAL REPORT 1 Aug 77 - 31 Oct 79 6. PERFORMING ORG. REPORT NUMBER 41696
7. AUTHOR(S) C.E. Jones M.W. Scott D.E. Schafer R.J. Hager		8. CONTRACT OR GRANT NUMBER(S) DAAK70-77-C-0194
9. PERFORMING ORGANIZATIONS NAME/AOORESS Honeywell Inc., Corporate Technology Center 10701 Lyndale Ave. So. Bloomington, MN 55420		10. PROGRAM ELEMENT,PROJECT,TASK AREA & WORK UNIT NUMBERS
11. CONTROLLING OFFICE NAME/AOORESS U.S. Army Night Vision and Electro-Optics Laboratory Fort Belvoir, VA 22060		12. REPORT OATE June 1980 13. NUMBER OF PAGES 131
14. MONITORING AGENCY NAME/AOORESS (IF OIFFERENT FROM CONT. OFF.) MERADCOM Procurement & Production Office Fort Belvoir, VA 22060 Symbol: BYRD/DRDME-PT-3		15. SECURITY CLASSIFICATION (OF THIS REPORT) Unclassified 15a. OECLASSIFICATION OOWNGRADING SCHEDULE

16. OISTRIBUTION STATEMENT (OF THIS REPORT)

17. DISTRIBUTION STATEMENT (OF THE ABSTRACT ENTERED IN BLOCK 20, IF OIFFERENT FROM REPORT)

18. SUPPLEMENTARY NOTES

This work was sponsored by Defense Advanced Research Projects Agency, ARPA Order No. 3211

19. KEY WOROS (CONTINUE ON REVERSE SIOE IF NECESSARY ANO IOENTIFY BY BLOCK NUMBER)

Indium-Doped Silicon; Photoconductive Sensors; X Level; Crystal Growth; Spectroscopy; Hall Measurements

20. ABSTRACT (CONTINUE ON REVERSE SIOE IF NECESSARY ANO IOENTIFY BY BLOCK NUMBER)

The objectives of this program were to develop a new growth technique for indium-doped silicon, to determine the trapping parameters for the centers in this material, and to identify and if possible eliminate the X-center, an indium-related complex.

The growth technique studied under this contract was the solution growth of silicon from an indium melt. Crystals doped with 1.6×10^{18} In/cm^3

FID-168 REV 11/74

DD FORM 1 JAN 73 1473 EOITION OF 1 NOV 55 IS OBSOLETE

UNCLASSIFIED

SECURITY CLASSIFICATION OF THIS PAGE (WHEN OATA ENTERED)

were grown by this technique at $\sim 1350^{\circ}C$. This is at the maximum in the indium concentration versus temperature curve and represents a concentration three to five times the values obtained from Czochralski or float-zone growth. The wafers grown have a uniformity of better than $\pm$ 5% by spreading resistance both axially and radially. Boron and phosphorus can be held to below 5×10^{12} atoms/cm^3 with the boron compensated to less than 10^8 electrically active boron atoms/cm^3. The indium-X-center concentrations can be held below the detection limit of about 5×10^{13}/cm. One-inch-diameter wafers with no voids or polycrystalline areas were grown but at present larger-diameter growths suffer from these defects. The current solution-growth dislocation count is ~ 1000 counts/cm^2.

The trapping parameters of indium and the indium-X center were measured as a function of temperature and electric field by deep-level transient spectroscopy. Both centers show the strong field dependence expected for coulombic traps. Two deep hole traps at E_v + 0.35 eV and E_v + 0.41 eV were found in indium-doped silicon.

X-centers were found associated with all of the other group IIIA dopants by optical absorption and deep-level transient spectroscopy techniques. The defects depend on carbon, and their annealing kinetics fit the reaction acceptor + carbon $\rightleftarrows$ X. The aluminum-X center has the stress symmetry of a $\{111\}$ trigonal defect. It was concluded that the best model for these defects is a nearest-neighbor carbon-acceptor pair. By growing with low-carbon materials, the X-center can be eliminated.

TABLE OF CONTENTS

LIST OF FIGURES

LIST OF TABLES

SECTION 1
INTRODUCTION

Areas of current interest in infrared detector development include the development of larger arrays, the use of cheaper materials, and the integration of the detectors and processing electronics onto the same chip. Silicon doped with various impurities can be used as a photodetector in many regions of the infrared. Silicon is available in large areas and the technology and equipment needed to process the detectors and coupled electronics is that used in the current silicon electronics industry. Because of this the production of chips with integrated detectors and electronics would be cheaper with silicon than with any other material. The yields, uniformity, and quality of silicon devices might be expected to be better for silicon than for any other less highly developed material and the development time and cost should be much less.

This report deals with the development of indium-doped silicon as a detector material.

Detector-grade indium-doped silicon should have high indium concentration, good uniformity over 2-inch-or-larger wafers, and a minimum concentration of electrically active shallow defects. A shallow defect complex which has been found in indium-doped silicon is the indium-X center. This center along with uncompensated boron can introduce thermal noise into the detector and require a lower temperature of operation than is needed if these defects are absent. In some applications the extra cooling required when X-levels are present results in a severe handicap.

The specific aims of this study effort were three fold:

1) Develop a new growth process which can produce better-quality indium-doped silicon than current Czochralski or float-zone techniques.

2) Determine the origin of the X-center and if possible eliminate it.

3) Determine the trapping parameters of centers in indium-doped silicon

This report reviews the results of the total study effort with emphasis on the results of the last reporting period. Many of the results are now published. Results which are not yet in the open literature are included in the appendices.

SECTION 2
SOLUTION GROWTH

DESCRIPTION OF THE TECHNIQUE

Solution growth is a technique for growing silicon crystals from a solution of silicon in molten indium. The apparatus is shown in Figure 1. The materials used are 0.999999 pure indium and the vacuum float-zone 20,000 Ω-cm silicon. A sandwich is formed with a silicon source crystal on top, an indium layer, and a seed crystal on bottom. The thin indium layer and the wafer-sized source and seed crystals provide for a minimum of material wasted in the growth process. At high temperatures silicon dissolves in the indium. A temperature gradient with the source hotter than the seed produces a silicon concentration gradient in the solution, with more silicon dissolved near the hotter source crystal. This concentration gradient moves silicon from the source to the seed where it recrystallizes. The recrystallized material contains the maximum indium concentration allowed at the growth temperature. The amount of material grown depends on the growth temperature and the temperature gradient. At 1300°C ∿ 10 mm of silicon can be grown in 24 hours with a 1.7°/mm temperature gradient.[1] The growth rate and the physics of the solution growth technique are discussed in detail in Appendix A.

---

[1] W. Scott and R.J. Hager, J. of Electron. Mater. 8, 581 (1979)

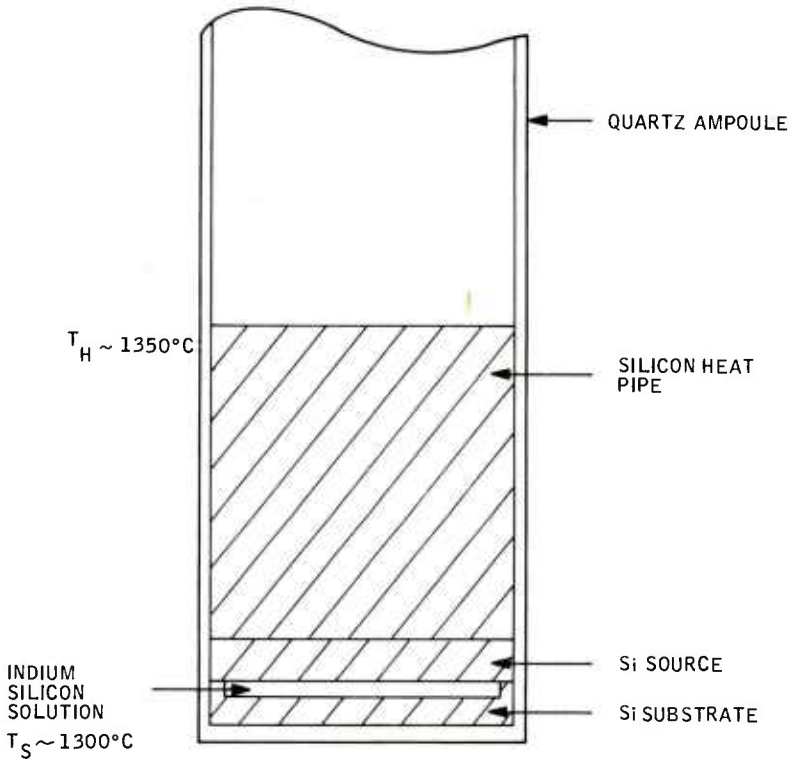

Figure 1. Schematic of the close-spaced solution-growth apparatus.

DOPANTS IN SOLUTION-GROWN MATERIAL

The solubilities of indium, oxygen, and carbon as a function of temperature in silicon have been measured with a series of solution growths. The indium concentrations were determined by Hall, resistivity, and optical absorption measurements (see Appendix A). The oxygen and carbon concentrations are measured by optical absorption (see Appendix B). The data are shown in Figure 2. The solubility of indium is retrograde, with the maximum being 1.6×10^{18} In/cm^3

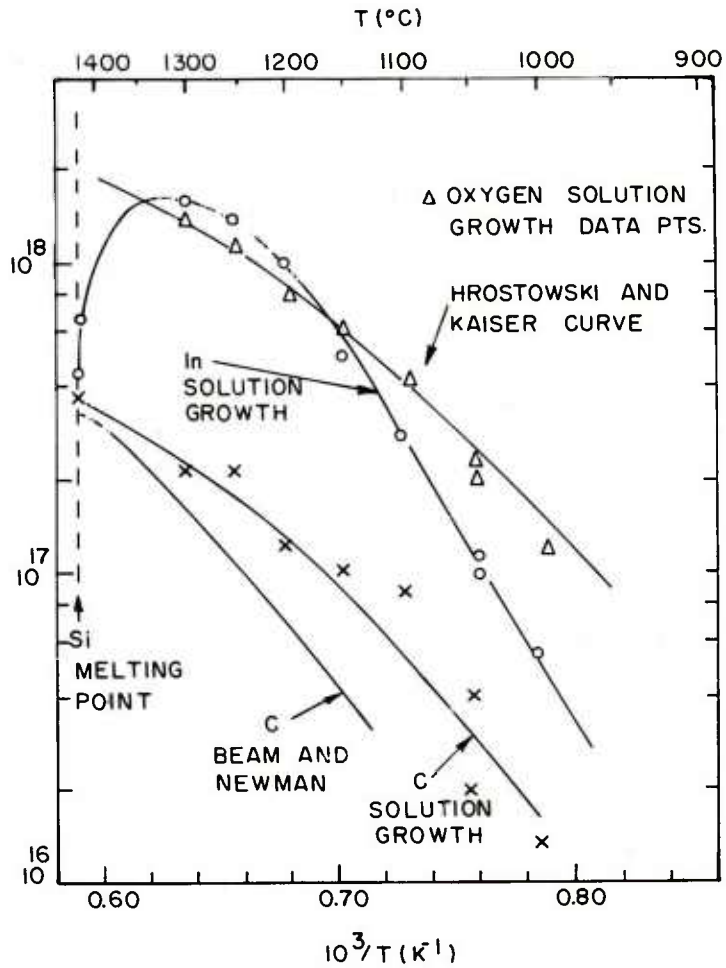

Figure 2. The maximum indium, carbon, and oxygen concentrations as a function of growth temperature as determined from solution growths. The solid lines represent the oxygen and carbon solubility curves obtained by Hrostowski and Kaiser[2] and Bean and Newman.[3] Data from Czochralski crystals are shown at the silicon melting point of 1420°C.

---

[2] H.J. Hrostowski and R.H. Kaiser, J. Phys. Chem. Solids 9, 214 (1958).

[3] A.R. Bean and R.C. Newman, J. Phys. Chem. Solids 32, 1211 (1971).

occurring at ∿ 1350°C. This concentration is about three times the best Czochralski values and five times the float-zone values obtained from growths at the silicon melting point of 1420°C. Oxygen seems to be introduced from the indium, since it is seen even in growths using low-oxygen float-zone silicon which has been isolated from the quartz walls. The oxygen concentrations seen in solution growths are always approximately the solubility limit for the growth temperature. This is seen in Figure 2 by comparing the solution growth data points and the oxygen solubility curve obtained by Hrostowski and Kaiser.[2] Carbon has been introduced from the silicon source and from graphite added to some growths. The carbon data shown are compared with the curve obtained by Bean and Newman.[3] The maximum substitutional carbon concentration seen in the solution growths is in the mid-10^{17} atoms/cm^3 range, which agrees with the more recent work of Newman[3] but is a factor of three lower than that reported in Newman's earlier work.[4] The carbon content can be controlled, and the use of low-carbon source and seed silicon materials has yielded crystals with carbon concentrations below our optical detection limit of ∿5 x 10^{15} atoms/cm^3.

Boron and phosphorous are introduced from the source and seed materials. Boron can also be introduced from the quartz holders. Solution growths made from vacuum float-zone silicon typically have boron and phosphorous concentrations less than 5 x $10^{12}/cm^3$ as measured by optical absorption using a bandgap bias light to populate the compensated boron and the phosphorous donors. These values are very close to those obtained from the original source

---

[4] R.C. Newman and J.B. Willis, J. Phys. Chem. Solids 26, 373 (1964)

and seed crystals, showing that the solution growth technique does not introduce any appreciable concentrations of these impurities. Hall data show that the boron concentrations are compensated at least down to the 10^8 carriers/cm^3 by the residual phosphorous. These data are shown in Figure 3.

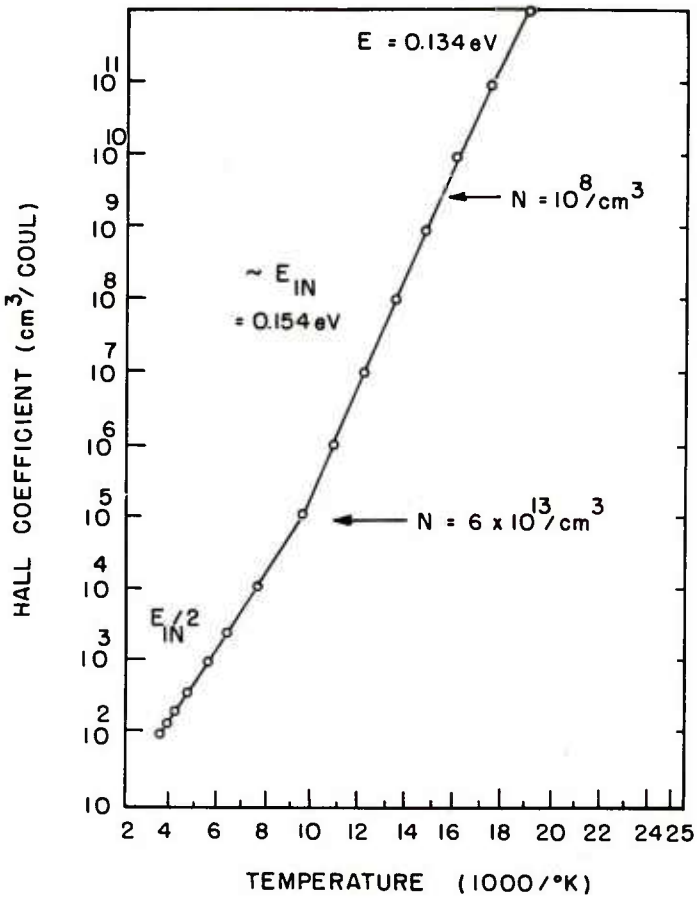

Figure 3. Hall data for solution-grown silicon showing indium dominating the free-carrier generation down to about the $10^8/cm^3$ level.

Optical absorption was also used to monitor the electrically active aluminum, gallium, and thallium concentration in the solution-grown material. The concentrations of all of these elements were below the optical detection limit of $\sim 5 \times 10^{12}/cm^3$ Al or Ga or $\sim 10^{15}$ Tl/cm^3.

Spreading resistance measurements have shown the solution-growth doping to be uniform to better than ±5% both axially and radially. This is shown in Figure 4, where data from Czochralski and float-zone crystals are shown for comparison. The Czochralski and float-zone samples show concentration drift from the center to the edge of a wafer and they also show striations due to the crystal rotation during growth. Solution growth is an equilibrium process carried out at a constant temperature with no motion to the materials. Growths near 1350°C are also at the broad top of the indium solubility curve so that small temperature variations make little difference in the indium solubility.

The X-center in indium-doped silicon has been found to depend on carbon and annealing temperatures.[5,6] The data are discussed in the section on X-center studies. Solution growths made from low-carbon, 20,000 Ω-cm vacuum float-zone silicon and annealed at 600°C for 6 hours have shown no detectable X-center concentration down to the optical detection limit of $\sim 5 \times 10^{13}/cm^3$. The Hall data of Figure 3 show no electrically active X-centers down to the $10^8/cm^3$ level. Thus, one result of this study has been the elimination of the indium-X center.

---

[5] R. Baron, J.P. Baukus, S.D. Allen, T.C. McGill, M.H. Young, H. Kimura, H.V. Winston, and O.J. Marsh, Appl. Phys. Lett. 34, 257 (1979).

[6] C.E. Jones, D.E. Schafer, W. Scott, and R. Hager, Bull. Am. Phys. Soc. 24, 276 (1979).

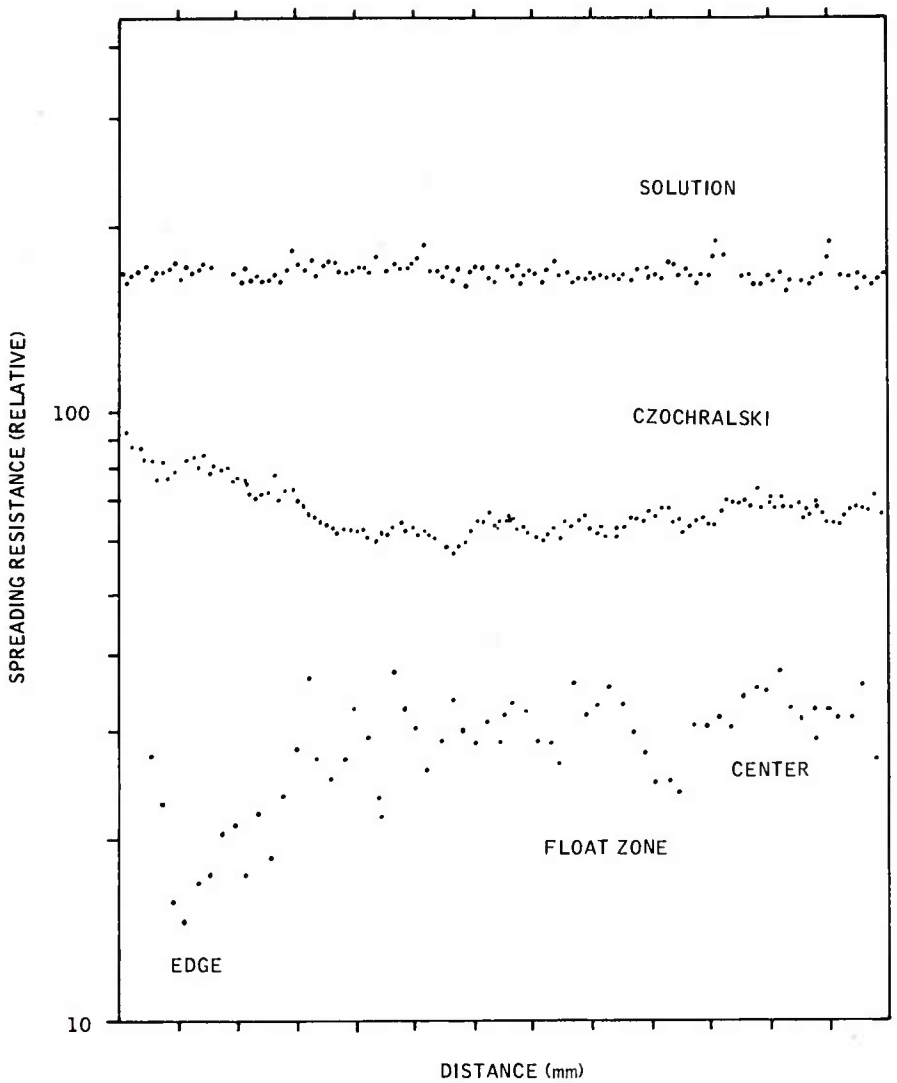

Figure 4. Spreading resistance measurements from edge to center of a solution growth, a Czochralski growth, and a float-zone growth for indium-doped silicon.

VOLUME PRODUCTION

Solution-grown indium-doped silicon has shown promise because of its high indium concentrations, good uniformity, and low impurity levels. Solution-grown silicon will not be practical for large-scale detector production unless it can be made in the volume needed, however.

A small furnace configuration has been designed and tested. This is shown in Figure 5. The system involves a cylindrical furnace area ∿5 inches in diameter by ∿2 inches high heated by a plate heater on the top. In the test furnace, a gradient of ∿1.5°C/mm over the temperature range of 1000 to 1420°C can be established vertically down from the plate heater. This could be maintained to better than ±0.1°C. The growth rate estimated for this gradient is ∿1 mm/day at 1200°C and 10 mm/day at 1300°C (see Appendix A). Test growths have been made between 1100° and 1200°C which fit this prediction. The furnace can produce wafers 2 to 3 inches in diameter.

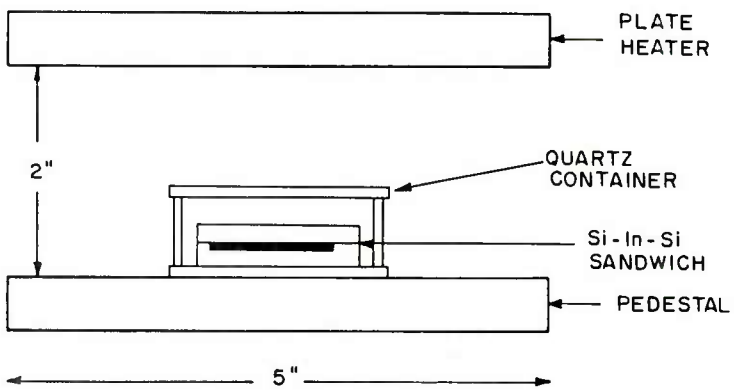

Figure 5. Furnace and sample arrangement for close-spaced solution growth.

The simple nature of the furnace design and its small size allow a large number of furnaces to be set up in parallel without undue cost. Parallel growth-furnaces coupled with the growth rates measured could produce adequate volumes of solution-grown crystals for detector needs.

CRYSTAL QUALITY

Most of the data on solubilities and purities have been taken on small samples on the order of 2 cm in diameter. To be useful for large-array production, crystals 2 inches in diameter or larger are needed. This is the minimum size which can be handled with ease on present silicon-device production lines. The wafers should be uniform in doping, single-crystal and void-free, and have low dislocation counts. The major effort in the last period of this contract was directed toward scaling-up the solution-growth diameter while maintaining crystal quality. Figure 6 is a photograph which shows the growth sizes. The larger the crystal area, the harder it has been to grow wafers without some voids or polycrystalline areas. Progress has been made from 1-cm-diameter wafers without these defects. At present, growths larger than 1 inch in diameter have all had some voids or polycrystalline areas. A series of solution growths have been made to try to determine the parameters affecting the start of polycrystalline growth and void formations.

Polycrystalline areas can be nucleated from defects in the seed layer, from particles in the melt, and from growth flaws. The quality of solution-growth material has been noted to drop at the height of the original indium solution, presumably due to impurities which float on the top of the original melt. The crystal quality for solution-growth runs with various indium melt depths running from 0.125 inch to 0.002 inch was checked. Again, a tendency for polycrystalline growth or complete crystal reorientation was found at the position of the top of the original indium layer. Better growths were obtained with thinner indium layers, with the optimum indium thickness being $\sim$0.005 inch.

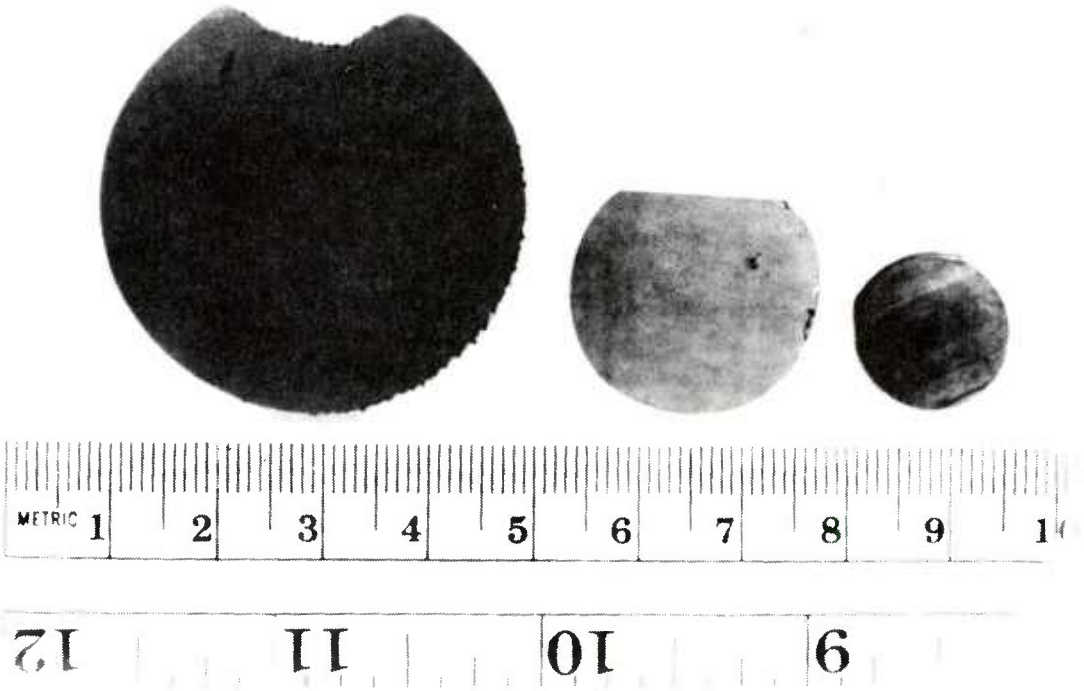

Figure 6. Progress in solution-growth wafer size from 1 cm in diameter in 1977, to 1 inch in diameter grown in 1978, to a 1.75-inch-diameter wafer grown in 1979.

Crystal cracking has been found when the indium spills out of the well and fuses the bottom of the seed crystal to the quartz ampoule. The differential contraction on cooldown causes the cracking. This has been prevented by placing the seed crystal on a silicon or quartz ring support which is smaller in diameter than the seed crystal.

Voids have been postulated to be due to trapped gas in the indium, indium vaporization, indium spillage, or incomplete indium-silicon wetting. Test runs have been made on pre-wetting, on preheating to drive off trapped gases, and on indium overpressures to prevent vaporization. Molten indium has a strong tendency to ball up and

not wet a silicon surface unless the temperature is raised to $\sim 1100^{o}C$. Solution growths are now put in a radiant heater and brought to $1100^{o}C$ for 10 minutes in argon or vacuum. The source-indium-seed sandwich is then X-rayed to see if any voids are present. Even after complete wetting, voids have been found to form during growth. This is especially true in vacuum growth. Indium vaporization seems to be a major cause for void formation. Indium and inert gas overpressures have helped to reduce this problem. Solution growths currently are done in a small quartz container which helps maintain the indium vapor in the growth region. This is shown in Figure 5. Some voids are still seen in the larger-area growths. Growths in saturated indium vapor or high-pressured inert gas have not been attempted yet but they may help to eliminate voids.

Dislocation counts have been made for solution-growth crystals over various orientations of substrates. The seed material has averaged 10 dislocations/cm^2. Some growths measured within a few mils of the seed have been as good as the seed quality. Most solution-growth material, however, has shown dislocation counts of $\sim 1000/cm^2$ independent of the substrate orientation. Figure 7 is a photograph of an etched solution-growth silicon surface.

For a more detailed discussion of solution growth, the reader is referred to Appendix A. The material in Appendix A was presented at the June 1979 IRIS Specialty Meeting on Infrared Detectors and covers the growth rates and impurity analysis in greater detail than is found in this section.

Figure 7. Solution-growth silicon etched with Wright etch to show dislocation and defects. The etch pit count shown is $\sim 1000/cm^2$.

SECTION 3
X-CENTER STUDIES

The X-center is an indium-related complex which is seen in Hall and optical absorption data at 0.12 eV.[7,8] This center is a source of noise in indium-doped silicon detectors unless the device is operated at a temperature of 40 to 50K to freeze it out. The normal operating temperature for an indium-doped detector should be 60 to 70K. The extra cooling needed when X-centers are present is a severe handicap in some applications.

There are several models which have been proposed for the X-center. Both the Hughes group of Baron et al.[5] and this group have seen a carbon dependence for the X-center concentration and have suggested a carbon-acceptor nearest-neighbor pair model.[6] The X-center concentration is seen to increase after irradiation and the AFML group has suggested that the center may involve interstitials or vacancies.[9] The energy of the In-X center is between that of aluminum and indium which has suggested Al-In distant pairs.[10]

During the course of this study, a number of experiments were performed to pin down the identification of the X-center. This work

---

[7] R. Baron, M.H. Young, J.K. Neeland, and O.J. Marsh, Appl. Phys. Lett. 30, 594 (1977).

[8] M.W. Scott, Appl. Phys. Lett. 32, 540 (1978).

[9] V. Swaminathan, J.E. Lang, P.M. Heminger, and S.R. Smith, Appl. Phys. Lett. 35, 184 (1979).

[10] M.C. Ohmer and J.E. Lang, Appl. Phys. Lett. 34, 750 (1979).

is described in Appendices C and D which are based on articles submitted for publication. The results are reviewed here. Two main conclusions have come out of this work on the X-center. The first is that:

- There is a class of X-center defects, with one X-center associated with each of the group IIIA elements in silicon.

With the indentification of the indium-X center as being an indium-related complex with an energy level about three-fourths that of the subsititutional indium,[5] we have been searching for similar defects in silicon doped with the other group IIIA acceptors. Optical absorption has shown similar defects in boron-doped,[11] aluminum-doped,[8] and gallium-doped,[11] silicon. The presence of these defects has helped to explain discrepancies sometimes observed in the activation energies measured for these dopants by Hall techniques and by optical absorption.[8,11] The indium-X level can also be seen in deep-level transient spectroscopy data. This is reported in Appendix B. A similar defect has now been identified in thallium-doped silicon, deep-level transient spectra (see Appendix D), completing the set for the group IIIA elements.

These X-centers are all electrically active acceptors having energies ∿80% of the corresponding group IIIA substitutional element's energy. The annealing behavior for the optically observed centers has been measured. None of the X-centers anneals out up to the melting point of silicon. The concentrations decrease with higher annealing temperature or increase with lower anealing temperatures. In all cases this can be done cyclically. The anealing kinetics for a number of samples with different doping levels can be fit to that expected for the reaction

[11] W. Scott and C.E. Jones, J. Appl. Phys. 50, 7258 (1979).

$$A + C \underset{\leftarrow}{\overset{K}{\rightarrow}} X \qquad (1)$$

where A is the group IIIA acceptor, C is carbon, and K is the equilibrium constant equal to

$$K = \frac{[X]}{[A]\,[C]} = K_o e^{-\Delta S/K_e \Delta H/KT} \qquad (2)$$

where ΔS is the change in the entropy and ΔH is the change in enthalpy for the reaction in Equation (1). These data are shown in Figure 8. The ΔH term is approximately equal to the X-center

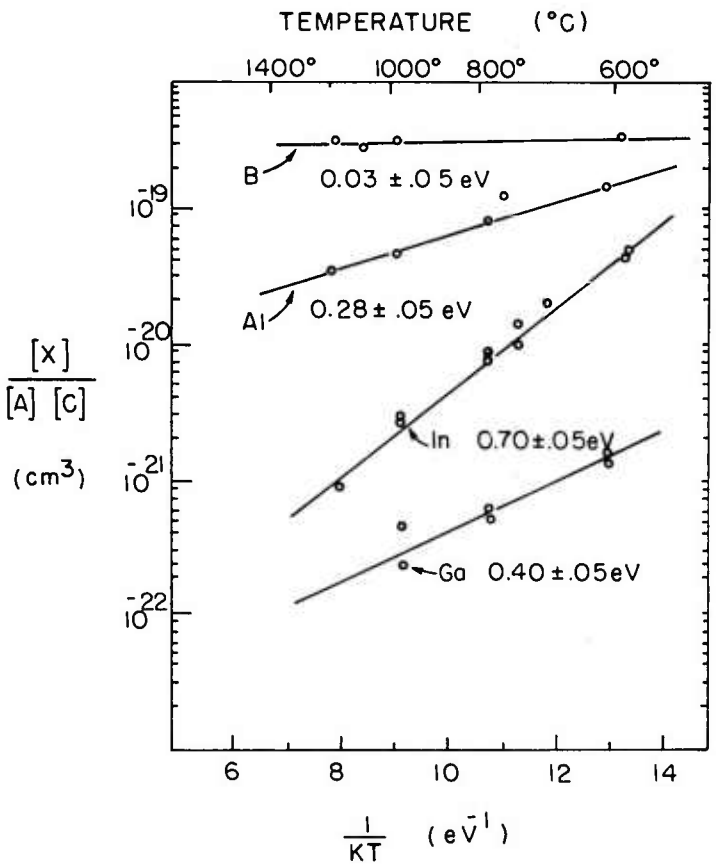

Figure 8. Normalized equilibrium concentrations of X-centers as a function of temperature. The quantity (X)/(A)(C) is equal to the equilibrium constant for the reactions $A + C \underset{\leftarrow}{\overset{K}{\rightarrow}} X$.

binding energy and these have been measured as being ~0.03 eV for boron-X, 0.28 eV for aluminum-X, 0.40 eV for gallium-X, and 0.70 eV for indium-X. The properties of the X-centers are listed in Table 1.

TABLE 1. X-CENTER PROPERTIES

Dopant	E(X) (meV)	E(ACC) Substitutional Dopant (meV)	E(X)/E(ACC)	[X]/[ACC] Pulled Si	E_A (eV)
B	37.1	44.3	0.84	10^{-2}	0.03
Al	56.3	68.5	0.82	10^{-2}-10^{-3}	0.28
Ga	57.0	72.7	0.79	10^{-4}-10^{-5}	0.40
In	112.8	156.0	0.72	10^{-2}-10^{-4}	0.70
Tl	180.0	246.0	0.73	10^{-2}	-

It is the similar X to substitutional acceptor energies, the similar annealing properties, and the defect binding energies which go in a smooth progression which have shown that these defects are members of a class of complexes of the same type.

The second result of the X-center studies is that:

- The model which best fits the X-center data is that of the nearest-neighbor carbon-acceptor pair.

The In-X-center concentration has been found to vary linearly with both indium and carbon. No dependences can be found on oxygen or boron; and aluminum and thallium were not detected. These data are presented in Appendix D. The aluminum-X stress symmetry has been determined to be that of a [111] trigonal defect (see Appen-

dix C). This rules out both substitutional single-atom defects and distant pairs. The high-temperature stability and the cyclic annealability of the X-centers is not consistent with interstitial or vacancy-related defects. All of the known interstitial or vacancy-related defects anneal within a few hundred degrees of room temperature and they cannot be cyclically annealed. The high-temperature stability and cyclic annealing do fit a model of a complex formed with substitutional atoms. The [111] symmetry and the dependence on a single carbon and a single indium fit the nearest-neighbor substitutional carbon-acceptor pair model. This model is shown in Figure 9.

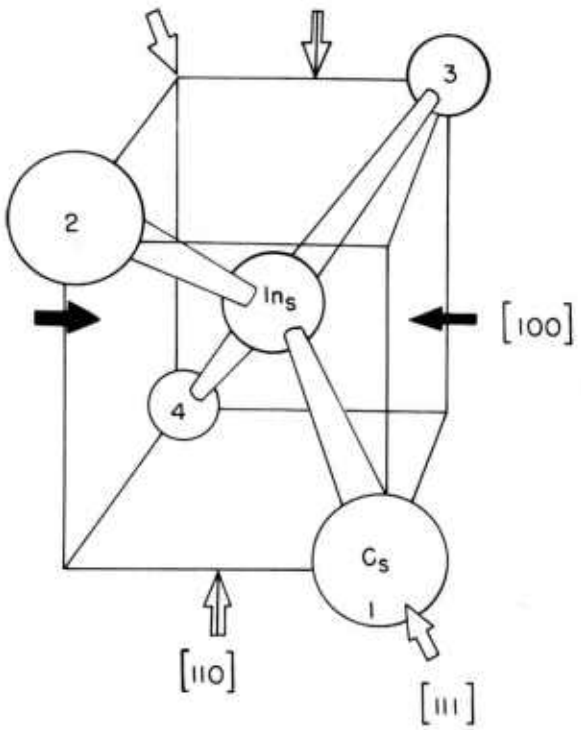

Figure 9. Model of the X-center as being a nearest-neighbor substitutional carbon-acceptor pair. Sites 1, 2,3, and 4 are different configurations for the carbon.

SECTION 4
TRAPPING STUDIES

Deep-level transient spectroscopy[12,13] has been used to investigate the trapping parameters of defects in indium-doped silicon. The In-X-center substitutional indium and two deeper hole traps at E_v + 0.31 eV and E_v + 0.45 eV were studied. The energy levels, concentrations emission rates, and capture cross sections were determined for these defects. These data were formalized and submitted for publication and are presented in Appendix B. This work is briefly reviewed below.

Deep-level transient spectroscopy (DLTS) measures the capacitance of a reverse-biased diode. This capacitance depends on the charge in the depletion region of the diode. In reverse bias, most of the traps in this region are empty. Short voltages pulses are used to bring carriers into this region, where some of the carriers are trapped. After the pulse, the trapped carriers are thermally emitted, producing a transient in the measured capacitance. Electronic processing is used to decompose the transient into a spectral form, with a peak for each defect displayed as a function of temperature and emission rate. The size of the peak can be related to the trap density, the change in the emission rate as a function of temperature gives the trap activation energy, and the peak amplitude as a function of the filling pulse time is related to the trap capture cross section. A DLTS spectrum for indium-doped silicon is shown in Figure 10.

---

[12] D.V. Lang, J. Appl. Phys. 45, 3014, 3023 (1974).

[13] G.L. Miller, D.V. Lang, and L.C. Kimmerling, in Ann. Rev. of Nat. Sci. 1, 377 (1977).

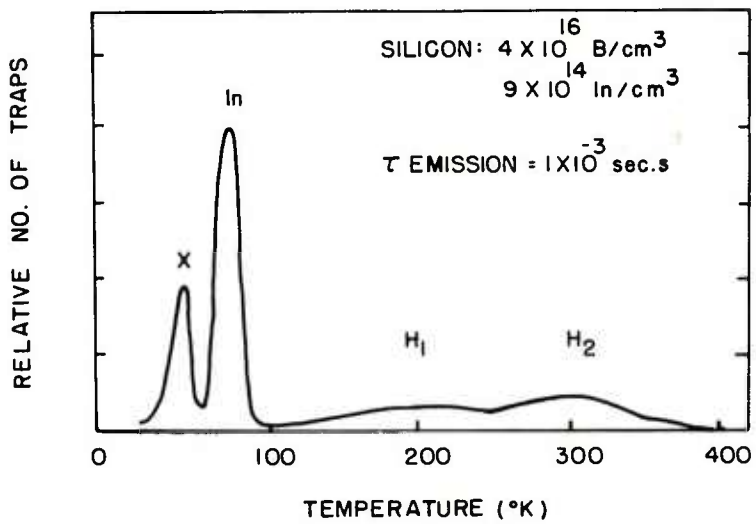

Figure 10. DLTS spectrum for indium-doped silicon.

Electric fields have been found to lower the thermal activation energies and thus increase the emission rates for both the In-X center and substitutional indium. These effects were measured experimentally as a function of electric field and temperature. The data could be fit by a theoretical model developed by Hartke[14] but the theoretical correction to zero field gives DLTS trap activation energies lower than optically measured energies.

The nitrogen temperature capture coefficients were measured as being 7.6×10^{-7} cm^3/sec for indium and 1.5×10^{-7} cm^3/sec for the In-X center. The temperature dependence for these coefficients was estimated as being 0.03 ± 0.02 eV for indium and 0.006 ± 0.005 eV for the In-X center. The capture coefficients for the hole

---

[14] J.L. Hartke, J. Appl. Phys. 39, 4871 (1968).

traps at E_v + 0.31 eV and E_v + 0.45 eV were estimated as being 2 x 10^{-9} cm^3/sec and 1.2 x 10^{-8} cm^3/sec, respectively.

Figure 11 shows the emission rates as a function of temperature for these traps and their effective thermal activation energies. The indium and indium-X-center data are also shown corrected to zero field by Hartke's[14] theory.

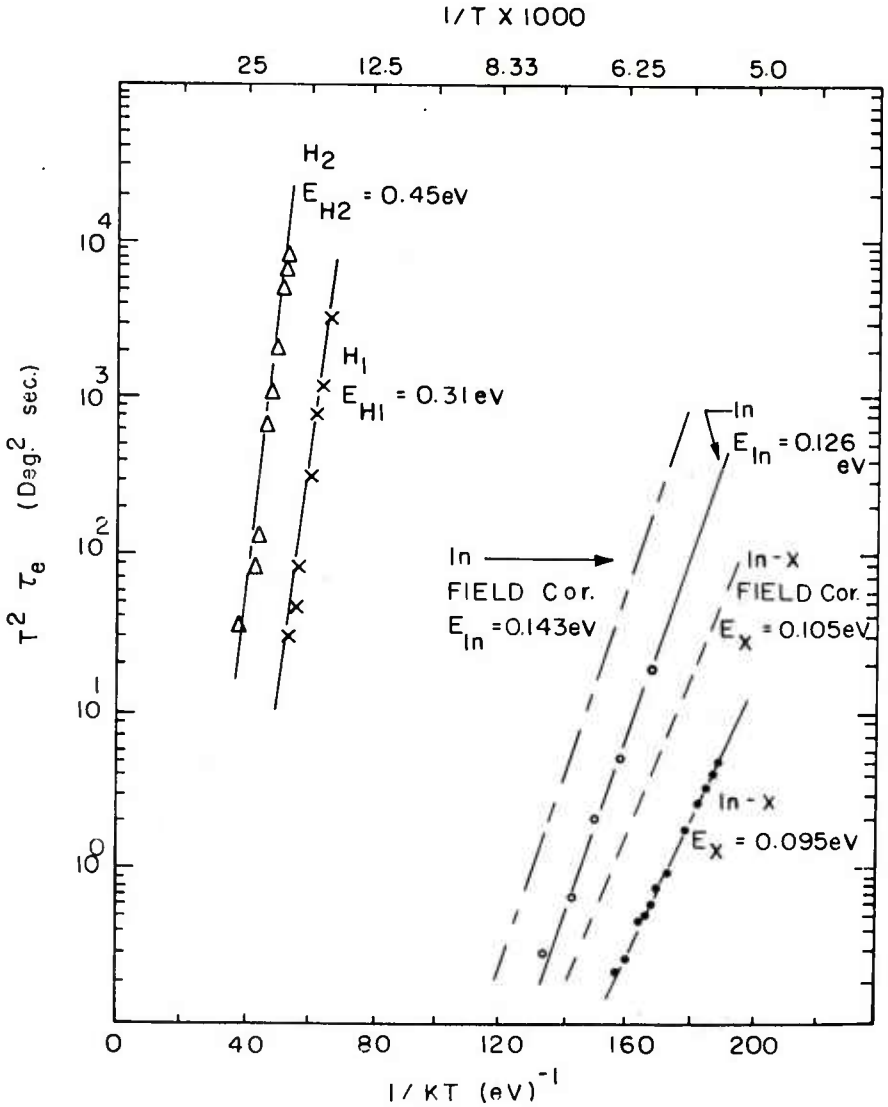

Figure 11. The emission rate of traps observed in indium-doped silicon as a function of temperature. The indium and indium-X center data are also shown corrected to zero field by the theory developed by Hartke.[14]

SECTION 5
ACCOMPLISHMENTS AND CONCLUSIONS

Significant progress was made in developing the solution-growth technique, in identifying and eliminating the In-X center, and in measuring the trapping parameters of defects in indium-doped silicon.

Solution growths provided a means of obtaining high indium concentrations with good uniformity and with low-boron and X-center concentrations. The technique can be used for volume production adequate for projected detector needs. The crystal quality improved greatly over the period of the contract but 2-inch-diameter wafers still show some voids or polycrystalline areas.

The X-centers were identified as a class of defects present in silicon doped with any of the group IIIA acceptors. The energy levels, optical spectrum, annealing properties, and binding energies were determined for most of these centers. The X-centers were found to depend on carbon and the best model for the defect was identified as a nearest-neighbor carbon-acceptor pair. The X-center can be eliminated by using low-carbon silicon starting materials in the solution growth technique.

The trapping parameters for substitutional indium, the indium-X center, and two deeper indium-related traps were measured by deep-level transient spectroscopy techniques near the detector operating temperatures. The electric field effects were determined for indium and the indium-X centers, and capture coefficients were measured for all four of the traps.

The specific accomplishments of the study effort are listed as follows:

- The solubility of indium in silicon was determined as a function of temperature.
- Indium-doped silicon was grown by solution growth at the maximum of the indium solubility curve at 1.6×10^{18} In/cm^3 with less than 10^8 electrically active boron atoms/cm^3.
- The X-centers were eliminated (less than 5×10^{13} In-X/cm^3 by optical measurements, less than 10^8 electrically active by Hall).
- X-centers related to boron, aluminum, gallium, indium, and thallium were identified.
- The X-center concentrations as a function of acceptor concentration, carbon concentration, and annealing temperature were determined.
- X-center binding energies of 0.03, 0.28, 0.40, and 0.70 eV were measured for the boron, aluminum, gallium, and indium-X centers, respectively.
- The nearest-neighbor carbon-acceptor pair model was identified as the best model for the X-center complex.
- The trapping parameters for indium, the indium-X center, and two indium-related hole traps at E_v + 0.31 eV and E_v + 0.45 eV were determined.

REFERENCES

1. W. Scott and R. J. Hager, J. Electron. Mater. 8, 581 (1979).

2. H. J. Hrostowski and R. H. Kaiser, J. Phys. Chem. Solids 9, 214 (1958).

3. A. R. Bean and R. C. Newman, J. Phys. Chem. Solids 32, 1211 (1971)

4. R. C. Newman and J. B. Willis, J. Phys. Chem. Solids 26, 373 (1964)

5. R. Baron, J. P. Baukus, S. D. Allen, T. C. McGill, M. H. Young, H. Kimura, H. V. Winston, and O. J. Marsh, Appl. Phys. Lett. 34, 257 (1979).

6. C. E. Jones, D. E. Schafer, W. Scott and R. Hager, Bull. Am. Phys. Soc. 24, 276 (1979).

7. R. Baron, M. H. Young, J. K. Neeland and O. J. Marsh, Appl. Phys. Lett. 30, 594 (1977).

8. M. W. Scott, Appl. Phys. Lett. 32, 540 (1978).

9. V. Swaminathan, J. E. Lang, P. M. Heminger and S. R. Smith, Appl. Phys. Lett. 35, 184 (1979).

10. M. C. Ohmer and J. E. Lang, Appl. Phys. Lett. 34, 750 (1979).

11. W. Scott and C. E. Jones, J. Appl. Phys. 50, 7258 (1979).

12. D. V. Lang, J. Appl. Phys. 45, 3014, 3023 (1974).

13. G. L. Miller, D. V. Lang and L. C. Kimmerling, in Ann. Rev. of Nat. Sci. 1, 377 (1977).

14. J. L. Hartke, J. Appl. Phys. 39, 4871 (1968).

APPENDIX A
SOLUTION GROWTH OF INDIUM-DOPED SILICON*

ABSTRACT

Indium-doped silicon has been grown from indium-rich solutions using a gradient-transport solution growth process. The growth temperatures were varied from 950^{o} to 1300^{o}C to determine the solubility limits of indium in silicon. The maximum indium concentration obtained was 1.6 x $10^{18}/cm^{3}$ at a growth temperature of 1300^{o}C but indications are that the maximum solubility is 2.5 x $10^{18}/cm^{3}$. The oxygen and carbon concentrations increased with the increased growth temperatures, suggesting solubility-limited values. The shallower, indium-X defect also increased with growth temperature, but could be reduced below 2 x $10^{13}/cm^{3}$ by removing carbon from the crystals. The uniformity in indium doping was typically ±5% across the crystal diameter.

INTRODUCTION

Indium-doped silicon is being investigated as an extrinsic photoconductor material for use in the 3- to 5-μm infrared region. A number of problems have arisen with this material, notably with

---

*This work was sponsored in part by the Defense Advanced Research Projects Agency under Order No. 3211, monitored by NV&EOL under Contract No. DAAK-77-C-0194. The authors are Walter M. Scott, Colin E. Jones, and Robert J. Hager, Honeywell Corporate Material Sciences Center, Bloomington, MN. The paper was presented at the June 1979 IRIS Specialty Meeting on Infrared Detectors, Minneapolis, MN.

the low indium concentration obtained by standard growth methods and the presence of a shallower defect level associated with the indium. Czochralski-grown crystals have been limited to a maximum indium concentration of $3.8 \times 10^{17}/cm^3$ before microprecipitates are observed in the crystals.[A-1] The concentration of indium in float-zone-grown crystals is generally even lower than this because of the low segregation coefficient of indium.[A-2] The limits to the indium solubility in silicon have not been previously reported in the literature to determine what improvement could be made in the doping levels in silicon crystals.

A shallower defect center associated with both indium and carbon,[A-3, A-4] and labeled as indium-X, has been observed in indium-doped silicon. Baron et al.[A-5] observed this defect in Hall coefficient measurements at an energy of about 0.11 eV. Subsequently, Scott[A-6] observed the infrared spectrum of an effective-mass-like

---

A-1 E.L. Kern, R. Baron, R.H. Walker, D.J. O'Connor, and O.J. Marsh, J. Electron. Mater. 4, 1249 (1975).

A-2 W.R. Runyan, Silicon Semiconductor Technology, (McGraw Hill, New York, 1965).

A-3 C.E. Jones, D. Schafer, W. Scott, and R.J. Hager, Bull. Am. Phys. Soc. 24, 276 (1979), and these proceedings.

A-4 R. Baron, J.P. Bankus, S.D. Allen, T.C. McGill, M.H. Young, H. Kimura, H.V. Winston, and O.J. Marsh, Appl. Phys. Lett. 34, 257 (1979).

A-5 R. Baron, M.H. Young, J.K. Neeland, and O.J. Marsh, Appl. Phys. Lett. 30, 594 (1977).

A-6 W. Scott, Appl. Phys. Lett. 32, 540, (1978).

defect associated with indium at an energy of 0.1128 eV. The origin of the defect is uncertain at this time, but it is known to exist in both Czochralski and float-zone-grown crystals.

Solution growth techniques such as gradient-transport solution growth and liquid-phase epitaxy (LPE) have been used to grow group III-V compounds for many years, but these techniques have not been extensively applied to silicon. Pfann[A-7] described the use of temperature-gradient zone melting as a means of producing large-area p-n junctions in silicon, and, more recently, Cline and Anthony[A-8] have explored the migration of liquid-metal droplets in silicon. An important feature of these solution growth procedures is that the crystals are grown below the melting point of silicon, so the retrograde solubility of the impurities can be used to obtain very heavily doped crystals.

In this paper we report the results of gradient-transport solution-growth of silicon from indium solutions. The growths were done as a function of temperature to determine the solubility limits of indium in silicon. Growth rates of about 4 mm/day have been achieved and crystals doped up to 1.6 x $10^{18}/cm^3$ with indium have been produced by this technique. Single crystals in excess of 2.5 cm diameter have been produced with a doping uniformity of ±5%. Indium-X concentrations <5 x $10^{13}/cm^3$ have been obtained in crystals with 7 x 10^{17} In/cm^3.

[A-7] W.G. Pfann, Solid State Physics, Volume 4, F. Seitz and D. Turnbull, Eds. (Academic Press, N.Y., 1957) pp. 424.

[A-8] H.E. Cline and T.R. Anthony, J. Appl. Phys. 48, 2196 (1977), and the references therein.

CRYSTAL GROWTH PROCEDURES

Solubility Limits

A schematic illustration of the growth apparatus used to determine the solubility limit of indium is shown in Figure A-1. It consists of a flat-bottomed quartz tube in which was placed a single-crystal silicon seed, high-purity (6N) indium, and a high-purity silicon source in the relative positions shown in Figure A-1. A tubular quartz spacer was used to hold the silicon seed in place during the growth and prevent it from buoying to the surface of the liquid indium. The apparatus was placed in a furnace with uniform temperature profile and a temperature difference established between the silicon source and the substrate by a flow of air directed at the flat bottom of the ampoule. The temperature of the silicon seed is maintained approximately 50°C colder than the source temperature throughout the growth process.

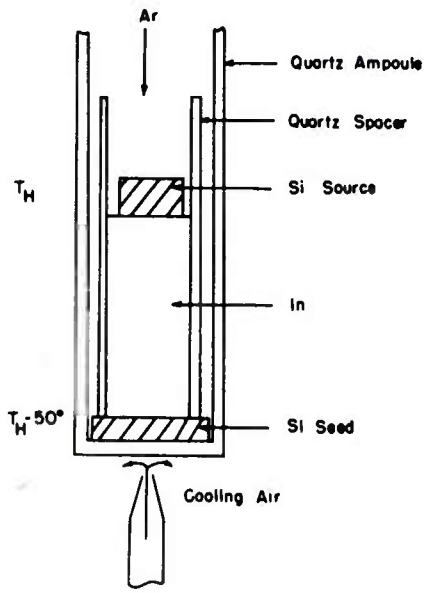

Figure A-1. Schematic of the solution-growth apparatus.

The temperature difference between source and substrate was determined by calibrating the system using a Pt-Pt (13% Rh) thermocouple. The capsule was loaded with the usual amount of indium and a standard substrate. A quartz tube containing the thermocouple was inserted into the indium to be in contact with the substrate. The apparatus was brought up to temperature, and the temperature profile in the indium measured. The profile was measured with the gas flow rate a parameter in order to be able to set any desired temperature difference across the indium column. The repeatability of the temperature setting was estaimated at about $\pm 5^{o}$C from these calibration measurements.

Large-Area Growth

The growth configuration was modified[A-9] to grow larger-area crystals (up to 2-inch diameter). The length of indium column was reduced to about 0.05 cm by containing the solution in a well formed in the silicon substrate. Other details of the growth remained basically the same as shown in Figure A-1.

RESULTS AND DISCUSSION

Electrical Evaluation

All the crystals were characterized by Hall coefficient versus temperature measurements on at least one sample from each growth taken from the single-crystal portion of the growth. A major problem in the electrical transport measurements of deep impurities in silicon is in determining the total concentration of

---

[A-9] C.E. Jones, D.E. Schafer, M.W. Scott, and R.J. Hager, "Studies of Indium-Doped Silicon," Semiannual Report, NVL Contract No. DAAK70-77-C-0194, 31 July 1978.

the impurities. Hall measurements provide a measure of the free-carrier concentration, but if all the impurities are not ionized at the temperature of measurement, then a specific model must be adopted before the total impurity concentration can be determined.

The free-carrier concentration, p, was determined from the Hall coefficient, R_H, from the expression

$$p = \frac{r}{eR_H}$$

where the scattering factor, r, was assumed to be unity. The carrier concentration is also determined from the charge neutrality condition

$$p + N_D^+ = N_A^-$$

where N_D is the concentration of ionized donors, and N_A^- is the concentration of ionized acceptors. By assuming a low concentration of compensating donors and a high concentration of indium relative to any other acceptor, this can be rewritten as

$$p = \frac{N_{In}}{1 + g \exp \frac{E_i - E_F}{KT}} \qquad \text{(A-1)}$$

where N_{In} is the total indium concentration, g is the ground-state degeneracy, E_i is the indium ionization energy, and E_F is the Fermi energy. In this expression the effects of the indium-excited states have been ignored, and only the ground state considered.

The hole concentration is also determined from the usual expression for nondegenerate bands

$$p = \frac{N_v}{1 + \exp\frac{E_F}{KT}} \qquad \text{(A-2)}$$

where N_v is the effective density of states in the valence band.

Combining Equations (A-1) and (A-2) gives the hole concentration as a function of the total indium concentration.

The values of the various parameters used in the calculation are the following:

$N_v = 4.8296 \times 10^{15} \, (m^*_h/m_o T)^{3/2}$

$m^*_m = 0.81$ at 300K (ref. A-10)

$E_i = 0.155$ eV

$g = 4$

The properties of the various crystals are summarized in Table A-1. The 300K electrical properties are listed along with the growth temperature and the calculated indium concentration. The boron concentration observed in the crystals is also listed in Table A-1, and was obtained from the exhaustion plateau observed in the Hall coefficient versus reciprocal temperature plot. The cases where no boron concentration is listed are those where the Hall coefficient versus reciprocal temperature curve did not have a boron exhaustion plateau.

A-10 H.D. Barber, Solid State Elect. 10, 1039 (1967).

TABLE A-1. SUMMARY OF ELECTRICAL EVALUATIONS

Crystal No.	Growth Temp (^{o}C)	$R_H(300)$ (cm^3/C)	$\rho(300)$ (Ω-cm)	Indium (cm^{-3})	Boron (cm^{-3})
1	946	620.0	2.17	1.8×10^{16}	
2	1005	281.0	1.28	6.0×10^{16}	
3	1008	317.0	1.03	5.2×10^{16}	1.0×10^{14}
4	1056	169.0	0.60	1.5×10^{17}	2.0×10^{15}
5	1056	198.0	0.74	1.1×10^{17}	
6	1056	213.0	0.75	1.0×10^{17}	5.0×10^{14}
7	1100	122.0	0.44	2.8×10^{17}	1.5×10^{15}
8	1150	87.5	0.36	5.1×10^{17}	1.0×10^{15}
9	1150	79.0	0.32	5.2×10^{17}	
10	1150	75.0	0.32	6.8×10^{17}	
11	1200	62.4	0.24	1.0×10^{18}	6.3×10^{15}
12	1200	57.0	0.26	1.1×10^{18}	
13	1250	52.5	0.26	1.4×10^{18}	
14	1300	45.5	0.24	1.6×10^{18}	
15	1300	45.0	0.21	1.7×10^{18}	

Recently, Sclar[A-11] published an analysis relating the 300K resistivity of silicon to the concentration of deep impurities in the crystal. The calculation takes into account the variation in mobility with free-carrier concentration and the usual mass-action equation to calculate the free-carrier concentration. His curve of 300K resistivity versus indium concentration is reproduced in Figure A-2 along with the values obtained here. As is obvious from the figure, the procedure used here agrees well with Sclar's calculated curve.

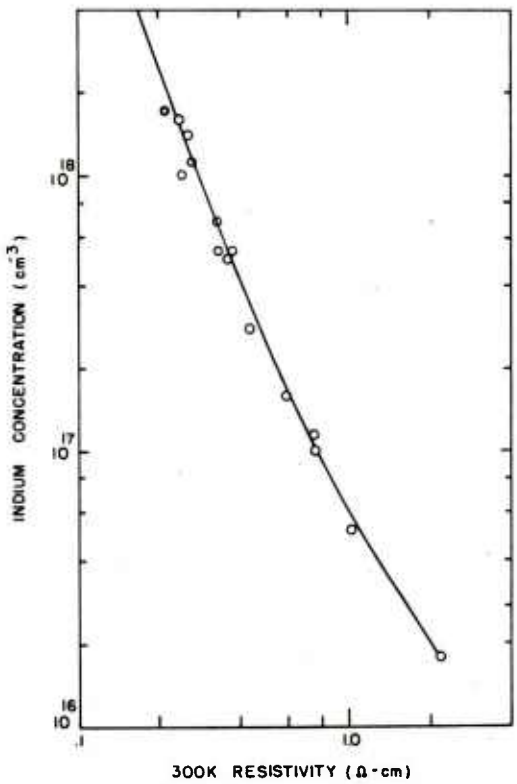

Figure A-2. Room temperature resistivity of indium-doped silicon as a function of the indium concentration. The circles are the measured values and the solid curve is taken from the calculations of Sclar (ref. A-11).

A-11 N. Sclar, IEEE Trans. Electron Devices ED-24, 709 (1977).

Solubility Limit

The indium concentration in the solution-grown crystals is shown in Figure A-3 as a function of the growth temperature. The maximum value of indium obtained in our growths has been $1.6 \times 10^{18}/cm^3$ at $1300^{o}C$. Higher growth temperatures were not attempted because of furnace limitations and problems with the quartz ampoules at higher temperatures.

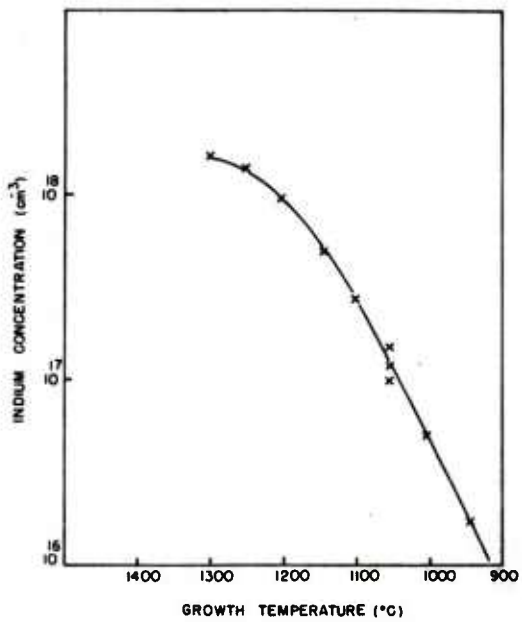

Figure A-3. Measured indium concentrations in solution-grown crystals at various growth temperatures.

Hall[A-12] has suggested that the distribution coefficient, k, of a solute having a low solid solubility should have a temperature dependence given by an equation of the type log k = B - A/T, where

---

[A-12] R.N. Hall, J. Phys. Chem. Solids 3, 63 (1957)

A and B are constants, and T is the absolute temperature. The values for distribution coefficient which we have obtained are shown in Figure A-4, and as is evident, they correspond to this type of relationship. The distribution coefficient for indium at the silicon melting point, k_o, is estimated to be 2.5×10^{-4} from our data. This is significantly lower than the value of 4×10^{-4} usually used for indium.[A-13] It was pointed out that this simple

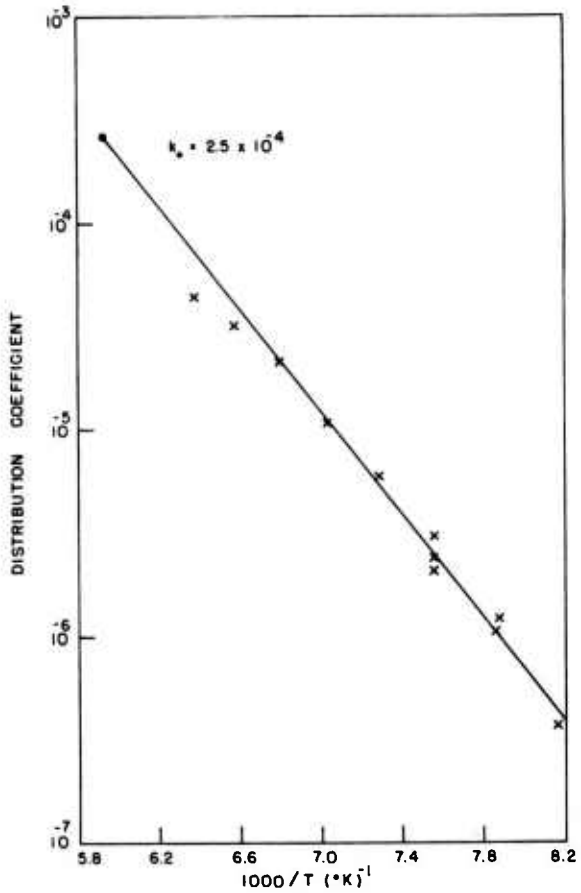

Figure A-4. Distribution coefficient, k, of indium in silicon as a function of reciprocal temperature. The distribution coefficient at the melting point, k_o, is 2.5×10^{-4}.

[A-13] F.A. Trumbore, Bell. Syst. Tech. J. 39, 205 (1960).

equation does not necessarily describe the temperature dependence of the distribution coefficient but empirically it has been found for a number of impurities in silicon and germanium. The fact that most of the data in Figure A-4 lie on a straight line would suggest that this relation applies to indium in silicon. In this case the crystals at the upper two temperatures may have been undersaturated. The solubility maximum estimated from the straight line is about 2.5 x $10^{18}/cm^3$, rather than the 1.6 x $10^{18}/cm^3$ which we have obtained.

Doping Uniformity

A major concern in producing material for focal planes is the uniformity of doping. This has been determined on solution-grown crystals using spreading resistance measurements, and the results are shown in Figure A-5 along with the results from Czochralski and float-zone indium-doped material. The solution-grown crystal is uniform to ±5%, or better. The Czochralski growth shows a

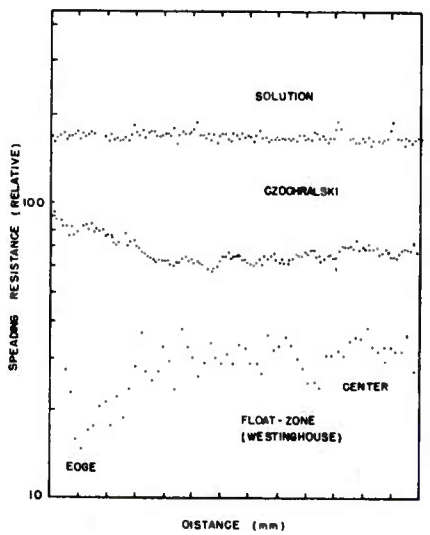

Figure A-5. Spreading resistance across a solution-grown crystal compared with spreading resistance across Czochralski and float-zone-grown crystals.

drift in doping level from the center to the edge along with some striations. Total variations across the entire crystal are about ±20%. Larger striations are also seen in the float-zone material, with a total variation from center to edge well in excess of ±20%.

Growth Rates

The growth rate can be computed from the standard expression:

$$J = -D \frac{\partial C_{Si}}{\partial x}\Big|_{x = \text{substrate}}$$

where J is the particle current in moles/cm^{2}sec, and C_{Si} is the silicon concentration in moles/cm^3. The growth rate at the substrate is given by

$$V(\text{cm/sec}) = J \frac{M_{Si}}{\rho_{Si}}$$

where M_{Si} is the molar weight of silicon, and P_{Si} is the density of the silicon crystal. In steady state the growth rate can be written

$$V(\text{cm/sec}) = D \frac{M_{Si}}{\rho_{Si}} \frac{(C_o - C_1)}{1}$$

since the concentration gradient will be constant throughout the solution. To characterize the growth process completely, we need to know only two parameters: (a) the diffusion coefficient, D, and (b) the silicon-indium liquidus (to obtain C_{Si}). The diffusion coefficient in liquid indium has been measured up to a

temperature of 1000°C, and is given by the expression[A-14]

$$D = 3 \times 10^{-4} \exp - \frac{2.5 \text{ kcal/mole}}{RT} \text{ cm}^2/\text{sec}$$

where R is the gas constant. The silicon-indium liquidus values used were obtained from the data of Thurmond and Kowalchick.[A-15]

The predicted growth rate in units of mm/day is shown in Figure A-6 as a function of the growth temperature. For a given temper-

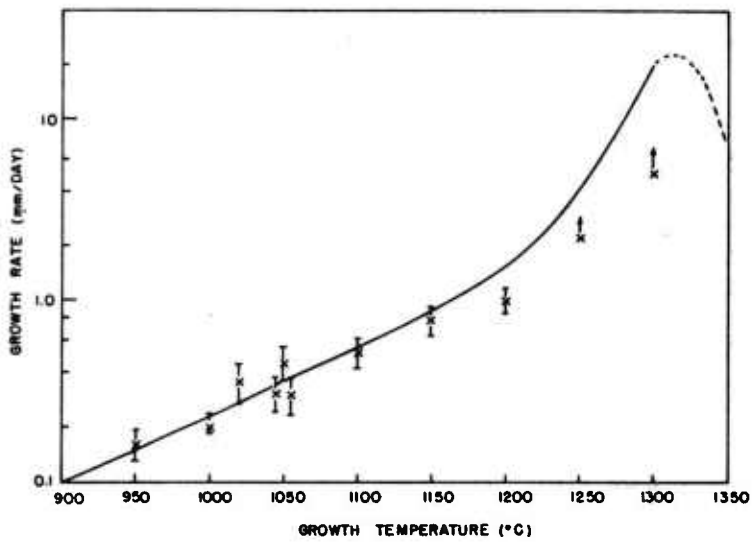

Figure A-6. Growth rates for diffusion through a 3-cm column of indium with a 50°C temperature difference from source to substrate. The solid line is calculated from a one-dimensional diffusion model.

A-14 The data for diffusion in liquids are summarized in: N.H. Nachtreib, Adv. Phys. 16, 309 (1967).

A-15 C.D. Thurmond and M. Kowalchick, Bell Syst. Tech. J. 39, 169 (1960)

ature gradient, the growth rate increases dramatically with increasing growth temperature up to about 1300°C because of the increased solubility of silicon in indium at the higher temperature. The slope of the liquidus, $\frac{dC}{dT}$, has a maximum near 1300°C, accounting for the maximum in growth rate. The maximum rate is expected to be in the 10 to 20-mm/day range under these growth conditions.

The measured growth rates are also shown in Figure A-6. In general, the measured values agree very well with calculated values, indicating that reasonable values of the parameters were used in the calculation. The errors assigned to the growth rates result from an uncertainty in the degree of melt-back of the substrate and also from an uncertainty in the amount of growth. On cooldown, material would precipitate on the solution-grown crystal, giving an uncertainty as to the length of the crystal. Some error also occurs in determining the length of time of the growth, since it requires some time for steady state to be reached. The growths were typically about 10 days, so this is judged to be only a small error. This uncertainty in growth rate is typically ±20% so still provides a sufficiently accurate comparison with the simple one-dimensional diffusion model.

Optical Evaluation

Optical absorption measurements were used to monitor the concentration of oxygen, carbon, boron, indium and the shallower indium-X defect in the crystals, and also determine if other, shallower impurities are introduced into the crystals by the solution growth process. The absorption spectrum of one of our solution-grown indium-doped silicon crystals in the 400- to 2000-cm^{-1} region is shown in Figure A-7. The principal indium lines are

marked as lines 1, 2, 3, and 4, to be consistent with the numbering system used by Onton et al.[A-16] for acceptors in silicon. The largest absorption line observed at 1134 cm^{-1} is due to oxygen. The broad absorption bands in the 400- to 1000-cm^{-1} region are lattice absorptions, and the broad absorption starting at 1200 cm^{-1} is due to ionization of the indium centers. The region of interest for monitoring the indium-X defect is between 700 and 1000 cm^{-1}, where there is appreciable lattice absorption. The lattice absorption bands were subtracted from the absorption spectrum as described earlier to observe these defect absorption lines.[A-17]

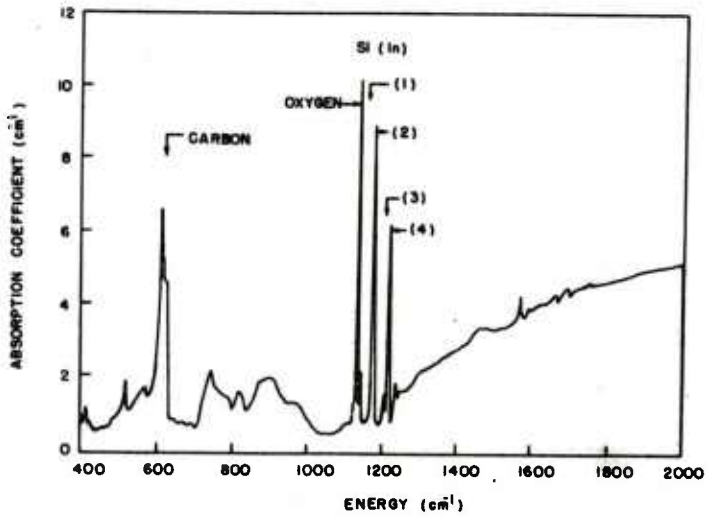

Figure A-7. Infrared absorption spectrum of silicon containing 1×10^{17} indium/cm^3. The major indium lines are numbered 1 through 4, and the absorption lines due to oxygen and carbon are also indicated.

A-16 A. Onton, P. Fisher, and A.K. Ramdas, Phys. Rev. 163, 686 (1967).

A-17 M.W. Scott, C.E. Jones, and R.J. Hager, "Studies of Indium-Doped Silicon," Semiannual Report, NVL Contract No. DAAK70-77-C-0194, 31 Jan 1978.

The shallower indium-X defect was previously shown to have an effective-mass-like absorption spectrum with the principal absorption lines at 800, 830, and 873 cm^{-1}.[A-6] The integrated intensity of the strongest line at 830 cm^{-1} was used to determine the concentration of this defect. The concentration of the indium-X defect in the as-grown crystals is listed in Table A-2. Since it is known[3,4] that the concentration of the indium-X defects varies with annealing temperature, the values in Table A-2 only represent the as-grown conditions. An important result to note in Table A-2 is the fact that the indium-X concentration can be made negligibly small in crystals where the carbon concentration is kept low, as in crystal 9.

TABLE A-2. SUMMARY OF CRYSTAL PROPERTIES FROM OPTICAL DATA

Crystal	Growth Temp. (°C)	[In]	[X]	[O]	[C]	[B]
3	1008	1.3×10^{16}	$<1.0 \times 10^{13}$	4.5×10^{16}	1.3×10^{16}	1.4×10^{14}
4	1056	1.7×10^{17}	$<4.5 \times 10^{13}$	8.0×10^{16}	3.75×10^{16}	2.35×10^{15}
6	1056	1.76×10^{16}	$<1.0 \times 10^{13}$	7.7×10^{16}	2.35×10^{16}	5.0×10^{14}
7	1100	4.2×10^{17}	4.5×10^{14}	1.7×10^{17}	1.0×10^{17}	5.5×10^{15}
8	1150	6.9×10^{17}	3.4×10^{14}	2.8×10^{17}	1.2×10^{17}	1.2×10^{16}
9	1150	5.24×10^{17}	$<9.0 \times 10^{12}$	2.13×10^{17}	$<3.3 \times 10^{15}$	$<2.5 \times 10^{13}$
13	1250	8.0×10^{17}	1.9×10^{15}	4.5×10^{17}	2.2×10^{17}	2.7×10^{14}
14	1300	9.5×10^{17}	2.2×10^{15}	6.2×10^{17}	2.0×10^{17}	$<1.0 \times 10^{13}$
16	1150	5.5×10^{17}	5.0×10^{13}	5.0×10^{15}	1.0×10^{17}	$<5.0 \times 10^{13}$

The concentrations of both oxygen and carbon were also measured in the crystals as a measure of crystal purity. The oxygen concentration was determined from the peak intensity of the 1134-cm^{-1} line at 8K, and the carbon concentration was determined from the intensity of the 606-cm^{-1} line. The conversion from peak absorption coefficient to doping level is taken from the literature using the room temperature values reported by Gaff et al.[A-18] for oxygen and by Newman and Willis[A-19] for carbon. The absorption coefficient for these lines was measured as a function of temperature to determine the appropriate conversion at 8K. The values used for the 8K measurements were 3.1 x $10^{16}/cm^3/cm^{-1}$ for oxygen, and 6.7 x $10^{16}/cm^3/cm^{-1}$ for carbon.

The oxygen and carbon concentrations are shown in Figure A-8 as a function of the growth temperature. The oxygen concentrations of four Czochralski-grown crystals are also shown in Figure A-8 for comparison. Both the oxygen and carbon concentrations increase with increasing growth temperatures, suggesting solubility-limited values. The oxygen concentrations obtained here agree reasonably well with the solubilities measured by Hrostowski and Kaiser.[A-20] In the case of carbon, there is significant scatter in the data, which could mean that all the crystals are not at the solubility limit at the particular growth temperature.

[A-18] K. Graff, E. Grallath, S. Ades, G. Goldback, and G. Tolg, Solid State Elect. 16, 887 (1973).

[A-19] R.C. Newman and J.B. Willis, J. Phys. Chem. Solids 26, 373 (1965).

[A-20] H.J. Hrostowski and R.H. Kaiser, Phys. Rev. 107, 969 (1957)

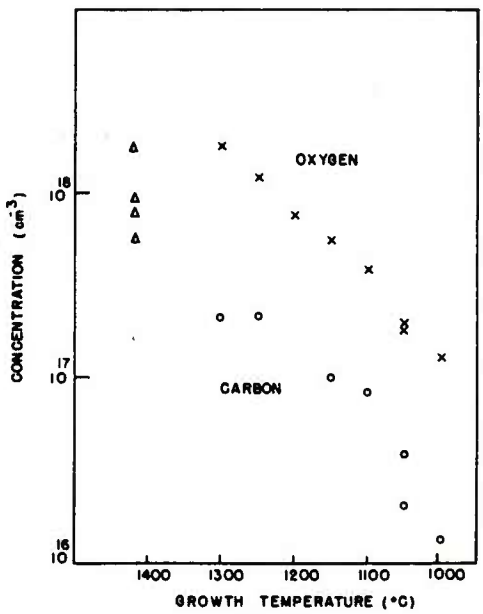

Figure A-8. The oxygen and carbon concentrations found in indium-doped silicon crystals. The oxygen concentration in solution-grown crystals is shown as X's and in Czochralski crystals as Δ's. The carbon concentration in solution-grown crystals is shown as O's.

SUMMARY

We have demonstrated that indium-doped silicon, doped at the solubility limits of indium, can be grown from an indium solution using the gradient-transport process. Growth rates of 4 mm/day have been obtained, making the technique feasible as a method of producing heavily doped silicon wafers in low-volume applications. The solubility limit of indium has, for the first time, been measured over the 950° to 1300°C temperature range. The maximum solubility obtained in the solution-grown crystals was $1.6 \times 10^{18} cm^3$, but the indications are that the maximum solubility

occurs at about 1300°C with a value of about $2.5 \times 10^{18}/cm^3$. Optical absorption measurements have verified that the concentration of the shallower indium-X defect is lower in the solution-grown crystals when the carbon concentration is kept low. Uniformity of the indium concentration has been shown to be ±5% across the crystal diameter, and the boron concentration has been at least equivalent to Czochralski crystals. The solution-growth, Czochralski-growth, and float-zone growth methods are compared in Table A-3.

TABLE A-3. COMPARISON OF GROWTH METHODS

Crystal	Solution Growth	Czochralski	Float Zone
$In(cm^{-3})$	10^{18}	$2 \text{ to } 3 \times 10^{17}$	1×10^{17}
$O(cm^{-3})$	(Solubility limit)	$\sim 10^{18}$	$< 10^{16}$
$C(cm^{-3})$	$\sim 10^{16}$	$> 10^{17}$	$\sim 10^{16}$
$B(cm^{-3})$	$< 5 \times 10^{13}$	$\sim 10^{14}$	$\sim 10^{12}$
$\Delta\rho/\rho$	±5%	±20%	>±20%

ACKNOWLEDGEMENTS

The authors would like to acknowledge the assistance of J.E. Sjerven making the optical measurements, and D.E. Schafer and J.L. Schmit for many helpful discussions.

REFERENCES

A-1. E.L. Kern, R. Baron, R.H. Walker, D.J. O'Connor, and O.J. Marsh, J. Electron. Mater. 4, 1249 (1975).

A-2. W.R. Runyan, Silicon Semiconductor Technology,(McGraw Hill, New York, 1965).

A-3. C.E. Jones, D. Schafer, W. Scott, and R.J. Hager, Bull. Am. Phys. Soc. 24, 276 (1979), and these proceedings.

A-4. R. Baron, J.P. Bankus, S.D. Allen, T.C. McGill, M.H. Young, H. Kimura, H.V. Winston, and O.J. Marsh, Appl. Phys. Lett. 34, 257 (1979).

A-5. R. Baron, M.H. Young, J.K. Neeland, and O.J. Marsh. Appl. Phys. Lett. 30, 594 (1977).

A-6. W. Scott, Appl. Phys. Lett. 32, 540, (1978).

A-7. W.G. Pfann, Solid State Physics, Volume 4, F. Seitz and D. Turnbull, Eds. (Academic Press, N.Y., 1957) pp. 424.

A-8. H.E. Cline and T.R. Anthony, J. Appl. Phys. 48, 2196 (1977), and the references therein.

A-9. C.E. Jones, D.E. Schafer, M.W. Scott, and R.J. Hager, "Studies of Indium-Doped Silicon," Semiannual Report, NVL Contract No. DAAK70-77-C-0194, 31 July 1978.

A-10. H.D. Barber, Solid State Elect. 10, 1039 (1967).

A-11. N. Sclar, IEEE Trans. Electron. Devices ED-24, 709 (1977).

A-12. R.N. Hall, J. Phys. Chem. Solids 3, 63 (1957).

A-13. F.A. Trumbore, Bell. Syst. Tech. J. 39, 205 (1960).

A-14. The data for diffusion in liquids is summarized in: N.H. Nachtreib, Adv. Phys. 16, 309 (1967).

A-15. C.D. Thurmond and M. Kowalchick, Bell Syst. Tech. J. 39, 169 (1960).

A-16. A. Onton, P. Fisher, and A.K. Ramdas, Phys. Rev. 163, 686 (1967).

A-17. M.W. Scott, C.E. Jones, and R.J. Hager, "Studies of Indium-Doped Silicon," Semiannual Report, NVL Contract No. DAAK-70-77-C-0194, 31 Jan 1978.

A-18. K. Graff, E. Grallath, S. Ades, G. Goldback, and G. Tolg, Solid State Elect. 16, 887 (1973).

A-19. R.C. Newman and J.B. Willis, J. Phys. Chem. Solids 26, 373 (1965).

A-20. H.J. Hrostowski and R.H. Kaiser, Phys. Rev. 107, 969 (1957)

APPENDIX B

DLTS STUDIES OF TRAPPING PARAMETERS FOR CENTERS IN INDIUM-DOPED SILICON*

ABSTRACT

Deep-level transient spectroscopy (DLTS) has been used to measure the low-temperature trapping parameters of defects in indium-doped silicon. Substitutional indium at E_v + 0.15 eV, the indium-X center at E_v + 0.11 eV, and two deeper indium-related centers at E_v + 0.31 eV and E_v + 0.45 eV were studied. Electric fields were found to lower the activation energies and increase the emission rates for the substitutional indium and the indium-X center. Theoretical models including the field effect on the barrier and thermally assisted tunneling were used to fit the data. The capture coefficients near liquid nitrogen temperature were estimated as being for substitutional indium, $C(In) = 7.6 \times 10^{-9}$ cm^3/sec exp (+0.031 eV/kT); for the indium-X center, $C(InX) = 7.7 \times 15^{-8}$ cm^3/sec exp (+0.006 eV/RT); for the E_v + 0.31 eV center, $C(H1) = 2 \times 10^{-9}$ cm^3/sec; and for the E_v + 0.45 eV center $C(H2) = 1.2 \times 10^{-8}$ cm^3/sec.

---

*Work done under DARPA Contract DAAK70-77-C-0194. The authors of this paper are Colin E. Jones and Gregory E. Johnson, Honeywell Corporate Material Sciences Center, Bloomington, MN. The paper was submitted to J. Appl. Phys. for publication.

INTRODUCTION

Silicon doped with indium is being studied as an infrared photodetector material in the 3-5 micron region. One of the problems with indium doping has been the formation of a shallow indium-related complex called the X-center.[B-1 - B-4] Holes thermally generated from these centers increase the background noise in indium-doped silicon detectors unless the system is cooled to around 45K to freeze out the X-centers.

In order to calculate the photodetector properties of indium-doped silicon, the trapping parameters for substitutional indium, the In-X center, and other defects common in this material must be known for temperatures in the 50K to 100K range. This paper describes the use of deep-level transient spectroscopy (DLTS) to measure the low-temperature trapping parameters of indium, the indium-X center at E_v + 0.11 eV, and two deeper hole traps at E_v + 0.31 eV and E_v + 0.45 eV.

B-1 R. Baron, M.H. Young, J.K. Neeland, and O.J. Marsh, Appl. Phys. Lett. 30, 594 (1977).

B-2 W. Scott, Appl. Phys. Lett. 32, 540 (1978).

B-3 R. Baron, J.P. Bankus, S.D. Allen, T.C. McGill, M.H. Young, H. Kimura, H.V. Winston, and O.J. Marsh, J. Appl. Phys. Lett. 34, 257 (1979)

B-4 C.E. Jones, D.E. Schafer, W. Scott, and R. Hager, Bull. Am. Phys. Soc. 24, 276 (1979) BL14, and IRIS Speca.

EXPERIMENTAL

Deep-level transient spectroscopy[B-5 - B-7] is the technique used to determine the concentrations, energies, and trapping parameters for defects in the indium-doped silicon. The test samples are n^+ p diodes made by thermally diffusing phosphorus into silicon doped with indium and boron. The indium concentrations ranged from 10^{16} In/cm^3 to 10^{13} In/cm^3. For each sample, the boron concentration was about 10 times that of the indium. The diodes are held in reverse bias which establishes a depletion region. Free carriers are pushed out of this region by the applied field and the traps are emptied. Short voltage pulses are used to collapse the depletion region, bringing in carriers, some of which are trapped at defects. After the pulse goes away, these trapped carriers are slowly emitted thermally. This produces a transient in the diode capacitance which is measured as a function of temperature. Electronic processing is used to separate the transient into a component for each trap and to display the data in a spectral form. The resulting peak heights are related to trap concentrations.[B-5,B-7] The peak positions give the trap emission rate as a function of temperature. The change in emission rate as a function of temperature is used to determine trap activation energies.[B-5,B-7] The saturation of the peak heights as a function of the filling pulse times can be used to calculate the capture cross sections.[B-6]

[B-5] D.V. Lang, J. Appl. Phys. 45, 3014 (1974).

[B-6] D.V. Lang, J. Appl. Phys. 45, 3023 (1974).

[B-7] G.L. Miller, D.V. Lang, and L.C. Kimmerling, Ann. Rev. of Mater. Sci. 7, (1977).

The DLTS-measured trap energies differ from the trap energies measured by Hall or optical techniques due to several reasons. Two of the most important are the temperature dependence of the capture cross section and the increase of the trap emission rates in an electric field. The mathematics for both of these corrections are reviewed in the next section. The experimental technique used to determine the field effect is described here.

The electric field in the diode depletion region goes from a maximum at the junction to zero at the end of the depletion region. The fields can be calculated as a function of position from Poisson's equation

$$\frac{\partial F(x)}{\partial x} = \frac{q(x)}{\varepsilon} \qquad \text{(B-1)}$$

where F(x) is the electric field and q(x) is the local fixed charge density which is measured by a CV profiler.[B-8] To measure the trap emission rate at a single field, two trap filling pulses are used. These are shown in Figure B-1. The first pulse is slightly larger than the second and it brings free carriers into traps in a slightly higher field region than the second pulse. Data are taken in such a way as to subtract the emission from the traps filled by the two pulses. The difference is due to the traps filled by the larger pulse and not filled by the smaller pulse. These traps are in a region, $\bar{x}$, which can be determined from the profiler data for x versus V and in an electric field, F(x), which is calculated from Equation (B-1). These effects are also shown in Figure B-1. By using various pulse heights, the position, x, can

---

[B-8] G.L. Miller, IEEE Trans. Electron. Devices, ED-19, 1103 (1972).

be moved from near the depletion region edge to near the junction and fields from zero to ∿ F max can be studied.

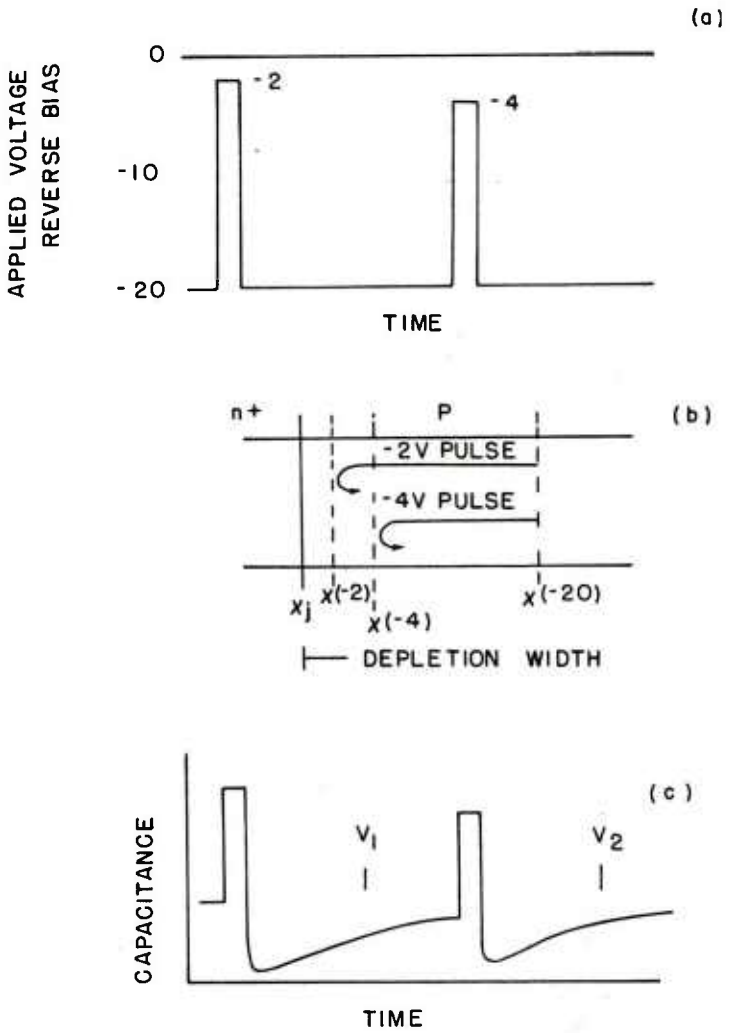

Figure B-1. Pulse schematic for double pulse DLTS (a) shows the applied voltage versus time, (b) shows the regions filled by the two pulses, and (c) shows the capacitance signal. The DLTS data are the difference between the voltage taken at V_1 and V_2.

RESULTS

A DLTS spectrum for Czochralski-grown indium-doped silicon is shown in Figure B-2. The peak directions (all upward) indicate that the traps are hole traps. Four traps are observed and they are labeled X, In, H_1, and H_2. The trap concentrations for the sample shown are:

$$\text{In-X} = \sim 1.4 \times 10^{15}/\text{cm}^3$$
$$\text{In} = \sim 3 \times 10^{15}/\text{cm}^3$$
$$H_2 = \sim 3 \times 10^{14}/\text{cm}^3$$
$$H_1 = \sim 1 \times 10^{14}/\text{cm}^3$$

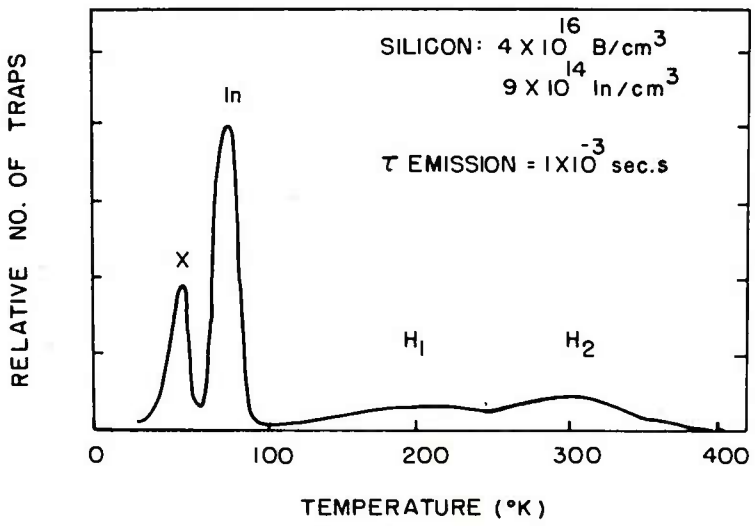

Figure B-2. The DLTS spectrum obtained for indium-doped silicon.

In equilibrium in neutral semiconductor material there are equal numbers of traps thermally emitting trapped carriers as there are empty traps capturing carriers. This equality in p-type silicon can be used to relate the trap emission time constant to its capture coefficient, giving

$$\tau_e = \frac{e^{E_T/KT}}{\frac{C2}{g}\left(\frac{2\pi m_d^* KT}{h^2}\right)^{3/2}} \qquad \text{(B-2)}$$

where

τ_e = Trap emission time constant

E_T = Trap energy relative to the valance band

C = Capture coefficient

g = Ground state degeneracy

m_d^* = Hole density of states effective mass

h = Plank's constant

Using the relation

$$\sigma = C\langle v\rangle \qquad \text{(B-3)}$$

the average thermal velocity $\langle v\rangle = (8KT/\pi m^*)^{1/2}$ can be calculated and Equation (B-2) can be put in the form

$$T^2\tau_e \simeq \frac{e^{E_T/KT}}{\sigma\frac{2K^2}{\pi^2 h^3 g} m_h^*} \qquad \text{(B-4)}$$

In this equation the density of states and velocity effective masses have been approximated as being equal. Both the In-X and the In centers show a strong field dependence. The double-pulse technique was used to measure the trap emission rate, τ, as a function of electric field and temperature. The data for substitutional indium are shown in Figure B-3, where it is plotted as $\ln T^2\tau$ versus $1/KT$ to fit Equation (B-4). In this form the data should be in a straight line, with the slope equaling the effective thermal activation energy.

The electric fields in the depletion region lower the trap activation energies and increase the trap emission rate. This is called the Poole-Frenkel effect and is shown in Figure B-4 for a coulomb-attractive trap. The change in emission rate for a coulomb trap in an electric field has been calculated by Hartke as being[B-9]

$$\frac{\tau_e(0)}{\tau_e(F)} = \left(\frac{KT}{\beta\sqrt{F}}\right)^2 \left\{1 + \left[\frac{\beta\sqrt{F}}{KT} - 1\right] e^{\beta\sqrt{F}/KT}\right\} + 1/2 \qquad \text{(B-5)}$$

where

$\tau_e(0)$ = Zero field emission rate

$\tau_e(F)$ = Emission rate in a field, F

β = $(e^3/\pi\varepsilon)^{1/2}$

B-9 J.L. Hartke, J. Appl. Phys. 39, 4871 (1968).

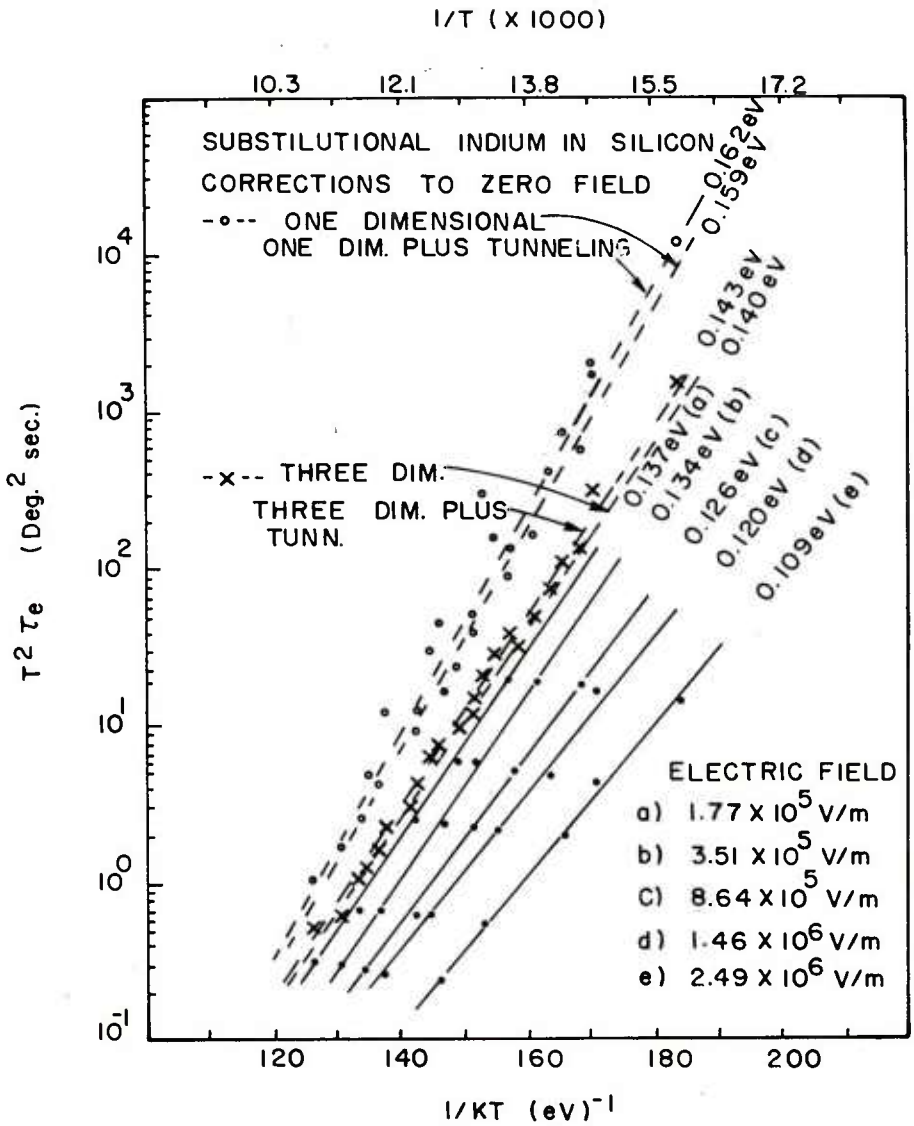

Figure B-3. The $T^2\tau_e$ data for the hole emission from indium in silicon for fields of 1.77×10^5 V/m to 2.5×10^6 V/m are shown by the solid lines in the lower right. The dashed lines are corrections of these data to zero field.

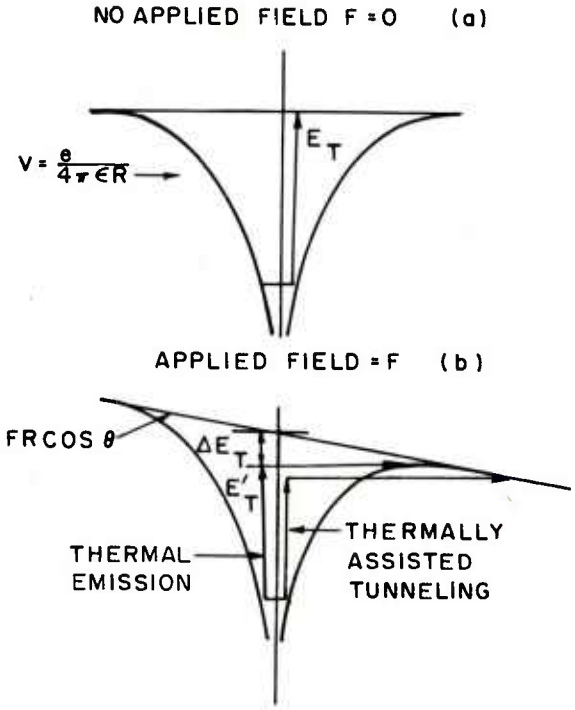

Figure B-4. The thermal activation energy of a coulombic trap in zero field is shown in (a). The change in trap energy (ΔE_T), the lowered activation energy (E'_T), and the thermally assisted tunneling effect are shown for an applied electric field in (b).

This is based on a three-dimensional model. A simpler formula based on a one-dimensional model is often used instead of this.[B-10]

$$\tau(O) = \tau(F)e^{\frac{\beta\sqrt{F}}{KT}} \qquad \text{(B-6)}$$

Another effect which increases the emission rate in a field is thermally assisted tunneling. This is also shown in Figure B-4.

[B-10] J. Frenkel, Phy. Rev. 54, 647 (1938).

A one-dimensional approximation has been developed to include this by Vincent, Chantre and Boise[B-11]

$$\tau(O) = \tau(F)\left\{ e^{\Delta E_T/KT} + \int_{\Delta E_T/KT}^{E_T/KT} \exp\left\{ Z - Z^{3/2}\left[\frac{4}{3}\,\frac{(2m^*)^{\frac{1}{2}}\,(KT)^{\frac{1}{2}}}{qh\bar{F}}\right]^{3/2} x \left[1 - \left(\frac{\Delta E_T}{ZKT}\right)^{5/3}\right]\right\} dz \right. \qquad \text{(B-7)}$$

where E_T is the trap energy and ΔE_T is $\beta\sqrt{F}$.

We have modified this to a three-dimensional form by defining an effective three-dimensional barrier change, ΔE_T^*, by

$$e^{\Delta E_T^*/KT} = \left(\frac{KT}{\beta\sqrt{F}}\right)^2 \left\{ 1 + \left[\left(\frac{B\sqrt{F}}{KT}\right) - 1\right] e^{\beta\sqrt{F}/KT} \right\} + 1/2 \qquad \text{(B-8)}$$

The data in Figure B-3 have been corrected to zero field values using the different models: the one-dimensional Poole-Frenkel model [Equation (B-6)], the three-dimensional Poole-Frenkel model [Equation (B-5)], the one-dimensional model, including tunneling [Equation (B-7)], and the three-dimensional model, including tunneling [Equation (B-8)]. Data for the In-X-center indium, and the two deeper traps are shown in Figure B-5. The data for the indium-X center and indium have been corrected for the three-dimensional Poole-Frenkel effect and thermally assisted tunneling by Equation (B-8). The activation energies measured were 0.095 eV for In-X and 0.126 eV for indium. The correction for electric field effects

---

B-11 G. Vincent, A. Chantre, and D. Bois, J. Appl. Phys. 50, 5484 (1979).

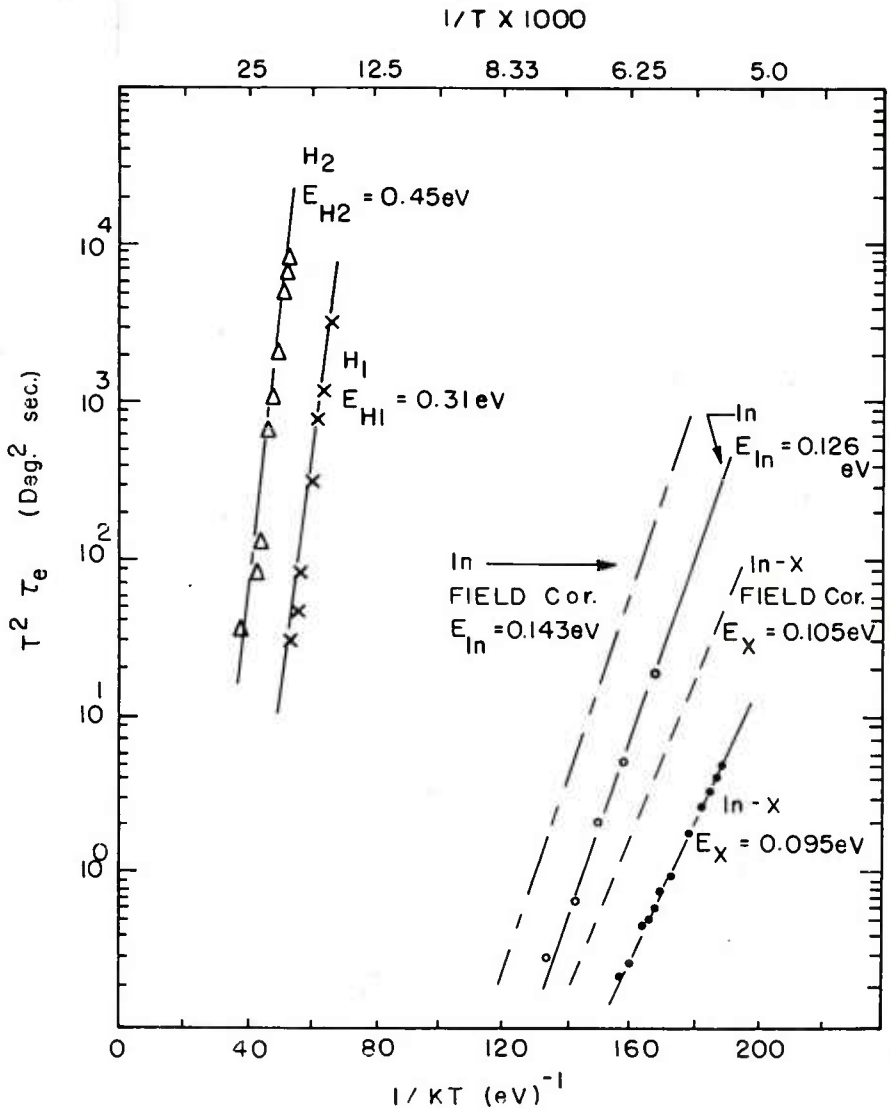

Figure B-5. The $T^2\tau_e$ data are shown for the H_1, H_2, In, and In-X centers in silicon in an electric field of $\simeq 8.6 \times 10^5$ V/m. The data for the In and In-X centers have been corrected to zero field by the three-dimensional coulomb correction, including thermally assisted tunneling. These are the dashed lines.

in Equation (B-8) gave corrected energies of 0.105 eV for In-X and 0.143 eV for indium. The experimental data for the deeper levels gave E_v + 0.31 eV and E_v + 0.45 eV for H_1 and H_2, respectively.

The DLTS techniques can be used to determine the capture coefficient as a function of temperature. For very short filling pulses, the free carriers are moved in and out of the depletion region too quickly to be trapped and no DLTS peak is observed. For very long fill pulses, all of the traps saturated. The peak amplitude as a function of filling time increases exponentially with a time constant equal to:[B-5]

$$\tau_f^{-1} \simeq Cp = \sigma \langle v \rangle p \qquad \text{(B-9)}$$

where p is the hole free-carrier concentration.

Data have been taken to determine the capture coefficients for the traps observed. The results for In and In-X are shown in Figure B-6. There is a slight temperature dependence for indium in this temperature region and very little temperature dependence for the In-X center. The data can be fit to an exponential form with

$$C_{In} = 7.6 \times 10^{-9}\ cm^3/sec\ e^{+0.031\ eV/KT} \qquad \text{(B-10)}$$

and

$$C_{In-x} = 7.7 \times 10^{-8}\ cm^3/sec\ e^{+0.006\ eV/KT} \qquad \text{(B-11)}$$

The accuracies of the activation energies are $\sim \pm 0.02$ eV for indium and ± 0.005 eV for indium X. The free-carrier thermal velocity has been estimated using $v = \sqrt{8KT/\pi m^*}$ with temperature-dependent effective mass data supplied by J. Lang of the Air Force Materials Laboratory. This allows the capture cross section

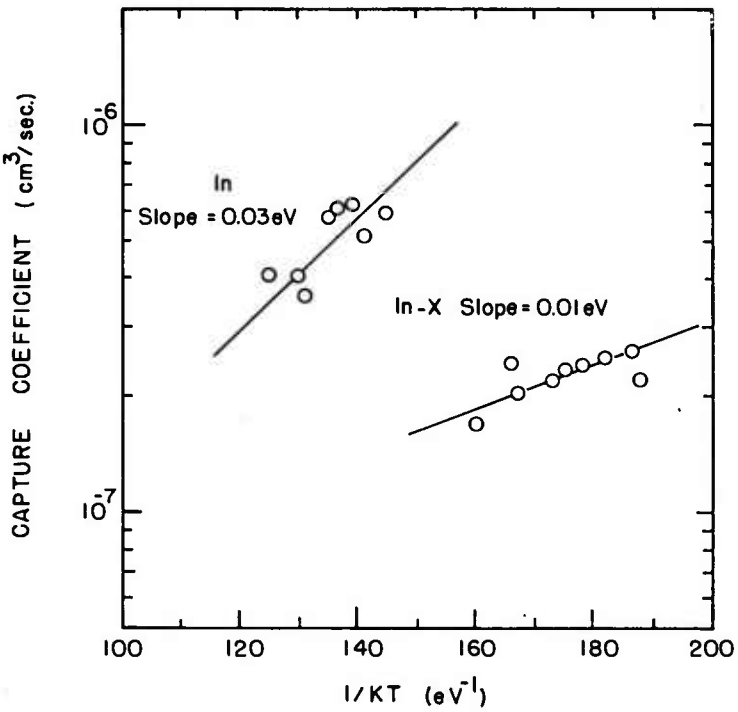

Figure B-6. Capture coefficients as a function of temperature for indium and the indium-X centers in silicon.

to be calculated as $\sigma = C/\langle v \rangle$. Values of the fill times, capture coefficients, and capture cross sections for indium and the indium-X center near 77 K are given in Table B-1.

TABLE B-1. TRAPPING PARAMETERS FOR In AND In-X

Temp. (K)	τ_f (ns)	p (cm^{-3})	<v> (cm/sec)	C (cm^3/sec)	σ (cm^2)
Indium					
96.7	30	10^{14}	1.08×10^{7}	3.17×10^{-7}	2.9×10^{-14}
77.4	12.5	10^{14}	9.84×10^{6}	8×10^{-7}	8.13×10^{-14}
Indium-X					
77.4	50	10^{14}	9.84×10^{6}	2×10^{-7}	2.03×10^{-14}
61.1	38	10^{14}	8.89×10^{6}	2.6×10^{-7}	2.92×10^{-14}

The capture coefficients for the two deep levels, H_1 and H_2, were estimated by fitting Equation (B-2). This assumes that there is no temperature dependence for their capture coefficients and that field effects on these centers are small. The g value used in Equation (B-2) was taken to be 2, which is what is expected for a nontetrahedral defect level. The values obtained are:

$$C_{H_1} = 2.0 \times 10^{-9} \text{ cm}^3/\text{sec} \qquad \text{(B-12)}$$

and

$$C_{H_2} = 1.2 \times 10^{-8} \text{ cm}^3/\text{sec} \qquad \text{(B-13)}$$

DISCUSSION

The DLTS spectrum shown in Figure B-2 is able to distinguish four hole traps in Czochralski-grown indium-doped silicon. The In-X center is very strong in the data shown; it is not always observed. Several models for the X-center have been proposed.[B-1, B-3, B-4] Evidence supporting a nearest-neighbor carbon-indium pair model has been presented by this group and Baron et al.[B-3, B-4, B-12] The identities of the deeper centers H_1 and H_2 are not known.

Both the indium and the indium-X center show the strong electric field effects expected for coulomb traps. The electric field in the diode depletion region lowers the effective trap activation energies and increases their emission rates. This was shown in Figures B-3 and B-5, where a 2.5×10^6 V/m electric field is shown to change the indium emission rate by one to two orders of magnitude and lower the indium activation energy by 0.035 eV. The data for indium shown in Figure B-3 was corrected for this field effect using one- and three-dimensional models. There is a significant difference between using the simple one-dimensional coulomb barrier lowering corrections of Equations (B-6) and (B-7) and the more accurate three-dimensional form in Equations (B-5) and (B-8). The emission rates for the two corrections differed by a factor of two to six over the temperature range studied and the activation energies differed by $\sim$ 0.02 eV. Because of this, the more accurate three-dimensional correction is used for the In-X and In data shown in Figure B-5.

B-12 C.E. Jones, D. Schafer, W. Scott, and R.J. Hager in the report of the IRIS Specialty Group on Infrared Detectors, June 1979, Minneapolis, MN.

The data reported are for samples with electric fields in the 10^5 V/m to 10^6 V/m range. For these fields and for the trap depths studied, the effect of thermally assisted tunneling is small. The tunneling correction is expected to be more important at higher fields.[B-12]

The capture coefficients for indium and the indium-X center were measured by the trap filling method of Equation (B-9). This technique involves the trap filling when the depletion region is decreased and it occurs in field free conditions. The indium trap filling occurred so quickly even in material doped to as low as 10^{14} B/cm^3 that there is appreciable scatter to the data shown in Figure B-6. The indium capture coefficient at 77K is given as 8×10^{-7} cm^3/sec. The activation energy is estimated at 0.03 eV ±0.02 eV for indium. Blakemore used a photoconductivity technique to determine an indium capture coefficient of $\sim 1 \times 10^{-6}$ cm^3/sec at 77K with an activation energy of $\sim$ 0.05 eV.[B-13] Forbes used a MOSFET technique similar to DLTS and measured a capture coefficient of 0.4 to 1.7×10^{-6} cm^3/sec at 77K with activation energy of 0.05 eV.[B-14] Forbes used bulk values of p for his calculations. Fields in the depletion region empty traps in this region, making the fixed charge here different from that in the bulk material. When the filling pulse is applied, carriers move in to neutralize the local fixed charge, making p in Equation (B-9) equal to the depletion region fixed charge not, as is often done, equal to the

---

[B-13] J.S. Blakemore, Can. J. Phys. 34, (1956).

[B-14] L. Forbes in "Characterization and Analysis of Indium-Doped Silicon Extrinsic Detector Material," (J. Backus, Hughes Res. Lab., T. McGill, C.I.T.; and L. Forbes, U. of C. Davis) Interim Technical Report 1, Dec. 1977, DARPA Contract DAAK70-77-C-0082, pg. 48-51.

free-carrier concentration in the neutral bulk semiconductor. The value of p needed for Equation (B-4) can be measured on a CV profiler which measures the fixed charge in the depletion region. Using a depletion region value of p lowers Forbes C value and also lowers his activation energy which would bring them closer to the values determined in this study.

The average capture coefficient value measured by DLTS and reported herein is very close to the values reported by Blakemore and Forbes. The indium capture coefficient activation energy of 0.03 ±0.02 eV has a large error range, but within the error range it is the same as that reported by the other two studies. This gives some confidence in the DLTS data for the indium-X center capture coefficient which has much less experimental error.

The magnitude of the indium and indium-X capture coefficients of 10^{-6} to 10^{-7} cm^3/sec are both large and in the range expected for coulomb traps. The capture coefficients estimated for H_1 and H_2 were smaller in the 10^{-8} to 10^{-9} range, which suggests that they may be neutral traps. The effect electric fields have on neutral traps is much less than that on coulombic centers. The capture coefficients calculated from Equation (B-2) for the H_1 and H_2 traps neglected any field dependence.

Trap energies measured by DLTS can be corrected for electric field effects and the temperature dependence of the capture cross section. Data to make both of these corrections have been measured for the In and In-X centers, as follows:

Center	E_{DLTS}	$+E_{Field}$	$-E_{\sigma}$	= E_{Trap}	Optical E_{Trap}
In	0.126 eV	+ 0.017	- 0.03	= 0.113 eV	0.156 eV
In-X	0.095 eV	+ 0.010	- 0.006	= 0.099	0.1128 eV

In these cases we are adding three terms each with an error of $\sim$ 0.01 eV and coming out low by 0.04 eV to 0.014 eV for In and In-X. Again, the In-X data had less experimental error for E_{σ} and the corrected DLTS trap energy is closer to the optical value. The field correction used also may be low. Using the one-dimensional formulas Equations (B-6) and (B-7) would give higher field corrections than the three-dimensional formulas. Better correlation between theory and experiment does not change the fact that the one-dimensional formulas were based on a less-accurate physical model, however. There is a large experiment error in the exponential dependence of the capture coefficients and these terms could be smaller, bringing the optical and DLTS energies closer.

CONCLUSION

The DLTS technique has identified four traps in indium-doped silicon. Two of these are the indium-X center and substitutional indium and two are unidentified deeper centers at E_v + 0.31 eV and E_v + 0.45 eV. Both indium and the indium-X center show the large electric field effects expected for coulomb traps. The electric field increases trap emission rates and decreases their activation energies. The emission rates and activation energies have been measured for a range of electric fields. Theoretical formulas have been able to correct these data to single-zero-field curves for indium and the indium-X center. The resulting zero-field trap activation energies are lower than the optically measured values, however.

The low-temperature capture coefficients for the four hole traps have been measured. Indium is the only one of these which has been previously reported in the literature and the DLTS values measured agree with the reported value for this trap. The indium hole trapping occurs so quickly that there is a large error in the DLTS determination of the temperature dependence of the capture coefficient and the DLTS corrected trap energy which uses these data. The data for the indium-X center have less experimental error but still yield a trap energy which is slightly lower than optical or Hall values.

The DLTS data provide the trapping parameters which can be used with optically measured energy levels to mathematically model trapping effects in indium-doped silicon.

ACKNOWLEDGMENTS

The authors would like to thank George Watkins and John Troxell of Lehigh University and Dave Lang and L.C. Kimmerling of Bell Laboratories for their help in setting up the DLTS apparatus.

REFERENCES

B-1. R. Baron, M.H. Young, J.K. Neeland, and O.J. Marsh. Appl. Phys. Lett. 30, 594 (1977).

B-2. W. Scott, Appl. Phys. Lett. 32, 540 (1978).

B-3. R. Baron, J.P. Bankus, S.D. Allen, T.C. McGill, M.H. Young, H. Kimura, H.V. Winston, and O.J. Marsh, J.Appl. Phys. Lett. 34, 257 (1979).

B-4. C.E. Jones, D.E. Schafer, W. Scott, and R. Hager, Bull. Am. Phys. Soc. 24, 276 (1979) BL14, and IRIS Speca.

B-5. D.V. Lang, J. Appl. Phys. 45, 3014 (1974).

B-6. D.V. Lang, J. Appl. Phys. 45, 3023 (1974).

B-7. G.L. Miller, D.V. Lang, and L.C. Kimmerling, Ann. Rev. of Mater. Sci. 7, (1977).

B-8. G.L. Miller, IEEE Trans. Electron. Devices, ED-19, 1103 (1972).

B-9. J.L. Hartke, J. Appl. Phys. 39, 4871 (1968).

B-10. J. Frenkel, Phy. Rev. 54, 647 (1938).

B-11. G. Vincent, A. Chantre, and D. Bois, J. Appl. Phys. 50, 5484 (1979).

B-12. C.E. Jones, D. Schafer, W. Scott, and R.J. Hager in the report of the IRIS Specialty Group on Infrared Detectors, June 1979, Minneapolis, MN.

B-13. J.S. Blakemore, Can. J. Phys. 34, 938 (1956).

B-14. L. Forbes in "Characterization and Analysis of Indium-Doped Silicon Extrinsic Detector Material," (J. Backus, Hughes Res. Lab., T. McGill, C.I.T.; and L. Forbes, U. of C. Davis) Interim Technical Report 1, Dec. 1977, DARPA Contract DAAK70-77-C-0082, pg. 48-51.

APPENDIX C

TRIGONAL STRESS SYMMETRY OF THE Al-X CENTER IN SILICON*

ABSTRACT

Electrically active complexes called X-centers have been identified associated with the group IIIA acceptors in silicon. The complexes are acceptors with an energy level ∿ 80% that of the corresponding group IIIA substitutional element. To provide the information needed to help identify these defects, the optical absorption spectra for the aluminum-X center have been measured under conditions of uniaxial stress. The data are interpreted in terms of a defect having trigonal [111] symmetry. Defect models which have been suggested involving single substitutional atoms or distance pairs do not fit the stress data. On the other hand, nearest-neighbor substitutional pairs or a substitutional atom next to a bond-centered or tetrahedral interstitial fit the data.

INTRODUCTION

Recent investigations of silicon doped with group IIIA acceptors (B, Al, Ga, and In) have revealed several shallow acceptor levels

---

*The authors of this paper are David E. Schafer, Colin E. Jones, and J.E. Sjerven, Honeywell Corporate Material Sciences Center, Bloomington, MN. The paper was submitted to J. Appl. Phys. for publication.

referred to as "X"-levels.[C-1 - C-4] Each X-level appears to be a complex involving a particular group IIIA impurity but with an ionization energy 20 to 25% lower than the corresponding substitutional group IIIA element in silicon. The structure of the X-center has not been firmly established. However, several models for X-centers have been suggested, including centers involving carbon-indium pairs,[C-4, C-5] indium interstitial or vacancy complexes,[C-6] and indium-aluminum pairs.[C-7] In the case of Si(In), the X-defect is of current technological interest in connection with the use of this material for a 3-5 micron photoconductor, since the shallower In-X level contributes excess thermal gen--eration-recombination noise and requires lower temperatures to achieve photon noise-limited operation.

Toward an eventual identification of the X-defect(s), we have investigated the behavior of the Al-X optical absorption spectrum under uniaxial stress. This has provided information about the symmetry and orientation of the Al-X defect. Although the X-defect in Si(Al) is not of as great current technological importance as

---

C-1 R. Baron, M.H. Young, J.K. Neeland, and O.J. Marsh, Appl. Phys. Lett. 30, 594 (977).

C-2 W. Scott, Appl. Phys. Lett. 32, 540 (1978).

C-3 W. Scott and C.E. Jones, J. Appl. Phys. 50, 7258 (1979).

C-4 C.E. Jones, D.W. Schafer, W. Scott, and R. J. Hager, Bull. Am. Phys. Soc. 24, 276 (1979).

C-5 R. Baron, J.P. Bankus, S.D. Allen, T.C. McGill, M.H. Young, H. Kimurg, H.V. Winston, and O.J. March, Appl. Phys. Lett. 34, 257 (1979).

C-6 V. Swaminathan, J.E. Lang, P.M. Heminger, and S.R. Smith, Appl. Phys. Lett. 35, 184 (1979).

C-7 M.C. Ohmer and J.E. Lang, Appl. Phys. Lett. 34, 750 (1979).

that in Si(In), it is the most amenable of the group IIIA X-centers to an optical study of this kind, having a relatively large optical cross section and having optical transitions easily separable from other nearby spectral features. Based on consistent trends in the ionization energies[C-2, C-3] and annealing behavior[C-4] of the X defects in B-, Al-, Ga-, and In-doped silicon, it seems likely at present that the various X-defects in these cases have related origins and that the structural information given here for the Al-X defect will be applicable to the other X-defects as well.

Experimental Procedure

Oriented samples of Czochralski-grown silicon with 3 to 5 x 10^{16} Al/cm^{-3} were cut with dimensions 0.6 x 0.45 x 0.13 inch, the transmission faces angle-lapped at about 0.5^{o} to prevent interference effects, and polished. They were mounted in a copper sample holder and compressed along the [111], [100] or [110] axis by differential thermal contraction relative to copper upon cooling to 10K, the temperature of the measurements. Some samples were mounted conventionally for stress-free data. Infrared absorption measurements were made using a Digilab FTS-14 Fourier transform spectrometer at a resolution of 2 cm^{-1}. In some of the measurements, light polarized either parallel or perpendicular to the stress direction with a wire grid polarizer was used.

Experimental Results

The optical absorption spectrum for unstressed aluminum-doped silicon in the 200-cm^{-1} to 450 cm^{-1} region is shown in Figure C-1. Data are shown for sample temperatures of 9K and 50K. The peaks at 245, 278, and 320 cm^{-1} are due to substitutional boron which is present in this sample as an impurity. The peaks at

339, 372, 404, and 414 cm^{-1} are due to the aluminum-X center. The general rise in the spectra toward larger wave numbers is due to the strong substitutional aluminum absorption which has its first peak at 440 cm^{-1}.

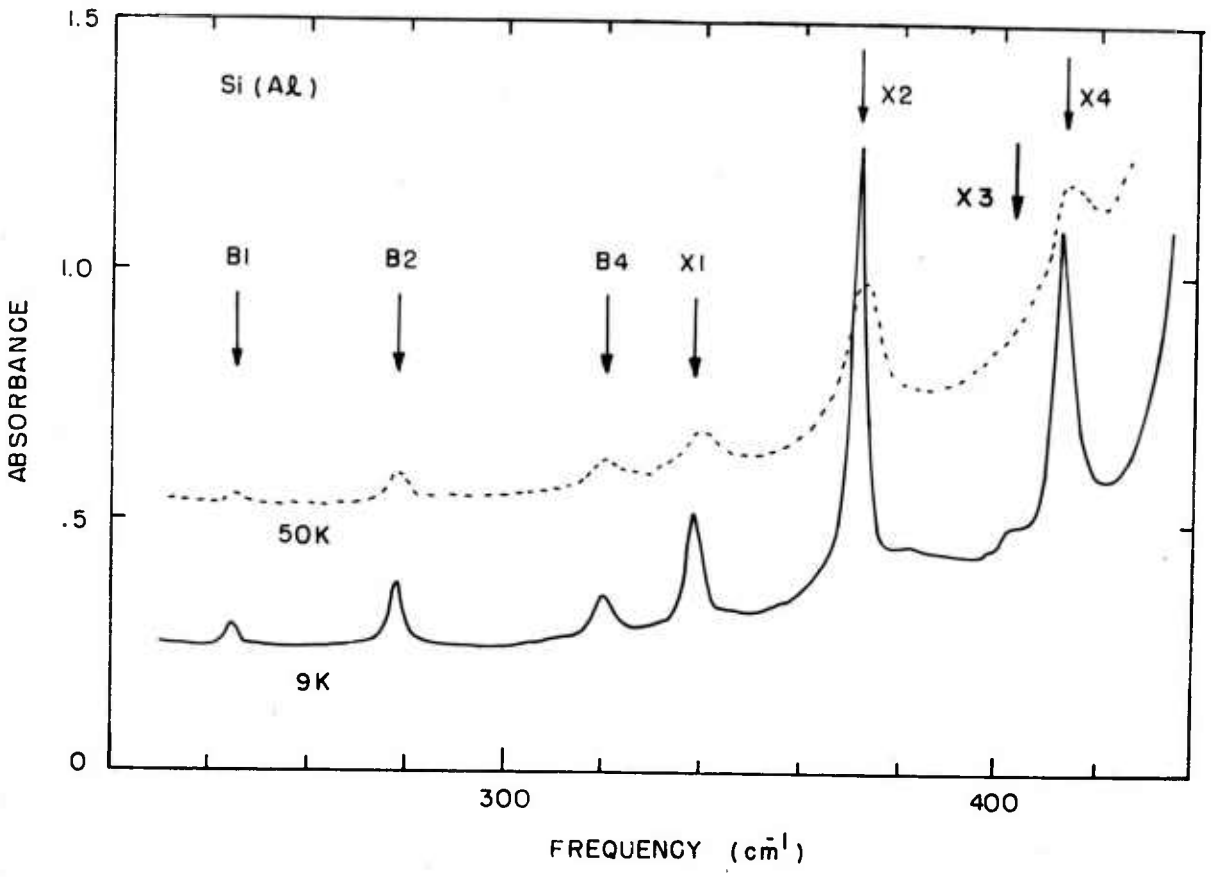

Figure C-1. The absorption spectrum of Czochralski-grown aluminum-doped silicon, showing lines due to the Al-X center (X1, X2, X3, X4) and due to residual boron (B1, B2, B4). Spectral resolution is 2 cm-1.

The absorption spectra with [100] and [111] uniaxial stress applied are shown in Figures C-2 and C-3, respectively. These data are taken at 10K with light polarized parallel and perpendicular to the stress directions.

For stress applied in the [110] direction there are two inequivalent directions for the optical beam. Data for [110] uniaxial stress with the optical beam in the $[1\bar{1}0]$ and [001] directions are shown in Figure C-4 and C-5, respectively.

Theory

The stress splittings and degeneracies of hydrogenic acceptor levels in silicon as predicted on the basis of symmetry properties are summarized in Figure C-6. These predictions are the basis for the analysis of the stress spectra presented below. The simplest picture of an acceptor in silicon, that of a positive hole attracted to a fixed negative ion via a spherically symmetric potential, is represented at the left of the figure. It consists of a 1s-like ground state with allowed optical transitions to three 2p-like excited states.[C-8] Since shallow acceptor levels generally arise from the four-fold degenerate J3/2 valence band maximum, the 1s and 2p hydrogenic states at the left of Figure C-6 are assigned net degeneracies of 4 and 12, respectively.[C-8] The level diagrams in the remainder of the figure represent the effects of various deviations from spherical symmetry, due to local structure or applied stress. In this figure, these effects are represented as small perturbations on the 1s-2p hydrogenic level structure.

[C-8] W. Kohn, in Solid State Physics, Vol. 5, p. 257, F. Setz and D. Turnbull, Eds. (Academic Press, New York, 1957).

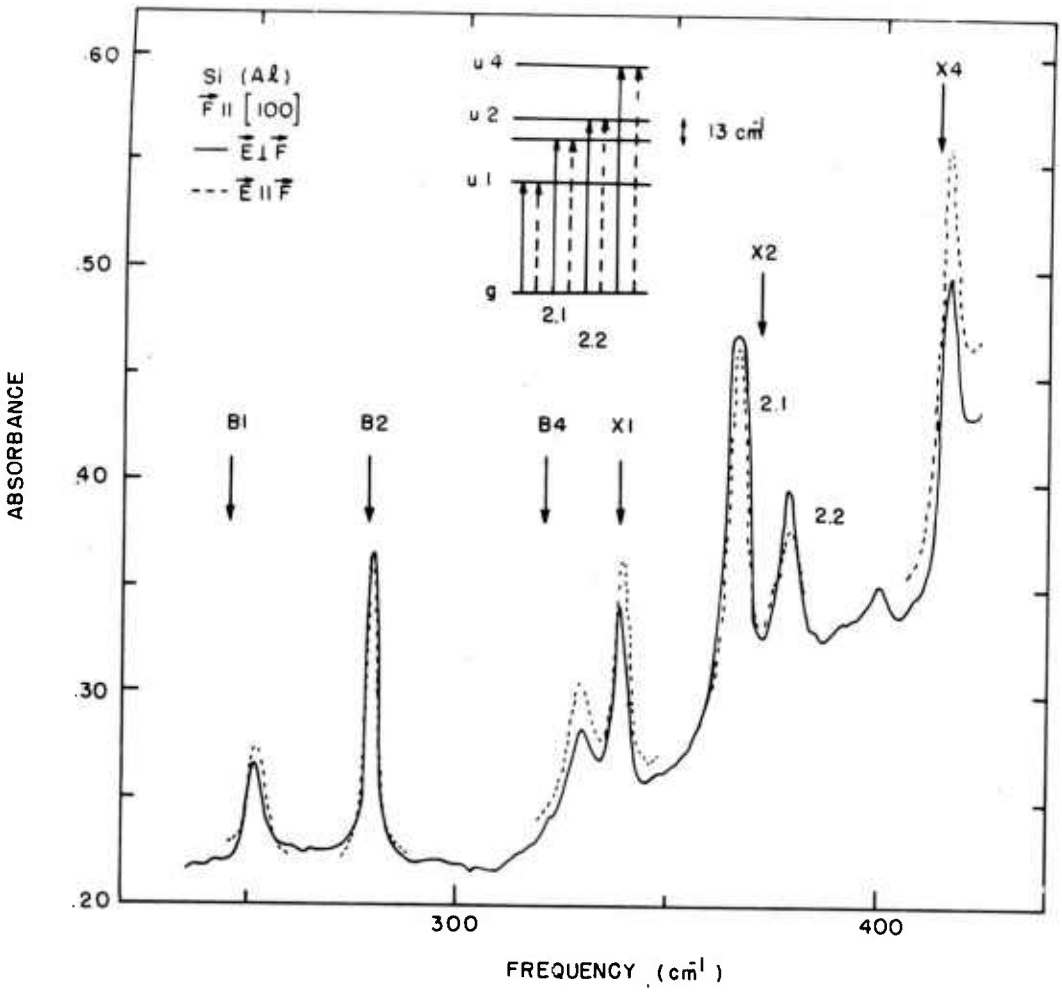

Figure C-2. The absorption spectrum of the material of Figure C-1 under [100] uniaxial compression near liquid-helium temperature. The inferred Al-X level splittings are also shown. The spectral resolution is 2 cm^{-1}.

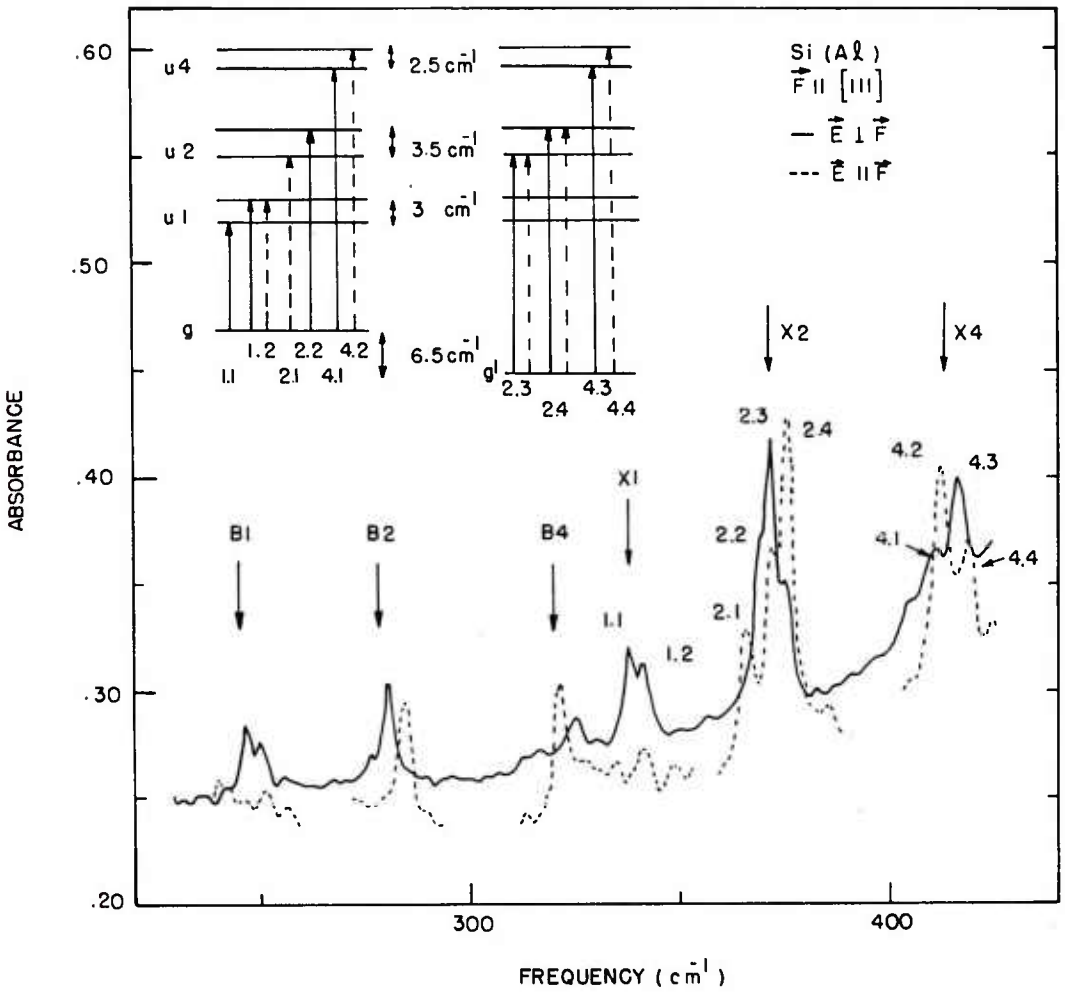

Figure C-3. The absorption spectrum of the material of Figure C-1 under [111] uniaxial compression. The inferred Al-X-level splittings are also shown, with two configurationally inequivalent subsets of the centers represented in two separate-level diagrams.

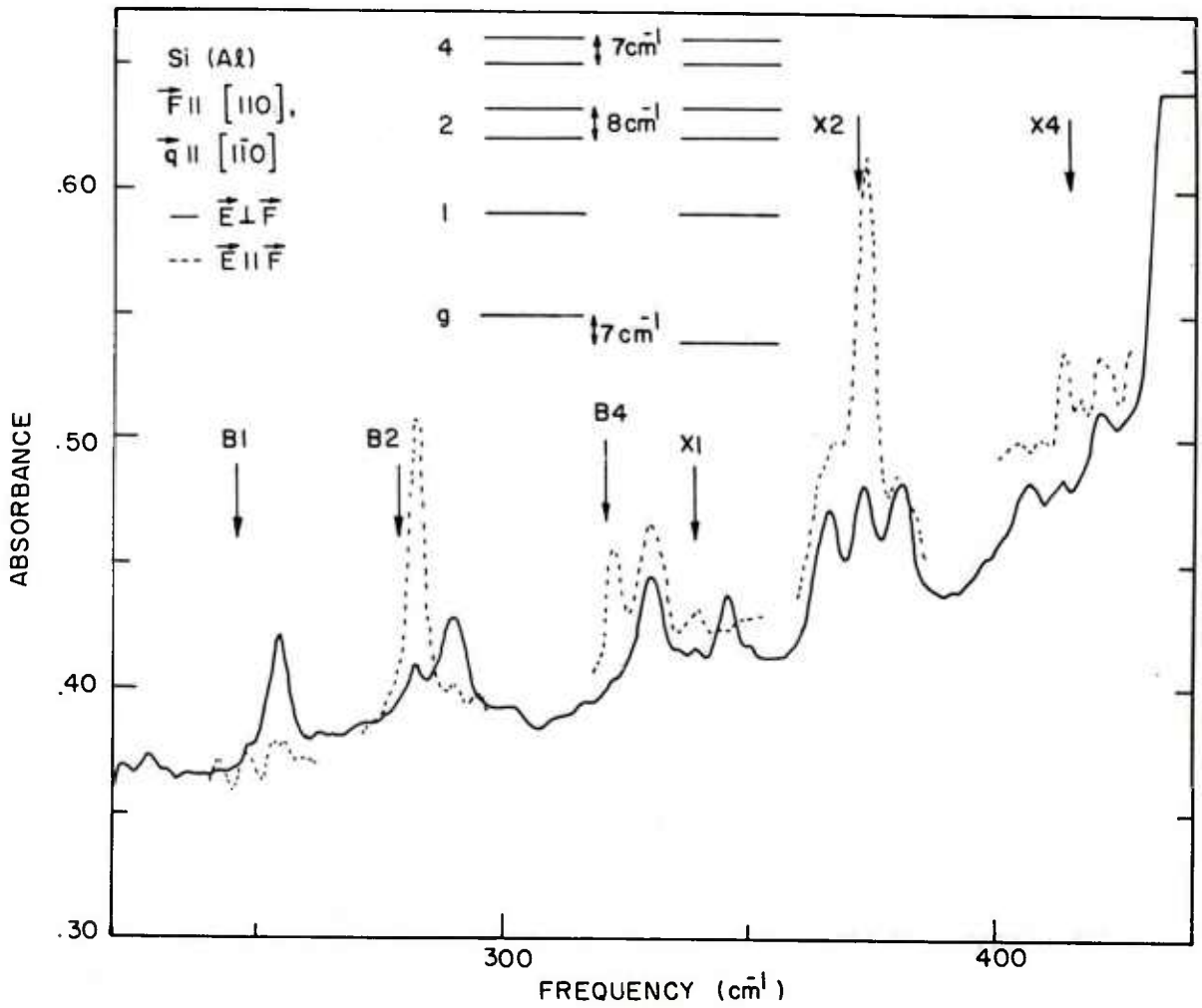

Figure C-4. The absorption spectrum of Al-doped silicon under [110] uniaxial compression with incident light along [1$\bar{1}$0]. The inferred level splittings are also shown, with two inequivalent subsets of the centers represented in two separate-level diagrams.

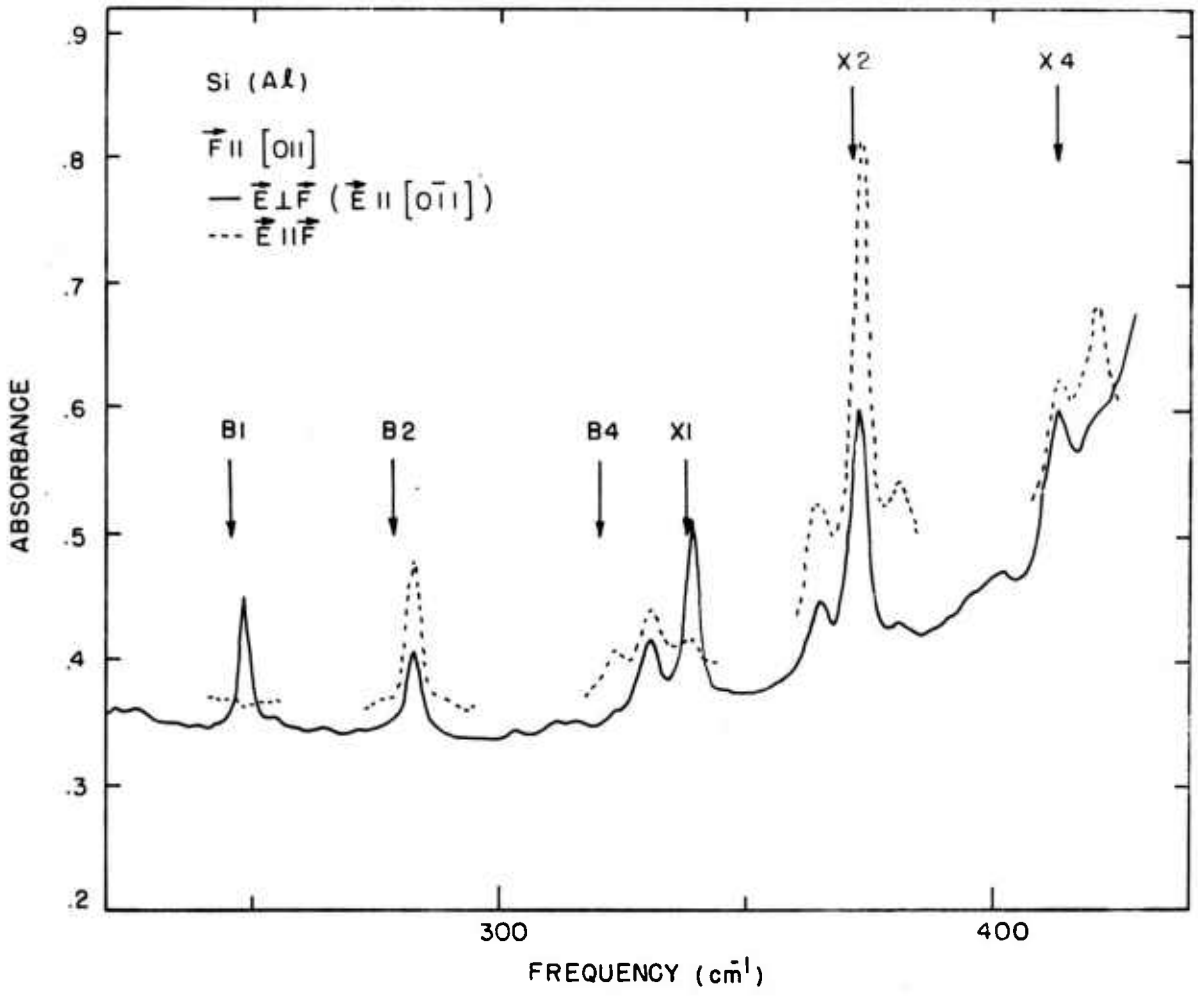

Figure C-5. The absorption spectrum of Al-doped silicon under [110] uniaxial compression with the incident light along [001]. The inferred level splittings are also shown, with two inequivalent subsets of the centers represented in two separate-level diagrams.

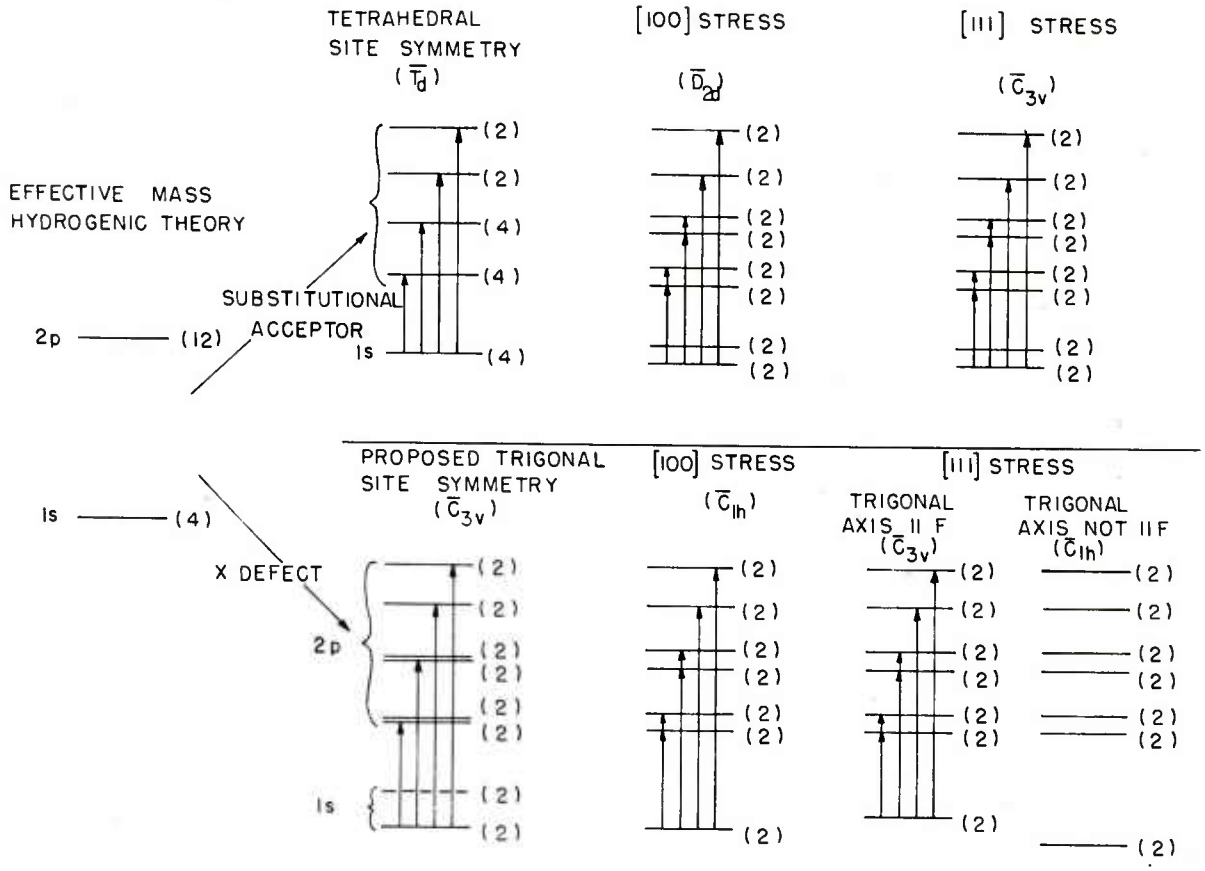

Figure C-6. Splitting patterns of 1s and 2p hydrogenic acceptor levels under the influence of local defect structure and applied stress, as predicted on the basis of symmetry changes. The upper half of the figure treats the case of a substitutional acceptor (tetrahedral symmetry), while the lower half depicts the case of a trigonal structure point group C_{3v}, with the threeefold axis oriented along any of the body diagonals of the cubic host structure.

The top half of Figure C-6 treats the usual case for group IIIA acceptors, that of a substitutional impurity in a tetrahedral environment. As indicated in the top center of Figure C-6, the local tetrahedral symmetry is expected to remove the 12-fold

degeneracy of the 2p excited state, splitting it into four components of degeneracy: 4, 4, 2, and 2. Such splitting and degeneracies have been observed for the most part in investigations of the absorption spectra of the group IIIA impurities,[C-9] with the possible exception of excited state 4, for which fourfold degeneracy has been suggested[C-9] rather than the value of two predicted by the effective-mass theory. The energy ordering of the fourfold and twofold degenerate states in Figure C-6 has been taken from the results for the substitutional acceptors. The additional symmetry-related effects of [100] and [111] applied stress are illustrated in the upper right portion of Figure C-6 and are qualitatively the same in each case, resulting in six 2p levels and two 1s levels all of degeneracy two. This is the maximum degree of splitting which these levels may undergo, since these levels have only the spin degeneracy of two left. Not all of the possible transitions are observed with the same intensity due to differing selection rules for the various transitions and polarizations.

Complex defects, as the X-centers may be, have a symmetry lower than tetrahedral. We describe the case of a trigonal [111] defect in some detail below and then sketch the effects expected for other defect symmetries. A trigonal defect has a point group (C_{3v} or D_{3d}) which is a subgroup of the tetrahedral group. The ground state is split by the nontetrahedral crystal field into two ground-state spin-doublets. The excited states are split into six components as shown in the lower left of Figure C-6. The excited states are spatially diffuse and have a node at the defect,

---

[C-9] A. Onton, P. Fisher, and A.K. Ramdas, Phys. Rev. 163, 1967. (See Figs. 7 and 25 Al-X absorption spectra.)

so the excited state splittings are not expected to be very large. The ground-state components are more strongly localized at the defect and they could be appreciably split.

The lower right hand side of Figure C-6 shows the splitting expected under applied uniaxial stress. The trigonal [111] complex has an added stress effect over that of a substitutional tetrahedral defect. A trigonal defect can be oriented along any of the four [111] cube diagonals. The crystal will contain equal numbers of defects in each of these orientations if the stress is applied at a low enough temperature so that the defect cannot reorient. If there are different angles between the four orientations and the applied stress, then the defects in the different orientations will be stressed different amounts. Optical data will show absorption from defects in each of the different orientations, giving rise to a superposition of several sets of stress spectra. This is called a configurational effect. The intensities of the lines from a particular orientation will not necessarily be in the same proportion to those of the other orientations, however, since the intensity of each transition changes with viewing angle.

The configurational effect is expected to occur predominantly in the ground state. Again, because the excited states are spread out and have a node at the defect, the stress splitting of the excited states is expected to arise mainly from the distortion of the bulk silicon lattice and is not expected to be strongly affected by the local atomic symmetry of the defect. Consequently, the stress-induced changes in these excited states (bottom half of Figure C-6) are represented in the figure as being the same as those of the tetrahedral defect (upper half of Figure C-6).

Under [100] stress, the different orientations for the trigonal [111] defect all make equal angles with the stress and will be affected in the same way, producing a single stress pattern in the optical data. For a [111] stress, one of the defect orientations is along the stress direction and three are at an angle to it, which would be expected to give a superposition of two stress patterns.

Application of [110] uniaxial stress also creates two distinct subsets of [111]-oriented centers, one with the trigonal axis perpendicular to the stress (two possible orientations) and the other with the trigonal axis not perpendicular to the stress (two more orientations). The resulting two level diagrams will be similar to those shown for the [111] stress case.

Similar sets of level diagrams can be drawn illustrating the stress effects expected for rhombic defects, which includes the [110]- and [100]-directed centers, and monoclinic defects. The patterns of splittings and degeneracies in these diagrams are similar to those for the trigonal defect illustrated here. The unique feature of the trigonal [111] defects is the lack of configurational effects for a [100] stress.

DISCUSSION

Figure C-1 shows the Al-X absorption spectrum in unstressed silicon at two temperatures. Three strong lines and one weak line (labeled X1 through X4) are observed, as well as three weak lines (labeled B1, B2, and B4) due to residual boron. As noted elsewhere,[C-2] the four Al-X lines are quite similar in their spacing and relative intensity to corresponding lines in the optical spectra of other shallow acceptors, suggesting that an effective-mass picture is appropriate for the Al-X-excited states. As

mentioned above, this is not surprising, since these states are not expected to interact strongly with the structural details at the defect.

The local crystal field of any nontetrahedral defect would split the ground state into two spin-doublet levels. The possible presence of ground-state splitting due to nontetrahedral defect symmetry was investigated through the second spectrum of Figure C-1, taken at 50K. At this temperature, any additional ground-state components less than about 10 meV above the observed ground state would have been thermally populated and revealed through additional optical transitions. The absence of any additional lines implies that any split-off ground-state component, if it exists, is either less than 2 meV away from the lower ground state (i.e., unresolvable) or more than 10 meV above it.

The apparent effective-mass nature of the Al-X-excited states was used in the analysis of the Al-X spectrum under applied stress. It was assumed that there would be a close correspondence between the stress behavior of these excited states and that of the (effective-mass-like) excited states of other shallow acceptors. Thus, the stress-induced changes in the nearby boron lines in Figure C-1 were used as a guide in attributing some of the observed Al-X line splittings to the Al-X excited states. Also, configurational effects (i.e., multiple orientations of a nontetrahedral defect relative to the stress direction) were neglected for the excited states, again because of their apparent weak interaction with structural details near the defect.

The Al-X spectrum under [100] stress, shown in Figure C-2, is the simplest of the three stress cases to discuss, since ground-state splitting does not appear to play a role; the observed spectral

changes can be accounted for by excited-state splitting only. In this case we estimate the expected Al-X excited-state splitting from the behavior of nearby boron lines B1 and B4. Previous investigations have shown that the upward shifts in these lines are due to splitting in the boron ground state.[C-9] Split-off downshifted partners to lines B1 and B4 observed in the earlier work[C-9] are not present in the spectrum of Figure C-2 because of depopulation of the upshifted split-off ground-state component associated with those transitions. Published values of excited-state to ground-state splitting ratios for boron acceptors[C-9] give splittings of 0, 14, and 0 cm^{-1} for boron-excited states 1, 2, and 4, respectively.

Returning to the Al-X absorption lines we find line splittings of 0, 13, and 0 cm^{-1} for lines 1, 2, and 4, respectively which is in good correspondence with the estimated boron-excited-state splittings. It is thus natural to attribute all of the observed Al-X line splittings to the excited states. No lines are observed which can be attributed to ground-state splitting. The inferred level structure in the stressed condition is shown in the upper part of Figure C-2.

Al-X centers which have different orientations relative to the applied stress would be expected to have slightly different ground-state energies. Any ground-state energy differences due to these configurational effects should produce extra lines in the spectrum. Depopulation of the higher-energy-defect orientations should not be possible in these samples. They are not highly compensated and the applied light does not empty any appreciable fraction of the centers. There are thus not enough ionized centers available to depopulate the higher-energy configurations.

Since no extra Al-X lines are observed for the [100] stress, there appears to be no configurational effect for this stress direction.

The [111] stress behavior (Figure C-3) shows a higher degree of line splitting than the [100] stress case. The same procedure described for [100] stress was followed in order to identify the Al-X excited-state splittings. However, in order to account for all of the observed transitions, the assumption of two ground-state components separated by about 6.5 cm^{-1} was required.

The polarization dependence of some of the absorption lines in Figure C-3 reveal differences from the stress behavior of tetrahedral substitutional acceptors. Specifically, the appearance of three distinct components of line 2 in the E||F polarization is inconsistent with the polarization selection rules for a tetrahedral, defect; the two stress-induced ground-state components in the tetrahedral case could undergo at most only one E||F transition each to any component of excited state 2, permitting at most two components of line 2. Defect structures of symmetry lower than tetrahedral, on the other hand, involve fewer selection rules for optical transitions and would not be inconsistent with the spectrum of Figure C-3. Again, the inferred arrangement of levels in the stressed condition is shown in the figure.

Two aluminum-X-center spectra under [110] uniaxial stress are shown in Figures C-4 and C-5. Analysis of observable changes in lines 2 and 4 as before (changes in line 1 are partly obscured by boron line 4) indicate two ground-state components.

Considering now the results of the three stress spectra collectively, we conclude that the Al-X defect is most likely to be of trigonal symmetry, with four possible orientations of the trigonal axis along the body diagonals of the cubic host structure.

The number of ground-state levels occurring for each direction of applied stress [one for [100] stress and two for [111] and [110] stress] corresponds to the number of inequivalent orientations expected for a defect of such symmetry.

Of the structures which have been proposed to date for X-centers, those having trigonal symmetry and which are therefore consistent with our conclusions here are illustrated in Figure C-7. These include nearest-neighbor pairs of substitutional impurities, a substitutional-bond-centered interstitial pair or a substitutional-tetrahedral interstitial pair. Distant pairs of impurity atoms or single substitutional impurities, on the other hand, are not con-

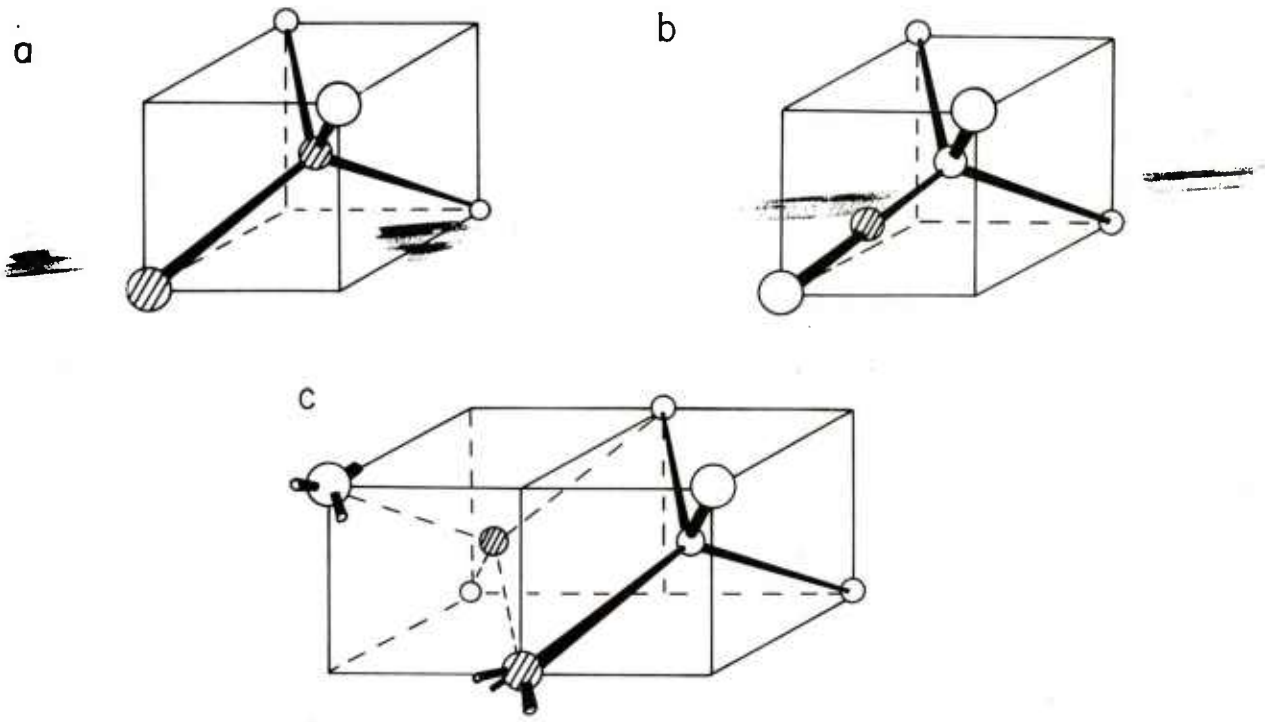

Figure C-7. Three defect structures having the trigonal, [111]-oriented symmetry discussed in the text: (a) nearest-neighbor impurity pair; (b) bond-centered interstitial impurity; and (c) a substitutional-tetrahedral interstitial pair.

sistent with the trigonal symmetry identified here. The association of the (presumably analogous) In-X defect with the presence of carbon impurities tends to rule out interstitial aluminum as a possible Al-X structure.

ACKNOWLEDGEMENT

We wish to acknowledge the assistance of R.J. Hager in providing the aluminum-doped silicon for this study.

REFERENCES

C-1. R. Baron, M.H. Young, J.K. Neeland, and O.J. Marsh, Appl. Phys. Lett. 30, 594 (977).

C-2. W. Scott, Appl. Phys. Lett. 32, 540 (1978).

C-3. W. Scott and C.E. Jones, J. Appl. Phys. 50, 7258 (1979).

C-4. C.E. Jones, D.E. Schafer, W. Scott, and R.J. Hager, Bull. Am. Phys. Soc. 24, 276 (1979).

C-5. R. Baron, J.P. Bankus, S.D. Allen, T.C. McGill, M.H. Young, H. Kimurg, H.V. Winston, and O.J. March, Appl. Phys. Lett. 34, 257 (1979).

C-6. V. Swaminathan, J.E. Lang, P.M. Heminger and S.R. Smith, Appl. Phys. Lett. 35, 184 (1979).

C-7. M.C. Ohmer and J.E. Lang, Appl. Phys. Lett. 34, 750 (1979).

C-8. W. Kohn, in Solid State Physics, Vol 5, p. 257, F. Setz and D. Turnbull, Eds. (Academic Press, New York, 1957).

C-9. A. Onton, P. Fisher, and A.K. Ramdas, Phys. Rev. 163, (1967). (See Figs. 7 and 25 for Al-X absorption spectra.)

APPENDIX D
CARBON-ACCEPTOR PAIR CENTERS (X-CENTERS) IN SILICON*

An electrically active complex called the X-center has long been known in indium-doped silicon. Similar defects have now been associated with the other group IIIA elements in silicon. These X-centers are acceptors with energies approximately 80% of the corresponding group IIIA substitutional atom's energy and with concentrations 10^{-2} to 10^{-5} of the corresponding group IIIA concentration. Doping studies show that the X-center concentrations depend on carbon and fit the reaction $A_s + C_s \overset{K}{\underset{\leftarrow}{\rightarrow}} X$, where A_s is the substitutional group IIIA acceptor, C_s is the substitutional carbon, and K is the equilibrium constant. The equilibrium constants as a function of temperature and the complex binding energies have been determined for all of the group IIIA X-centers except thallium. The binding energy for the complex increases from 0.03 eV for the boron-X center to 0.70 eV for the indium-X center. The complexes do not anneal out up to the melting point of silicon and they can be cyclically annealed. Stress studies on the aluminum-X center show that the complex has [111] trigonal orientational symmetry. The dependence on carbon, the stress symmetry, and the high-temperature stability of these centers all suggest a model for these complexes of a nearest-neighbor substitutional carbon-acceptor pair. Mathematical modeling using extended Huckel calculations confirms that this defect should

---

*Work done under DARPA contract DAAK70-77-C-0194. The authors of this paper are Colin E. Jones, David E. Schafer, Walter M. Scott, and Robert J. Hager, Honeywell Corporate Material Sciences Center, Bloomington, MN. The paper was submitted to J. Appl. Phys. for publication.

have a single energy level slightly shallower than the substitutional acceptor.

INTRODUCTION

Carbon and oxygen are the major residual impurities in silicon. Carbon is often detected at concentrations of 10^{17} C/cm^3 in Czocharlski and 10^{16} C/cm^3 in float-zone silicon. Most of this carbon is in isolated substitutional sites and is electically inactive. This paper discusses the properites of a class of electrically active defects which we believe to be carbon-acceptor complexes.

Historically, a shallow acceptor called the X-center has been seen in Hall[D-1] and optical absorption data[D-2] in indium-doped silicon. This center is known to involve indium. It is electrically active, having an acceptor level at E_v + 0.11 eV, and it occurs in pulled silicon at concentrations 0.1 to 0.5% of the indium concentrations. Silicon crystals doped with indium or other group IIIA elements are being studied as infrared photodetector materials. In these devices, even at the low concentration levels seen, 10^{13} X/cm^3 to 10^{15} X/cm^3, the X-center is a source of thermal noise in the photodetectors. To eliminate this noise, the detectors have to be cooled to freeze out the X-centers. This involves operating the detectors at a lower temperature than would be needed if there were no X-levels present. In some applications, this extra cooling is a severe handicap.

D-1 R.Baron, M.H. Young J.K. Neeland, and O.J. Marsh, Appl. Phys. Lett. 30, 594 (1977).

D-2 M.W. Scott, Appl. Phys. Lett. 32, 540 (1978).

Several models have been suggested for the indium-X center. The center has been found to depend on carbon, and substitutional indium-carbon pair model has been suggested.[D-3, D-4] The energy level of the defect, between indium and aluminum, has also suggested In-Al distant pairs.[D-5] The fact that the X-center concentration increases with irradiation has suggested that the center may be an indium-interstitial or vacancy-related defect.[D-6] Finally, EPR data have shown transition metal ions and acceptors form complexes.[D-7] This has suggested Fe_i-In_s pairs for the X-Center.[D-8]

This paper has two major aims. The first is to show that there is an X-center for each of the group IIIA elements in silicon. The second is to present the optical, thermal, and chemical evidence we have obtained which supports the identification of these defects as being nearest-neighbor substitutaional carbon-acceptor pairs.

[D-3] R. Baron, J.P. Bankus, S.D. Allen, T.C. McCill, M.H. Young, H. Kumura, H.V. Winston, and O.J. Marsh, Appl. Phys. Lett. 34,

[D-4] C.E. Jones, D.E. Schafer, W. Scott, and R.J. Hager, Bull. Am. Phys. Soc. 24, 276 (1979) BL14.

[D-5] M.C. Ohmer and J.E. Lang, Appl Phys. Lett. 34, 750 (1979).

[D-6] V. Swaminathan, J.E. Lang, P.N. Heminger, and S.R. Smith, Appl. Phys. Lett. 35, 184 (1976).

[D-7] G.W. Ludwig and H.H. Woodbury in Solid State Physics, 13, F. Switz and D. Turnbull, Eds. (Academic Press, New York, 1962), p. 223.

[D-8] J. Schneider talk presented at the International Conference on the Physics of Pure Semiconductors, Stockholm, Sweden, 3-5 Sept. 1979.

EXPERIMENTAL

Several experimental techniques were used to characterize the samples and to determine the properties of the X-center. These include low-temperature infrared absorption, thermal annealing, deep-level transient spectroscopy (DLTS) and Hall analysis.

Infrared Sepctroscopy

Transmittance measurements were made using a Digilab FTS-14 Fourier transform spectrometer at a resolution of 2 cm^{-1}. The samples were lapped and polished with about 0.5^{o} taper to eliminate interference fringing and cooled to about 8K for the measurements. The transmittance was converted to absorption coefficient in the usual way[D-9] and digitally stored in the spectrometer. The transmittance of a high-purity vacuum float-zone-grown crystal measured and used as a reference to subtract out any lattice absorption, particularly in the 400- to 1000-cm^{-1} region. Signal averaging of 1200 to 2400 scans was used to increase the signal-to-noise ratio to obtain sufficient accuracy with the low concentrations.

The samples were taken from a variety of sources and grown by a variety of different growth techniques. Most of the indium-doped crystals were grown by a solution-growth process developed in our laboratory,[D-10] with a few grown by the Czochralski method,

---

D-9 T.S. Moss, Optical Properites of Semiconductors (Academic Press, New York, 1959) p. 14.

D-10 W. Scott and R.J. Hager, J. Electron. Mater. 8, 581 (1979).

and one float-zone-grown crystal. [D-11] The aluminum-doped and gallium-doped samples were obtained from crystals grown in our laboratory by the Czochralski technique. The boron-doped crystals were purchased from Dow-Corning and consisted of crystals which were grown by the Czochraliski method and crystals which were grown by the float-zone method. The results we obtained did not appear to be unique to any one particular growth method nor to any source of crystals. The specifics on crystal identifications are not emphasized here for this reason, but where appropriate, any further crystal identification is included with the results being discussed.

The concentrations of the group IIIA acceptor in the crystals are determined from the room temperature Hall coefficient for the case of indium-doped silicon, and from the resistivity curves recently published by Sclar for boron-, aluminum-, and gallium-doped silicon. [D-12]

Low-temperature optical absorption shows a series of peaks due to transitions from an s-like ground state to p-like effective-mass excited states.[D-13] The concentrations determined from the Hall and resistivity data hve been used to determine a calibration constant relating the area of the strongest of these peaks at 8K to the concentration of the group IIIA element. The 8K optical spectrum was then used on most samples to determine acceptor concentration.

[D-11] Float-zone indium-doped silicon supplied by Dr. Sumner of U.S. Army NVL.

[D-12] N. Sclar, IEEE Trans. Electron. Devices Ed-24, 709 (1977).

[D-13] D. Schechter, J. Phys. Chem. Solids 23, 237 (1962).

Both interstitial oxygen and substitutional carbon have vibrational bands which can be seen in the IR absorption. The relationship between the peak absorption and the oxygen or carbon concentrations has been estimated at room temperature and is given in ASTM F120-75 and F121-76 for oxygen and in Newman and Wills[D-14] for carbon. Samples were measured at room temperature using these calibration factors to determine the oxygen and carbon concentrations. The same samples were then measured at 77K and 8K to determine low-temperature calibration factors. The wavelengths and the 8K calibration constants are given in Table D-1 for the acceptors and for carbon and oxygen. The concentrations of the X-centers were determined solely from optical absorption measurements as will be described in detail in the next section.

TABLE D-1. OPTICAL CALIBRATION FACTORS AT 8K

Impurity	Line (cm^{-1})	Concentration (cm^{-3})
Boron	279	[B] = peak area/6.6 x 10^{-14}
Boron	666	= peak/6 x 10^{-15}
Aluminum	472	= area/2.4 x 10^{-14}
Gallium	$\sim$ 510	= area/ 2 x 10^{-14}
Indium	1175	= area/5 x 10^{-16}
Thallium	1907	= area/8.5 x 10^{-17}
Carbon	600	= α peak x 6.7 x 10^{16}
Oxygen	1136	= α peak 3.09 x 10^{16}
B-X	184	= area/9.5 x 10^{-14}
Al-x	373	= area/4 x 10^{-14}
Ga-X	381	= area/4 x 10^{-14}
In-X	830	= area/3.5 x 10^{-15}
Phosphorus	315	= area/9.94 x 10^{-14}

D-14 R.C. Newman and J.B. Willis, J. Phys. Chem. Solids 26, 373 (1965).

Thermal Annealing

The X-center concentrations depend on the sample's last annealing temperature. Before the infrared spectra are taken, the samples are placed in a furnace in dry N_2 gas and annealed until equilibrium X-center concentrations are reached. The equilibrium condition was checked by annealing the samples for a longer time at the same temperature to see if the concentration changed. For float-zone silicon, the annealing times used were $\sim$ 12 hours and near 600°C and $\sim$ 6 hours near 1000°C. For Czochralski silicon $\sim$ 4 hours near 600°C and $\sim$ 2 hours near 1000°C were used. These times are conservative and are not the minimum times needed for equilibrium. Baron et al. used 0.5 hour and 1 hour anneals at 650°C and 850°C, respectively, for Czochralski crystals[D-3] but they found these times to be inadequate for float-zone crystals. We found that a 6-hour anneal is too short for equilibrium to be reached at 600°C for float-zone crystals. Once equilibrium is reached, the X-level concentrations in float-zone and Czochralski silicon follow the same curves as is shown later in Figure D-8. The time to reach equilibrium is much slower in float-zone crystals however.

Deep-Level Transient Spectroscopy

Deep-level transient spectroscopy (DLTS)[D-15, D-16] has been used to study trapping in indium and thallium doped silicon. This technique measures the capacitance of a reverse-biased diode. The

---

[D-15] D.V. Lang, J. Appl. Phys. 45, 3014 and 3023.

[D-16] G.L. Miller, D.V. Lang, and L.C. Kimmerling, Am. Rev. of Mater. Sci. 7, (1977).

capacitance depends on the fixed charge in the depletion region. N^+p diodes were made in silicon doped with boron as well as indium or thallium. The boron concentration is held to about 10 times that of the indium or thallium. Short voltage pulses are used to bring free carriers into the depletion region where some of them are trapped. After the filling pulse, these trapped carriers are thermally emitted, producing a transient in the observed capacitance. The signal is processed electronically to provide a "spectral" display with a peak for each trap. The peak heights can be related to the trap concentration and the peak position gives the emission rate as a function of temperature. The change in the emission rate with temperature is used to calculate the trap energy.

Hall Technique

D-C Hall data were also taken on many of the samples over the temperature range of 40K to 300K. The Hall coefficient, resistivity, and mobility were measured. A computer program which does a multivariable least squares fit to these data was used on some samples to fit concentrations and energy levels.

RESULTS

In indium-doped silicon, an indium-dependent acceptor level called the X-level has been observed in Hall data.[D-1] This level occurs at 0.113 eV, 72% of the substitutional indium's energy, and in concentrations $\sim 10^{-2}$ to 10^{-4} times that of the indium in pulled crystals. This level was subsequently seen in the infrared optical absorption spectra.[D-2] Figure D-1 shows an absorption spectra for Czochralski-grown indium-doped silicon showing the 606-cm^{-1} carbon band, the 113-cm^{-1} oxygen band, and

the indium lines near 1200 cm^{-1}.

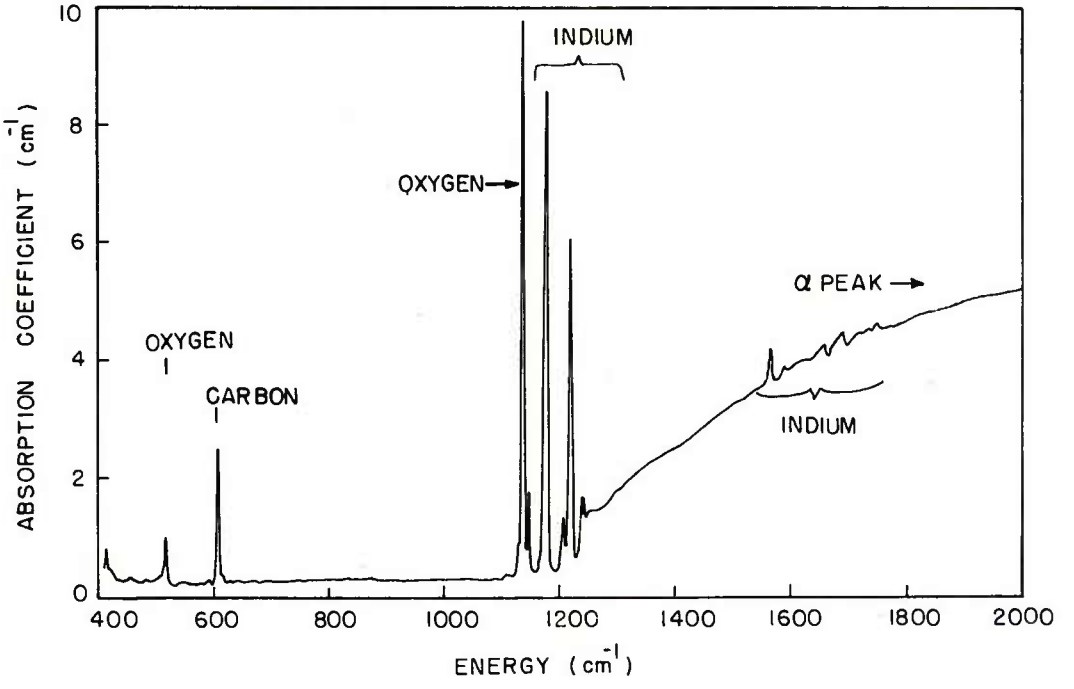

Figure D-1. Optical absorption spectrum of indium-doped silicon at 8K showing the prominent indium lines in addition to the lines due to oxygen and carbon.

Figure D-2, a scale expansion of the region lower in energy than the indium lines, shows a weak absorption spectra, labeled X, which has the same characteristic four-line acceptor effective-mass spectra as indium has.[D-2, D-13] This type of spectra arises from transitions from an s-like ground state to p-like excited states. The s-state penetrates the acceptor's core region and differences in local screening shift this level's energy different amounts in different acceptors. The p-type excited states have a node at the core and they are diffuse enough so that their energies are the same as those calculated by effective mass

theory for all of the substitutional group IIIA acceptors. Thus, the s-state energy shift changes the infrared absorption energy for various acceptors, while the constant p-like final states give the same characteristic pattern to all the acceptor infrared spectra.

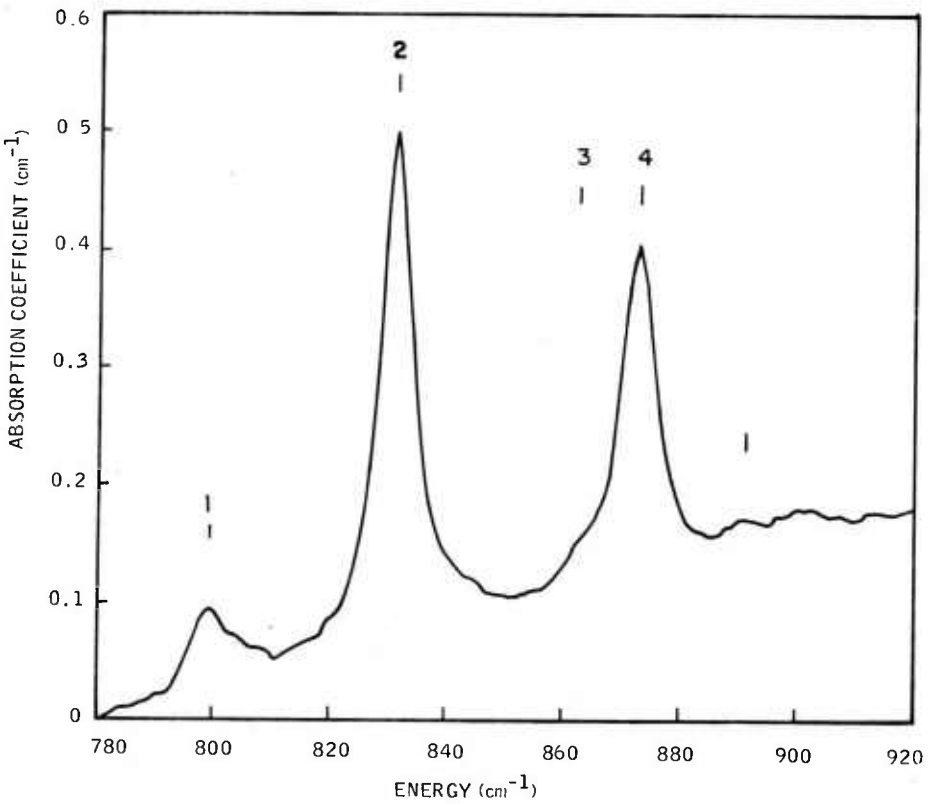

Figure D-2. Optical absorption spectrum of indium-doped silicon at 8K showing the indium-X lines for a sample with 4 x 10^{17} In/cm^3.

The energy for an acceptor can be found by adding the energy seen in the optical absorption spectra for the s-to-p transition to the calculated effective mass energy of the p-state to the continum. When this is done for the lines labeled X, an energy of

0.112 eV is obtained, which is the same value as measured by the Hall technique for the In-X center.

The optical spectra for silicon doped with the other group IIIA elements (B, Al, Ga, and Tl) have now been studied. In every case except for thallium, a defect spectrum is observed at energies slightly less than the substitutional acceptor's energy, with intensities down 10^{-2} to 10^{-5} in magnitude. These spectra have been designated as B-X, Al-X, Ga-X, and In-X spectra and are shown in Figure D-3 along with the substitutional boron spectrum for comparison. It is seen that in each case the number of lines, intensity ratios, and line splittings are similar to those observed in the boron acceptor effective-mass spectrum. The energy differences are listed in Table D-2 showing the same characteristic spacing as the boron acceptor spectrum. Having identified the spectra as being acceptor effective-mass-like spectra, the X-center energy can be obtained by adding the measured s-to-p optical absorption energy to the calculated effective-mass p-to-continuum energy. These energies are given in Table D-3. The ratios of the X to acceptor energies are seen to run in a smooth progression from 0.84 for boron to 0.72 for indium.

As was described in the previous experimental section, Hall and resistivity data were used to determine the calibration factors so that the group IIIA acceptor concentrations could be found from the strong (no. 2) s-to-p optical cross sections at 8K. These data are plotted in Figure D-4. The optical cross sections for the s-to-p absorption varies smoothly with the acceptor energy. Deeper acceptors have smaller s-like wave functions and smaller cross sections. The curve drawn through the data for the substitutional acceptors was used to estimate the calibration factors for the X-centers. These are also shown in Figure D-4,

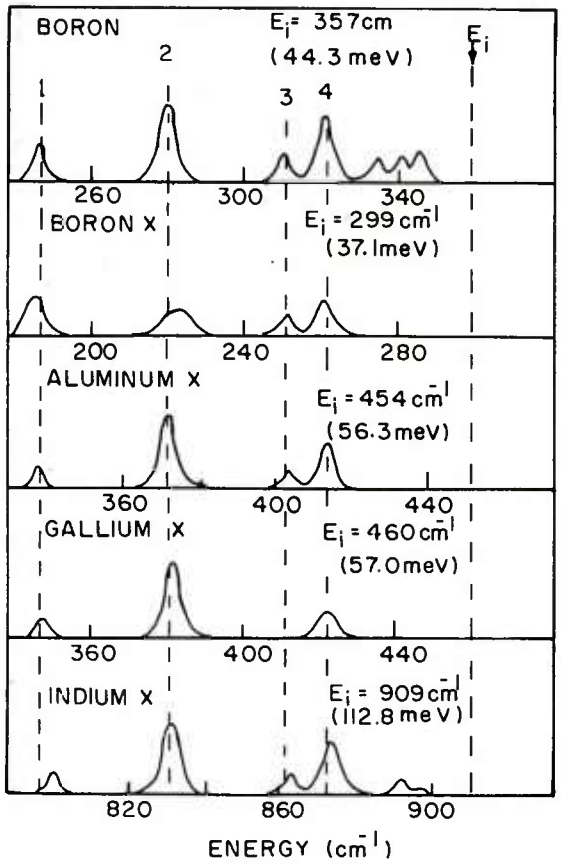

Figure D-3. Absorption spectra of substitutional boron in silicon and of the X-centers observed for boron, aluminum, gallium, and indium.

and the corresponding calibration factors from peak area to concentration are listed in Table D-1. The concentrations for all of the X-centers are then calculated from the area of the strong (no. 2) peak in the absoprtion spectra at 8K. The X-center concentrations observed run from about 10^{-2} to 10^{-5} those of the substitutional group IIIA acceptor concentrations.

TABLE D-2. OPTICAL ENERGIES AND SPACINGS FOR THE X-CENTER AND BORON

Defect	Energy (cm^{-1})				Spacings (cm^{-1})		
	Line 1	Line 2	Line 3	Line 4	Lines 1 to 2	Lines 2 to 3	Lines 2 to 4
Boron	245	279	310	323	34	31	44
B-X	184	220	250	261	36	31	41
Al-X	338	372	404	414	34	32	42
Ga-X	347	381		423	34		42
In-X	799	831	863	873	32	32	42

TABLE D-3. X-CENTER DATA

Dopant	E(X) (meV)	E(ACC) Substitutional Dopant (meV)	E(X)/E(ACC)	[X]/[ACC] Pulled Si	E_A (eV)
B	37.1	44.3	0.84	10^{-2}	0.03
Al	56.3	68.5	0.82	10^{-2}-10^{-3}	0.28
Ga	57.0	72.7	0.79	10^{-4}-10^{-5}	0.40
In	112.8	156.0	0.72	10^{-2}-10^{-4}	0.70
Tl	180.0	246.0	0.73	10^{-2}	--

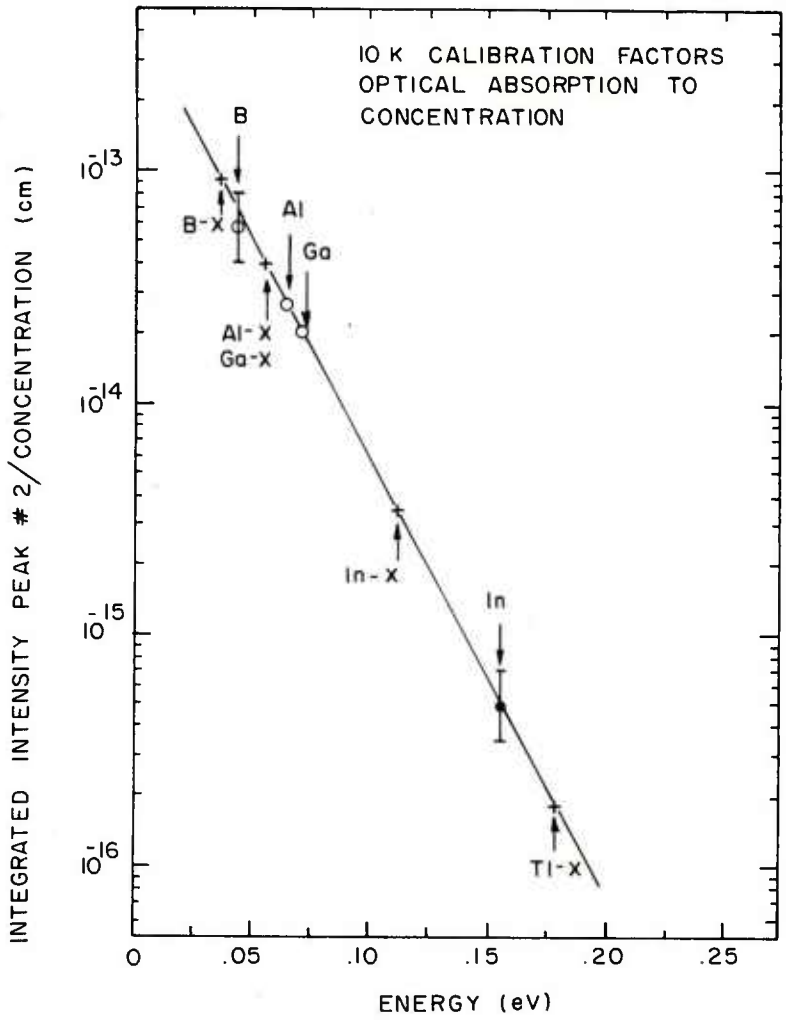

Figure D-4. Calibration factors for converting the area of peak no. 2 in the acceptor absorption spectra at 10K to concentration. The B, Al, Ga, and In points are experimental data. The X-center factors are estimated from these data.

The indium-X center was also observed in deep-level transient spectroscopy.[D-17] A spectrum for indium-doped silicon is shown in part (a) of Figure D-5. Four hole traps are seen in the spectrum. The DLTS energies were measured at 0.095 eV, 0.126 eV,

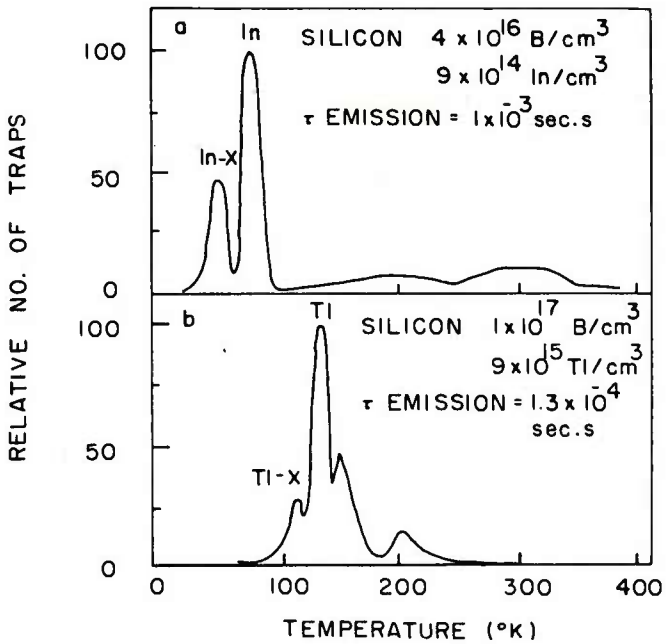

Figure D-5. DLTS spectra for indium-doped silicon (a) and thallium-doped silicon.

0.31 eV and 0.45 eV. Electric fields lower the observed energies of acceptors [D-18] and this was found to be the case for the first two traps.[D-17] A correction for the electric field effects derived by Hartke[D-18] was applied to these two traps. The corrected energies are ∿ 0.11 eV and ∿ 0.143 eV near the proper indium-X and indium energies of 0.113 eV and 0.15 eV. a DLTS spectrum for thallium-doped silicon is shown in part (b) of Figure D-3. The

---

[D-17] C. Jones and G. Johnson, IRIS Specialty Group in Infrared Detectors, Minneapolis, MN (June 1979). Also sub. J. Appl. Phys. 1980.

[D-18] J.L. Hartke, J. Appl. Phys. 39, 4871 (1968).

structure is similar to that in the indium spectrum, with a major peak for the major dopant, thallium, a weaker lower energy peak to its left, and two higher-energy peaks. Again, the DLTS energy for the major dopant, thallium, is low, being $\sim$ 0.20 eV instead of 0.245 eV, and the lower-energy peak occurs at $\sim$ 0.14 eV. If a field correction is assumed for the first two peaks of $\sim$ 0.40 eV to bring the thallium energy up to its proper value, the peak marked Tl-X would have an energy of $\sim$ 0.18 eV. Hall and optical absorption data were taken on adjacent pieces of thallium-doped silicon crystal. The optical absorption showed $\sim 10^{16}$ Tl/cm^3 but no shallower X-like level. The thallium concentrations and energies determined from the optical data were put into the computer program fitting the Hall data and the program was allowed to determine the parameters for any other acceptors needed to fit the data. The computer fit the Hall data with 9.3×10^{15} thallium and another acceptor at 0.18 eV and 4×10^{14}/cm^3 concentration, confirming the DLTS data on the lower-energy defect.

The Tl-X center at $\sim$ 0.18 eV is much deeper than the other X-centers, giving it tighter wave functions and a smaller optical cross section. This fact and the low thallium concentrations (10^{16} -10^{17}/cm^3) in the samples studied would make it very hard to observe a Tl-X absorption spectrum. As yet, we have been unable to distinguish an X-type spectrum in the thallium infrared data.

The concentrations of the X-centers have been observed to change, depending on annealing. Data for the indium-X-center concentration is presented in Figure D-6. Different concentrations are seen in different samples but in all of these samples the X-center concentration decreases as the temperature increases and can be fit to an exponential form[D-3, D-4]

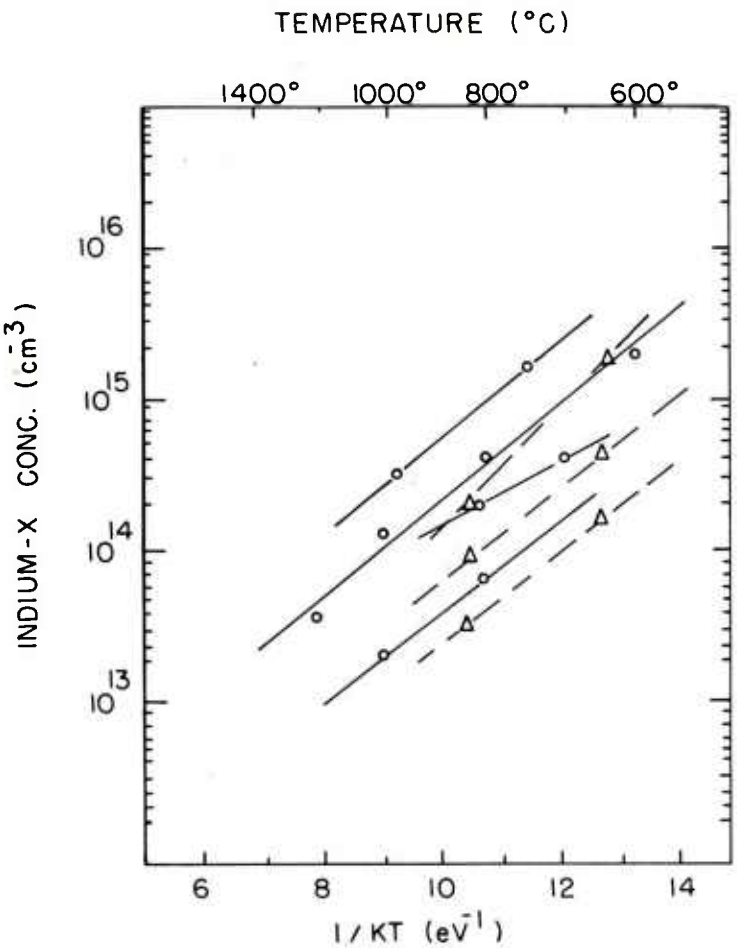

Figure D-6. Indium-X-center concentration as a function of annealing temperature (circles are Honeywell data, triangles are Hughes data[D-3]).

$$[\text{In-X}] = [\text{In-X}]_o e^{E_A/KT} \qquad \text{(D-1)}$$

with an activation energy E_A of 0.70 eV. The X-centers do not anneal out up to the silicon melting point and the annealing is cyclic. The concentration can be lowered by annealing at a high temperature and then brought back to its original value by annealing it at its original annealing temperature.

The infrared absorption spectra have been used to monitor the X-center, carbon, oxygen, boron, aluminum, gallium, indium, and thallium concentrations. The data for indium-doped silicon are shown in Figure D-7. The indium-X-center concentration is normalized to the indium concentration and plotted with respect to carbon, oxygen, indium, and boron. The aluminum, gallium, and thallium concentrations were all too small to be detected optically, placing the electrically active concentration of aluminum at less than $2 \times 10^{12}/cm^3$, of gallium at less than $2 \times 10^{12}/cm^2$, and of thallium at less than $2 \times 10^{15}/cm^3$. The X-center concentrations used in Figure D-7 were all adjusted to 600°C equilibrium values using Equation (D-1).

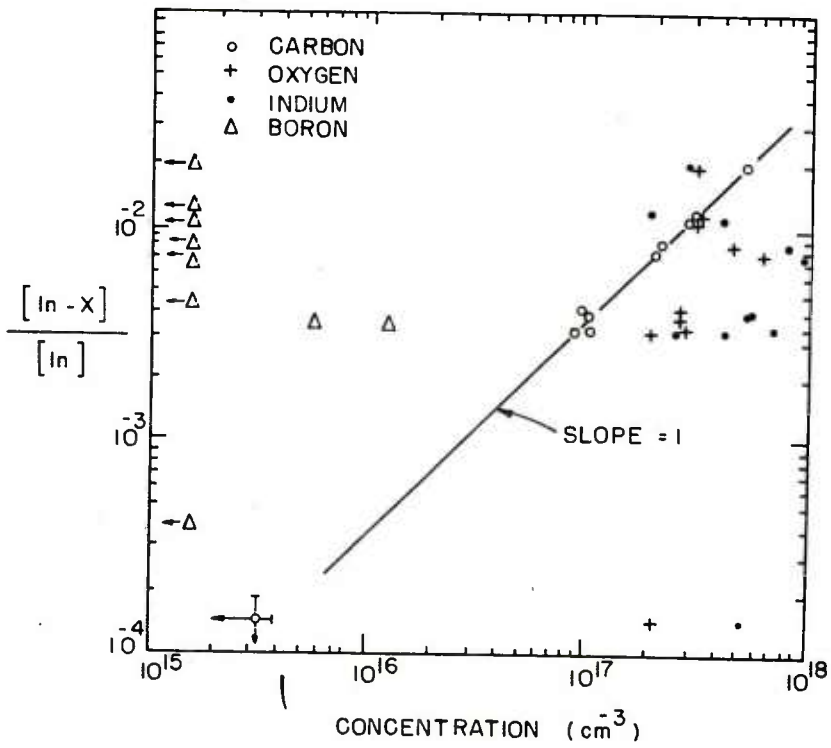

Figure D-7. Normalized indium-X-center concentrations ([In-X]/[In]) versus carbon, oxygen, boron, and indium concentrations. The X-concentrations have been adjusted using the data from Equation (D-1) to 600°C equilibrium values.

The data in Figure D-7 for indium-doped silicon show no In-X-center dependence on oxygen, boron, or more than one indium atom per complex. There is a linear relationship seen between the [X]/[In] ratio and the carbon concentration. The slope of the line through the data is 1, implying the X-center depends on only a single carbon per complex. The carbon dependence shown in Figure D-7 is the same as that reported by the Baron et al. group for the samples they measured.[D-3] The carbon dependence was checked by growing two crystals out of indium[D-10] with low-carbon, vacuum float-zone silicon as the source and seed material. One sample was intentially carbon-doped. The two samples grown had the same indium, oxygen, and aluminum concentrations, with the undoped sample having less than $5 \times 10^{15} C/cm^3$ and no measurable X-centers ($<5 \times 10^{13} X/cm^3$), while the carbon-doped sample had $9 \times 10^{16} C/cm^3$ and $2 \times 10^{15} X/cm^3$ after a 600°C anneal. This confirms the carbon dependence of the In-X center seen in Figure D-7.

The simplest reaction between carbon and an acceptor is

$$C + A \underset{\leftarrow}{\overset{K}{\rightleftarrows}} X \qquad \text{(D-2)}$$

The equilibrium constant, K, for this reaction is equal to[D-19]

$$K = \frac{[X]}{[A][C]} = K_o e^{\Delta F/kT} \qquad \text{(D-3)}$$

where the brackets denote concentration and ΔF is the difference in the Gibbs' free energy for the reaction in Equation (D-2). The data in Figure D-6 has been renormalized to $[X]/[In][C]$ to fit

---

[D-19] R.A. Swalin, Thermodynamics of Solids, (John Wiley & Sons, New York, 1962) Chapter 14.

Equation(D-3). These data, along with similar annealing data for the boron, aluminum, and gallium-X centers are shown in Figure D-8. The fact that the normalization of Equation(D-3) has collapsed the indium-X data in Figure D-6 to a single line is another strong piece of evidence supporting the dependence of the X-centers on a single carbon and a single acceptor atom.

The Gibbs' free energy difference in Equation (D-3) is $\Delta F = \Delta H - T\Delta S$, where ΔH is the change in enthaply and ΔS is the change in entropy.

$$K = K_o e^{-\Delta S/k} e^{\Delta H/kT} \qquad \text{(D-4)}$$

In this model the slopes of the lines in Figure D-8 can be related to ΔH, which would be expected to be close to the defect binding energies (0.03 $\pm$ 0.05 eV for the boron-X center, 0.28 $\pm$ 0.05 eV for the aluminum-X, 0.40 $\pm$ 0.05 eV for the gallium-X, and 0.70 $\pm$ 0.05 eV for the indium-X center). The infinite temperature intercept is related to the defect entropy. Differences in vibrational frequencies or configuration can change the intercept value.

Mott and Gurney use an Einstein model where each atom has three vibrational modes of a single frequency.[D-20] The entropy per mode is given as

$$S_{vib} = k \ln \frac{h\nu}{kT} \qquad \text{(D-5)}$$

[D-20] N.F. Mott and R.W. Gurney, Electronic Process in Ionic Crystals.

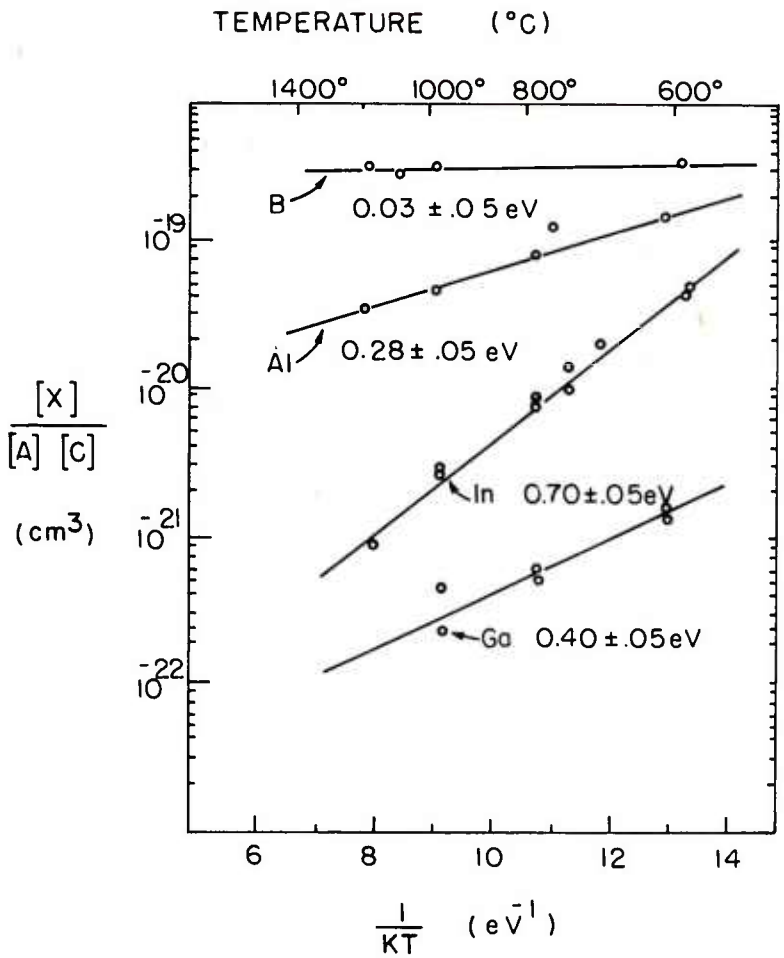

Figure D-8. Normalized equilibrium concentration of the X-centers as a function of temperature. The quantity $[X]/[A][C]$ is equal to the equilibrium constant for the reaction $A_s + C_s \underset{\leftarrow}{\overset{K}{\rightarrow}} X$.

The lighter atoms in the group IIIA series would be expected to have higher frequency modes and higher infinite temperature intercepts. Boron is the only acceptor with a radius smaller than silicon. Because of this, it could sit off-center from the substitutional site, giving rise to a configurational entropy term

and further raising the boron intercept. These effects are seen as a general trend in the infinite temperature intercepts.

The tetrahedral radii for the atoms in question are:[D-21]

Carbon	0.774 Å
Boron	0.853
Silicon	1.173
Gallium	1.225
Aluminum	1.23
Indium	1.405
Thallium	1.47

Carbon and boron are smaller than silicon, while the other group IIIA elements are larger. Baron et al[D-3] suggested that the indium-X-center binding energy could be due to strain relief of the substitutional indium by a nearest-neighbor carbon. The small boron binding energy and the increase in binding through the group fits this suggestion. The fact that the boron-X center is bound at all and the 0.12 eV difference in binding for the aluminum and gallium-X centers with the same acceptor radii say that there is also a small component to the X-center binding energy due to the defects' electronic bonding.

Stress Symmetry

The absorption spectrum of the aluminum-X center has been studied as a function of uniaxial stress. A full analysis of the stress data is being published in an associated article. A summary of the stress data is shown in Figure D-9 and a review of the restuls is given here.

D-21 J.C. Phillips, Bonds and Bands in Semiconductors, (Academic Press, New York, 1973 p. 22

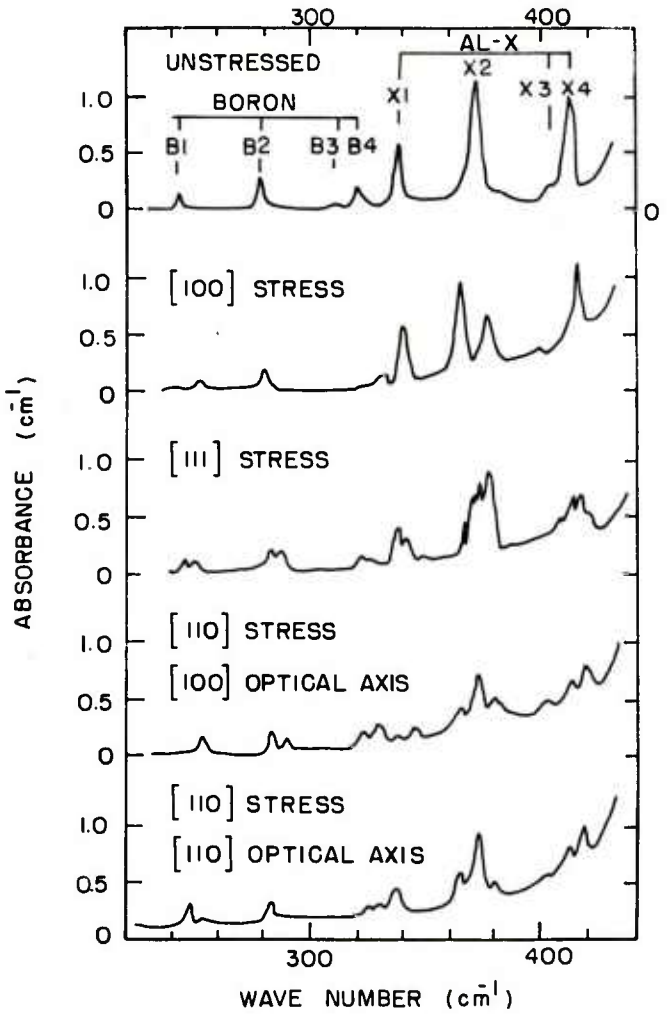

Figure D-9. Absorption spectra showing substitutional boron and the aluminum-X center at 8K under unstressed and [100], [111], and the two inequivalent [110] uniaxial stress conditions.

Multiple lines are introduced into the optical data by the stress due to two effects. The first is the splitting of degenerate levels by the stress and the second is that a complex defect can have several possible orientations relative to an applied stress. The second effect is called a configurational effect. The data

shown in Figure D-9 can be explained by a model involving the following assumptions:

1. The X-center ground state is an orbital singlet with spin degeneracy g = 2.

2. The excited states will split in the same way as the excited states of the substitutional acceptors.

3. The structure not explained by assumptions 1 and 2 is due to configurational effects.

Assumption 1 is due to the fact that no optical absorption lines could be identified as being due to a split-off ground state. A substitutional acceptor has a ground-state degeneracy of four but the crystal field from any nontetrahedral complex would be expected to split these into two spin-doublet levels. Spectra taken up to 50K showed no sign of populating this second level, so the local crystal field is presumed to have split these levels into two spin doublets more than 10 meV apart. Assumption 2 rests on the argument that the excited states are very diffuse and have a node at the defect. Figure D-3 shows optical transitions from a ground state to the excited states. The X-center crystal field has not perturbed the excited states, as is shown by the effective-mass-like spectra. The stress effects for the excited X-center levels should then be the same as for a substitutional acceptor like boron. The sample shown in Figure D-9 has both aluminum-X and substitutional boron in it which can be seen in the same region of the spectrum. The [100] stress data for the aluminum-X center have approximately the same form as that of boron. The [111] and [110] stress spectra are more complex than the boron spectra. The extra lines in the latter two stress directions can be explained by two inequivalent orientations of the X-complex relative to the stress direction. The only defect symmetry

in which the possible orientations would make equal angles with a [100] stress but two different angles with respect to a [111] or a [110] stress is a trigonal [111] oriented defect. Each of the four equivalent [111] directions of such a defect structure makes the same angle with respect to a [100] stress but there are two angles formed between these directions and a [111] or [110] stress.

DISCUSSION

A Class of Defects

In the first part of this paper a group of defects in silicon was singled out for study. These defects occurred in silicon doped with a group IIIA acceptor, with one defect being associated with boron, aluminum, gallium, indium, and thallium. The concentrations observed in Czochralski-grown silicon are $\sim 10^{-2}$ to 10^{-5} those of the corresponding group IIIA element's concentration. The optical, Hall, and DLTS data have shown that these centers are electrically active acceptors having energies $\sim$ 75% to 85% that of the respective substutional group IIIA element's energy. All of these centers showed the same high-temperature stability and cyclic annealing properties. Taken as a whole, the similarities in properties for the defects we have called X-centers strongly identifies them as being a class of similar defect complexes. Specifically:

- Each X-center is seen in silicon doped with a different group IIIA acceptor.
- The X-center energies are all $\sim$ 80% those of the corresponding acceptor's energy.

- They are all stable up to the silicon melting point, with larger concentrations resulting from lower-temperature annealing.
- They can be cyclically annealed.
- The annealing kinetics all fit $A + C \rightleftarrows X$ reaction kinetics.
- The binding energies follow a smooth progression through the group.

X-Center Model

Aluminum has been suggested as being involved in the In-X center.[D-5] If this is true, we feel substitutional aluminum should have been seen after high-temperature anneals when the X-center is broken apart. The concentrations expected are in the $10^{15}/cm^3$ range for some samples and this is far above the possible compensation levels which could make it go undetected. Iron has also been suggested.[D-8] So far, we have not seen iron in the DLTS data but iron cannot be eliminated on the basis of our data. The chance exists that iron is completely tied up in complexes that we cannot detect.

Figure D-7 shows a linear relationship between the indium-X-center concentration and carbon. No relationship is seen for boron, aluminum, or oxygen. Figure D-8 shows that normalizing the indium-X concentration to both indium and carbon collapsed the indium annealing curves in Figure D-6 to a single curve. This normalization fits the form predicted from the thermodynamics of the reaction $A + C \overset{K}{\rightleftarrows} X$, where $K = K_o \exp(E_{A/KT}) = [X] / [A][C]$. Two

indium-doped crystals grown from the same materials, except that one was carbon-doped, had no measurable In-X in the undoped crystal and 2 x 10^{15}in-X/cm^3 in the carbon-doped crystal. All of these factors identify the X-centers as involving carbon and a group IIIA acceptor.

The irradiation data[D-6] suggested that vacancies or interstitials may be involved in the X-centers. The annealing temperatures for some of the known acceptor interstitial or vacancy-related defects are given in Table D-4. These annealing temperatures are all within a few hundred degrees of room temperature. In none of these cases can the defect concentrations be cyclically annealed. Once a vacancy or interstitial center is annealed to a low concentration, reannealing at a lower temperature does not bring back the original concentration. It is the high thermal stability and cyclic annealability of the X-centers that leads us to the conclusion that they involve substitutional atoms and not interstitials or vacancies.

The X-centers have a binding energy tending to form the complex, while thermal energy tends to break the components apart. This fits the concentration versus annealing data shown in Figure D-8. Again, if the components of the complex are substitutional atoms, they are not eliminated when the complex is thermally broken apart. This explains the ability to cyclically break up and then reform the complexes when the sample is brought to equilibrium at high and then low temperatures.

The X-center model suggested by the data now involves a substitutional acceptor and a substitutional carbon atom. It is the stress data which puts these atoms at nearest-neighbor sites. The

TABLE D-4. ANNEALING TEMPERATURES FOR SOME INTERSTITIAL AND VACANCY-RELATED DEFECTS

Defect	Approx. Annealing Temperatures[a] (time = 1000 sec)
V^{O}	150K
$V^{=}$	70K
P-V	400K
As-V	440K
Sb-V	460K
Al-V	500K
Al_s-Al_i	520K
C_s-C_i	550K
Al_i	500K
V-V	550K
O-V	600K

[a]Data complied by H.J. Stein, Radiation Effects in Semiconductors (Eds. J.W. Corbett and G.D. Watkins, Gordon and Breach, London 1971) pp. 125-140, and R.C. Newman, Infrared Studies of Crystal Defects (Taylor and Francis, London, 1973).

nearest-neighbor axis in silicon is in the [111] directions, which was the symmetry found from the stress data. The model is shown in Figure D-10. Distant pairs would not be expected to show the distincy [111] stress symmetry.

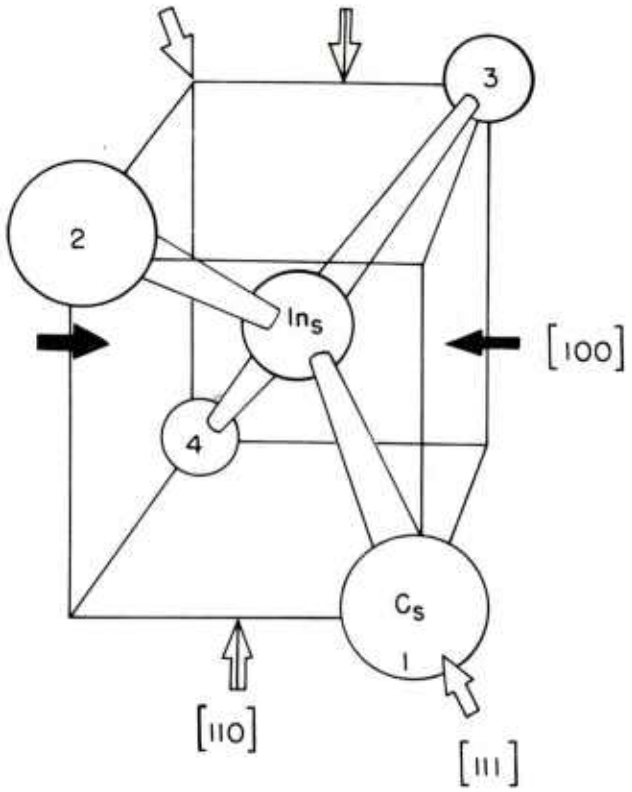

Figure D-10. Model of the indium-X center showing the stress axis. The carbon atom can occupy nearest neighbor sites 1, 2, 3, or 4, giving rise to the different configurations under stress.

X-Center Energy Level Calculation

To determine if the nearest-neighbor substitutional acceptor-carbon pair is a reasonable model for the X-centers, a calculation was made to estimate this model's expected energy levels.

A mathematical technique which has been used to obtain reasonable results for the energy levels, wave functions, and configurations for defects in diamond and silicon is the extended Hückel cluster

technique.[D-22-D-26] A defect is surrounded by three shells of silicon atoms in the normal crystal lattice positions. The cluster is then treated as a large molecule and a liner combination of atomic orbitals (LCAO) technique is used to calculate the energy levels and wave functions.

The molecular orbitals, Ψ_i, are taken as a linear combination of Slater functions, ϕ_v, representing the valence atomic orbitals of the cluster atoms:

$$\Psi_i = \sum_v C_{vi}\phi_v \qquad \text{(D-6)}$$

$$\phi_i = N_i \; r^{n-1} e^{-\xi r} Y_{ln} \qquad \text{(D-7)}$$

where N_i is a normalization constant, ξ is an orbital exponent related to the atomic screening, n is the principal quantum number, and Y_{ln} is a spherical harmonic. The energies of the molecular orbitals are calculated as

$$E_i = \frac{\langle \Psi_i | H | \Psi_i \rangle}{\langle \Psi_i | \Psi_i \rangle}$$

D-22 R.P. Messmer and G.D. Watkins, Phys. Rev. B7, 2568 (1973).

D-23 C. Weigel, D. Peak, J.W. Corbett, G.D. Watkins, and R.P. Messmer, Phys. Stat. Sol. b 63, 131 (1974).

D-24 V.A. Singh, C. Weigel, J.W. Corbett, and L.M. Roth, Phys. Stat. Sol. b 81, 637 (1977).

D-25 K.L. Yip, Phys. Stat. Sol. b 66, 619 (1974).

D-26 C.E. Jones, Bull. Am. Phys. Soc. 22, 382 (1977) EO14.

where H is the Hamiltonian operator. The energies are minimized with respect to the coefficients, C_{vi}, giving rise to the secular equations

$$\sum_{v} (H_{\mu v} - E_i S_{\mu v}) C_{vi} = 0 \qquad \text{(D-9)}$$

where

$$H_{\mu v} = \langle \phi_\mu | H | \phi_v \rangle \qquad \text{(D-10)}$$

and

$$S_{\mu v} = \langle \phi_\mu | \phi_v \rangle \qquad \text{(D-11)}$$

The extended Huckel method involves approximating the $H_{\mu v}$ matrix elements by

$$H_{\mu\mu} = -I_\mu \qquad \text{(D-12)}$$

$$H_{\mu v} = \frac{1}{2} K (H_{\mu\mu} + H_{vv}) S_{\mu v} \qquad \text{(D-13)}$$

where I_μ is an emperical ionization energy and K is a constant taken to be 1.75. The secular equations (D-9) are solved for the molecular orbital energies, E_i, and the molecular orbital coefficients, C_{vi}. The total energy in the extended Hückel technique is taken as being

$$E_{total} = \sum_{i} n_i E_i \qquad \text{(D-14)}$$

where n_i is the occupation number of the ith state.

The calculations were first run on some known test cases: pure silicon, substitutional indium, substitutional carbon, and interstital carbon. The parameters used are given in Table D-5. The results are shown in Figure D-11. The pure silicon calculation gave a bandgap of 1.01 eV, with E_c 7.4 eV below the vacuum level and with an 11-eV-wide valance band. This compares well with the experimental values of 1.16 eV for the bandgap, with E_c 5.4 eV below the vacuum level and a 13.6-eV-wide valance band. Carbon substitutional gave no defect levels in the gap as is the experimentally observed case. Carbon interstitial in the split [100] configuration suggested by EPR results[D-27] gave a deep donor level as is seen experimentally. Substitutional indium gave a calculated level at E_v + 0.166 eV close to the actual level at E_v + 0.156 eV.

The position of a defect's energy level has been found to depend on the interaction of the defect's atomic levels and the levels of the same symmetry in the host crystal's bands.[D-28] The good results for the pure-silicon bandgap and bandwidths and the good results for the indium and carbon test defects suggest that as crude as the extended Hückel approximation is, it may be calculating a reasonable average density of states for the silicon crystal. This gives some reason to suggest that the technique should be able to be used to describe other similar defects.

[D-27] G.D. Watkins and K.L. Brower, Phys. Rev. Lett. 36, 1329 (1976).

[D-28] H. Hjalmarson, Thesis, U. of Illinois, Physics Dept. (1979).

TABLE D-5. PARAMETERS USED IN EXTENDED HUCKEL CALCULATIONS

Atom	Wave Function	Energy (eV)	Exponent
Silicon	3s	-14.66[f]	1.6344[a]
	3p	- 8.068	1.4284[a]
Surface silicon	3s	- 8.1	1.63[a]
Indium	5s	-11.47[c]	1.9023[b]
	5p	- 5.787	1.6940[b]
Carbon	2s	-19.20[e]	1.6083[a]
	2p	-11.79	1.5679[a]
Aluminum	2s	-10.62[d]	1.3724[a]
	2p	- 5.986	1.3552[a]
Oxygen	2s	-13.62	2.2458
	2p	-17.19	2.2266[a]

[a]E. Clementi and D.L. Raimondi, J. Chem. Phys., 38, 2686 (1963).

[b]E. Clementi, D.L. Raimondi, and W.P. Reinhardt, J. Chem. Phys. 47, 1300 (1967).

[c]C. Moore, Atomic Energy Level VIII Circular of the NBS No. 467 (1958).

[d]W. Lotz, J. Opt. Soc. Am. 60, 206 (1970).

[e]S. Huzinaga, "Approximate Atomic Functions."

[f]G.D. Watkins, private communications.

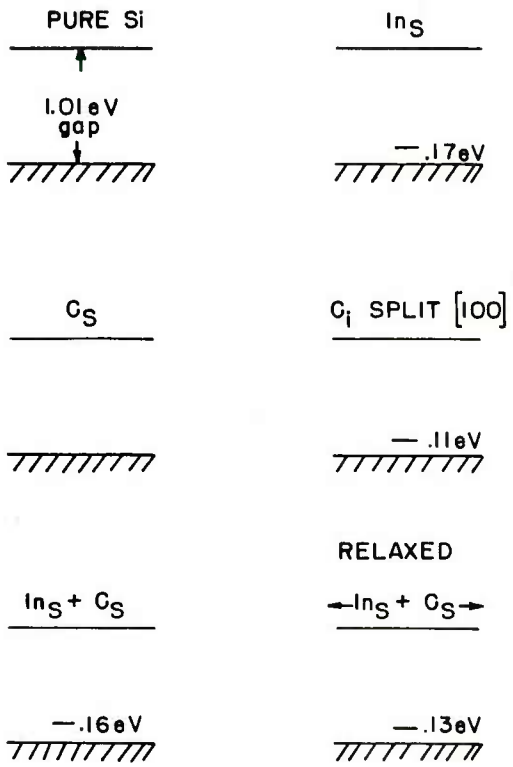

Figure D-11. Energy levels calculated for pure silicon, substitutional carbon, interstitial carbon, and substitutional indium to test the extended Hückel cluster technique shown in the top diagrams. The bottom diagrams are for the indium-X-center model of a nearest-neighbor substitutional carbon-indium pair in the substitutional sites and in a relaxed minimum-energy configuration.

The extended Hückel theory does not include charge interations, and clusters with atoms having differences in Pauling electronegativity greater than 1.2 have been found to give poor results.[D-29] Silicon, indium, and carbon have electronegativities of 1.8, 1.7, and 2.5, all within 0.8 of each other.

D-29 R.T. Sanderson in Chemical Periodicity (Reinhold Publishing Co., New York, 1969) p. 34.

With this background, the nearest-neighbor substitutional carbon-acceptor pair model for the indium-X center was then calculated. A single energy level slightly shallower than that of the substitutional indium was found. The total energy of the complex can be reduced by letting the atoms relax, with the indium and the carbon moving away from each other. In this configuration the energy level for the defect is 0.13 eV, close to the actual X-center energy of 0.113 eV.

The wave function corresponding to the 0.13 eV level is a bonding molecular orbit between the indium and the three neighboring silicons. The carbon neighbor does not take part in this bond. This explains why the complex relaxes to a minimum-energy configuration by moving the indium and carbon away from each other and closer to their bonding neighbors. The energy levels for the carbon acceptor pair are also shown in Figure D-11.

The fact that the extended Hückel cluster calculation came out with an energy level for the carbon-indium pair which is close to the measured In-X-center energy gives some further support to the model. In this case it is probably of more interest to take a different view. That is that the experimental data of the dependence on carbon and an acceptor, the high-temperature cyclic annealing, and the [111] stress symmetry have established the X-center model and that the calculations give us some insight into this defect's bonding, wave functions, and minimum-energy configuration. The combination of the experimental data and the theoretical calculation gives a good total picture of the carbon-acceptor pair (or X-center) defects.

Application Note

One of the reasons for interest in X-centers was their adverse effect on extrinsic silicon infrared detectors. With the identification of the carbon dependence for these centers, it has been possible to produce low-carbon detectors with no measurable X-level concentrations.

CONCLUSIONS

The data for the X-centers in silicon yields two major results:

1. A class of defects called X-centers exists. There is one of these centers corresponding to each of the group IIIA elements boron, aluminum, gallium, indium, or thallium in silicon.

2. The model for these centers which best fits the data is a nearest-neighbor substitutional carbon-acceptor pair.

REFERENCES

D-1. R. Baron, M.H. Young, J.K. Neeland, and O.J. Marsh, Appl. Phys. Lett. 30, 594 (1977).

D-2 M.W. Scott, Appl. Phys. Lett. 32, (1978).

D-3 R. Baron, J.P. Sankus, S.D. Allen, T.C. McGill, M.H. Young, H. Kimura, H.V. Winston, and O.J. Marsh, Appl. Phys. Lett. 34, 257 (1979).

D-4 C.E. Jones D.E. Schafer, W. Scott, and R. J. Hager, Bull. Am. Phys. Soc. 24, 276 (1979) BL14.

D-5 M.C. Ohmer and J.E. Lang, Appl. Phys. Lett. 34, 750 (1979).

D-6 V. Swaminathan, J.E. Lang, P.M. Heminger, and S.R. Smith, Appl. Phys. Lett, 35, 184 (1976).

D-7 G.W. Ludwig and H.H. Woodbury in Solid State Physics, 13, F. Seitz and D. Turnbull, Eds. (Academic Press, New York, 1962), p. 223.

D-8 J. Schnedier talk presented at the International Conference on the Physics of Pure Semiconductors, Stockholm, Sweden, 3-5 Sept. 1979.

D-9 T.S. Moss, Optical Properties of Semiconductors (Academic Press, New York, 1959), p. 14.

D-10 W. Scott and R. J. Hager J. Electron. Mater. 8, 581 (1979).

D-11 Float-zone indium-doped silicon supplied by Dr. Sumner of U.S. Army NVL.

D-12 N. Sclar, IEEE Trans. Electron. Devices Ed-24, 709 (1977).

D-13 D. Schechter, J. Phys. Chem. Solids 23, 237 (1962).

D-14 R.C. Newman and J.B. Willis, J. Phys. Chem, Solids 26, 373

D-15 D.V. Lang, J. Appl Phys. 45, 3014 and 3023.

D-16 G.L. Miller, D.V. Lang, and L.C. Kimmerling, Am. Rev. of Mater. Sci. 7, (1977).

D-17 C. Jones and G. Johnson, IRIS Specialty Group on Infrared Detectors, Minneapolis, MN (June, 1979). Also sub. J. Appl. Phys. 1980.

D-18 J.L. Hartke, J. Appl. Phys. 39, 4871 (1968).

D-19 R.A. Swalin, Thermodynamics of Solids, (John Wiley & Sons, New York 1962) Chapter 14.

D-20

D-20 N.F. Mott and R.W. Gurney, Electronic Processes in Ionic Crystals.

D-21 J.C. Phillips, Bonds and Bands in Semiconductors, (Academic Press, New York, 1973) p.22.

D-22 R.P. Messmer and G.D. Watkins Phys. Rev. B7, 2568 (1973).

D-23 C. Weigel, D. Peak, J.W. Corbett, G.D. Watkins, and R.P. Messmer, Phys. Stat. Sol. b 63, 131 (1974).

D-24 V.A. Singh, C. Weigel, J.W. Corbett, and L.M. Roth, Phys. Stat. Sol. b 81, 637 (1977).

D-25 K.L. Yip, Phys. Stat. Sol. b 66, 619 (1974).

D-26 C.E. Jones, Bull, Am. Phys. Soc. 22, 382 (1977) EO14.

D-27 C.D. Watkins and K.L. Brower, Phys. Rev. Lett. 36, 1329 (1976).

D-28 H. Hjalmarson, Thesis, U. of Illinois, Physics Dept. (1979).

D-29 R.T. Sanderson in Chemical Periodicity (Reinhold Publishing Co., New York, 1969) p. 34.